

Recent Progress in Rechargeable Sodium-Ion Batteries: toward High-Power Applications

Xiangjun Pu, Huiming Wang, Dong Zhao, Hanxi Yang, Xinping Ai, Shunan Cao, Zhongxue Chen,* and Yuliang Cao*

The increasing demands for renewable energy to substitute traditional fossil fuels and related large-scale energy storage systems (EES) drive developments in battery technology and applications today. The lithium-ion battery (LIB), the trendsetter of rechargeable batteries, has dominated the market for portable electronics and electric vehicles and is seeking a participant opportunity in the grid-scale battery market. However, there has been a growing concern regarding the cost and resource availability of lithium. The sodium-ion battery (SIB) is regarded as an ideal battery choice for grid-scale EES owing to its similar electrochemistry to the LIB and the crust abundance of Na resources. Because of the participation in frequency regulation, high pulse-power capability is essential for the implanted SIBs in EES. Herein, a comprehensive overview of the recent advances in the exploration of high-power cathode and anode materials for SIB is presented, and deep understanding of the inherent host structure, sodium storage mechanism, Na^+ diffusion kinetics, together with promising strategies to promote the rate performance is provided. This work may shed light on the classification and screening of alternative high rate electrode materials and provide guidance for the design and application of high power SIBs in the future.

1. Introduction

The exhaustion of fossil fuels has accelerated advancements in exploiting renewable energy sources; to cope with ever-growing energy demand and better make use of sustainable energy, multiscale energy storage systems (ESSs) have been intensively developed in recent years. Among various candidates, lithium-ion battery (LIB) is considered as the pioneer technology which

can provide both high energy density and large output power, accordingly has captured the markets of portable electronics (W level) and electrical vehicles (KW level). Nevertheless, the implementation of LIB into grid-scale ESS (MW) is constantly postponed due to cost and safety issues. Although the lithium iron phosphate (LiFePO_4) battery is seeking a participant opportunity in the grid-scale battery market, the rising cost of lithium resources, as opposed to their reserves, is likely to be the primary concern for its potential application. Recently, sodium-ion battery (SIB) emerges as an attractive and promising alternative because of the practically inexhaustible, ubiquitous and low cost sodium resources.

Despite the similar electrochemistry to the well-established LIBs technology, SIBs exhibit lower specific capacity and working potential than LIBs, thus demonstrating inferior energy density. For instance, the most advanced full sodium-ion bat-

tery based on $\text{O}_3\text{-Na}_{0.9}[\text{Cu}_{0.22}\text{Fe}_{0.30}\text{Mn}_{0.48}]\text{O}_2$ cathode and hard carbon anode developed by Hu and co-workers delivered a practical energy density of 100 Wh kg^{-1} with an average operation voltage of 3.2 V, far lower than the energy density and working potential ($>200 \text{ Wh kg}^{-1}$, 3.7 V) achieved for present LIBs. Overall, the SIBs are almost impossible to enter the market for portable electronics and electric vehicles. The good news is that both LIBs and SIBs technologies for electricity storage system are currently at much earlier stages of development, therefore, SIBs still hold a great chance in case their electrochemical performance is enormously improved and their cost is largely reduced.

The primary technology characteristics used in assessing a battery's potential for use in grid-scale energy storage applications include storage and operation properties, such as energy and power density, efficiency, scale, response time, lifetime and cost. Up to date, over 10 000 papers on SIBs have been published, implying SIBs are attractive and full of promise. However, most of these works focused on the design, synthesis and modification of new electrode materials with enhanced operating voltage and energy density, few of them paid attention to the power capability of the batteries. In practical terms, power density rather than energy density is often a more important parameter for SIBs in electricity storage system. Apart from

X. Pu, H. Wang, D. Zhao, Prof. S. Cao, Dr. Z. Chen
Key Laboratory of Hydraulic Machinery Transients
Ministry of Education

School of Power and Mechanical Engineering
Wuhan University
Wuhan 430072, China

E-mail: zxchen_pmc@whu.edu.cn

Prof. H. Yang, Prof. X. Ai, Prof. Y. Cao
Hubei Key Laboratory of Electrochemical Power Sources
College of Chemistry and Molecular Sciences
Wuhan University
Wuhan 430072, China
E-mail: ylcao@whu.edu.cn

 The ORCID identification number(s) for the author(s) of this article can be found under <https://doi.org/10.1002/smll.201805427>.

DOI: 10.1002/smll.201805427

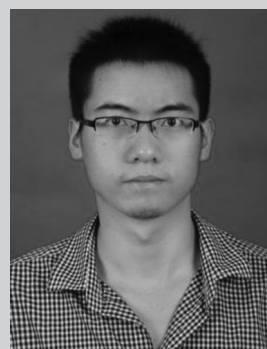
the general function for smoothing out the fluctuations from renewable energy sources (wind, solar, etc.) and reducing the need for “peaker” plants, grid-level battery also provides short-term emergency backup power, and contributes in frequency regulation by delivering active power when the grid frequency is dropping below a certain lower threshold and charge when the frequency is above a certain upper threshold. The amount of energy charged and discharged is proportional to the frequency deviation, and the discharge duration time varies from 1 to 15 min, with shallow charge and discharge for 20 to 40 cycles per day. In this context, power capability of SIBs is essential for their successful applications in electricity storage system (Figure 1).

Generally, the power capability of a SIB depends critically on the speed at which Na^+ ions and electrons migrate through the electrolyte and bulk electrode. For a long time, sodium ion is widely recognized as having sluggish movement compared with lithium ion due to its large ionic radius. However, recent studies have revealed that there are a great number of SIBs, either half or full cells, exhibit high power characteristics, thus providing a compelling rationale to enable SIBs to serve as a high power supply when proper material and rational design are elaborately established. Unfortunately, there is no evident borderline between high energy and high power batteries; accordingly, no common standard that defines high power battery is given until now. Particularly, most previous works only investigate the rate performance of a single electrode (cathode or anode), this will bring out relatively great deviation in evaluating the power capability of a full battery since all the factors related to the power performance should be considered, such as the voltage gap between the cathode and anode, the electrochemical kinetics of both electrodes, battery design and manufacture, and so on. Nonetheless, the power output of a full SIB depends mostly on the electrochemical characteristics of its cathode and anode, in this sense, the property of a single electrode can be assessed to predict its potential application in high power SIBs.

Now, there is no commonly accepted standard with which to define high power electrode materials; this will bring a challenge to select practicable alternative electrodes for grid-scale SIBs from a vast number of cathodes and anodes reported so far. Despite this, we can still gauge their application prospect according to the requirements of current electricity storage system. In this context, electrode materials which are capable of discharging in 1–15 min and cycling shallowly for 20–40 times a day are included within the scope of this review. Specifically, an output power density of at least 2 KW kg^{-1} is essential for a single cathode in a half cell with sodium metal as anode (strictly speaking, power density could only be used to evaluate full batteries, but we can still get a hint about their rate capabilities by half cell's data in massively published works, so the power density provided below is calculated based on the mass of cathode if it is not specified), considering the capacity of most state-of-art cathode materials are around 100 mAh g^{-1} , the operating voltage of the cathodes at 10 C ($\approx 1000 \text{ mA g}^{-1}$) should be kept above 2.0 V . For anode materials, it is logically required that the working potentials should be low, generally in the range of $0\text{--}1.0 \text{ V}$ (vs Na/Na^+). Especially for high power application, anode materials should be able to tolerate high current



Xiangjun Pu received his B.Sc. degree in 2016 in energy chemical engineering from Wuhan University, China. Now, he is pursuing a Ph.D. degree in energy storage and conversion science. His research objective is to design green and sustainable materials, and advanced electrolytes for rechargeable batteries.



Zhongxue Chen received his B.Sc. degree in 2007 and Ph.D. degree in 2012 from Wuhan University, and worked as a visiting scholar in the Pennsylvania State University from 2010 to 2011. Currently, he is an associate professor in the School of Power and Mechanical Engineering in Wuhan University. His research interests focus on energy storage/conversion materials and devices.



Yuliang Cao received his Ph.D. degree in 2003 from Wuhan University, and then he worked as a visiting scholar in Pacific Northwest National Laboratory from 2009 to 2011. He is now a professor in the college of chemistry and molecular sciences, Wuhan University. His research interests focus on developing advanced energy storage materials (e.g., carbonous materials, alloy nanocomposite anodes, transition metal oxide cathodes, phosphate framework materials, and novel safety electrolytes) for lithium/sodium ion batteries.

impulses (10 C) and eliminate the sodium-dendrite hazard. Up to date, there have been many review papers published on electrode materials and full cells of SIBs. However, to the best of our knowledge, there is no special review on high power SIBs as well as high rate electrode materials. In this review, we will present the most recent progress on high power cathode and anode materials for sodium-ion batteries, focusing on the fundamental aspects of synthesis, structure and electrochemistry. Special attention is given to the discussions of crystal structure characteristics, and sodium storage mechanisms of typical electrode materials, also the effects of their intrinsic structure features and nonstructural engineering on the sodium ion

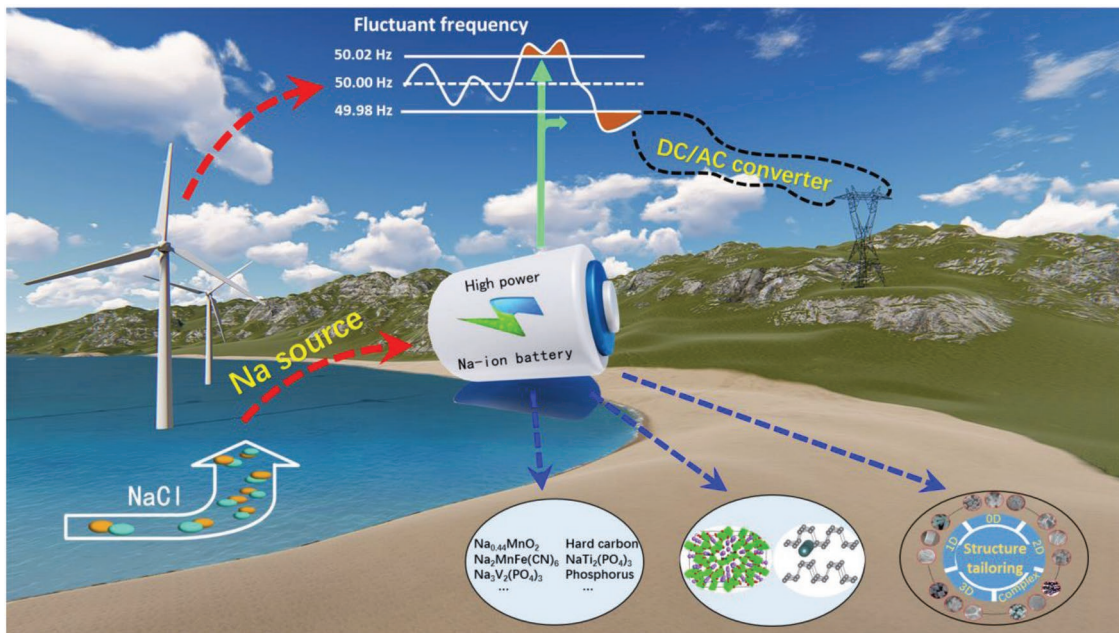


Figure 1. Schematic illustration of high power Na-ion battery in energy storage system.

intercalation/deintercalation kinetics are discussed in details. The main goal is to offer the reader a clear vision of promising candidates for high power electrode materials, for this purpose, our perspectives on the major challenges and future developments toward the commercialization of grid-scale SIBs are provided at the end of this review.

2. Cathode Materials

The operating voltage of SIB depends mainly on the potential gap between the positive and the negative electrodes, and the positive electrode is considered as the bottleneck for boosting the power output of SIBs, so major efforts have been dedicated to developing advanced cathode materials. Generally, researches on cathodes for SIBs focus on three major types of compounds. The first one is sodium transition metal oxides. These materials have high reversible capacity and high working voltage. Even so, most of them still suffer from irreversible phase transition, air instability and insufficient battery performance. Another type is Prussian blue analogues, these compounds exhibit favorable operating voltage, cycling stability and rate capability, the main obstacles for their practical application would be control of lattice defects, thermal instability and low tap density. Lastly, polyanionic compounds are another class of promising cathode materials that have drawn considerable attentions due to their structure stability, high safety and small volume change with cycling. Up to date, numerous iron-, vanadium-, and manganese-based polyanion compounds have been investigated.

2.1. Transition Metal Oxides

$\text{Na}_x\text{TM}\text{O}_2$ oxides ($0 < x \leq 1$; TM = Fe, Cr, Co, Mn, Ni, V, Cu, and mixtures of them) are an assorted and appealing class

of cathode materials which own open structures, compositional and electrochemical tenability and activity. These materials could be sorted into two kinds: tunnel and layer structures. Interestingly, some of the above $\text{Na}_x\text{TM}\text{O}_2$ oxides exhibit better performance than their lithium counterparts, which is probably because the distinctly different size of Na^+ (1.02 Å) and TM ion (<0.7 Å) can avoid cation mixing. For example, rhombohedral $\alpha\text{-NaFeO}_2$ (Fe^{3+} : 0.645 Å) was reported to have electrochemical activity toward sodium storage,^[1] whereas, stable layered rock-salt LiFeO_2 was unable to be obtained, because Fe^{3+} and Li^+ (0.76 Å) cations have similar ion size and they are prone to cation mixing, resulting in structure deterioration.

2.1.1. Tunnel Oxides

In the tunnel structured families, Na_xMnO_2 oxides are typical cathodes and attractive in utilization in SIBs due to the cost-efficient of Na and Mn elements. Specifically, $\text{Na}_{0.44}\text{MnO}_2$ is the most extensively studied compound. In its crystal structure, sodium ions can be located in wide S-shaped and narrower tunnels. It is expected that only the large S-shaped tunnels can offer diffusion path to accommodate the relatively large size of sodium ions (Figure 2a,b), therefore, the x of tunnel Na_xMnO_2 varies over the range of 0.22–0.66 during charge and discharge process with a series of phase changes (Figure 2c).^[2–4]

It has been revealed by many researchers that $\text{Na}_{0.44}\text{MnO}_2$ is prone to form single-crystalline nanorods morphology (Figure 2d), which shortens the diffusion path lengths for both electron and Na^+ transport and provides a beneficial microstructure for Na^+ insertion/extraction. Zhou et al. reported early a single phase $\text{Na}_{0.44}\text{MnO}_2$ was successfully synthesized by hydrothermal method, which showed a power density of $\approx 2700 \text{ W kg}^{-1}$ without obvious capacity decay at high rate.^[5] Later, Liu and co-workers investigated the effect

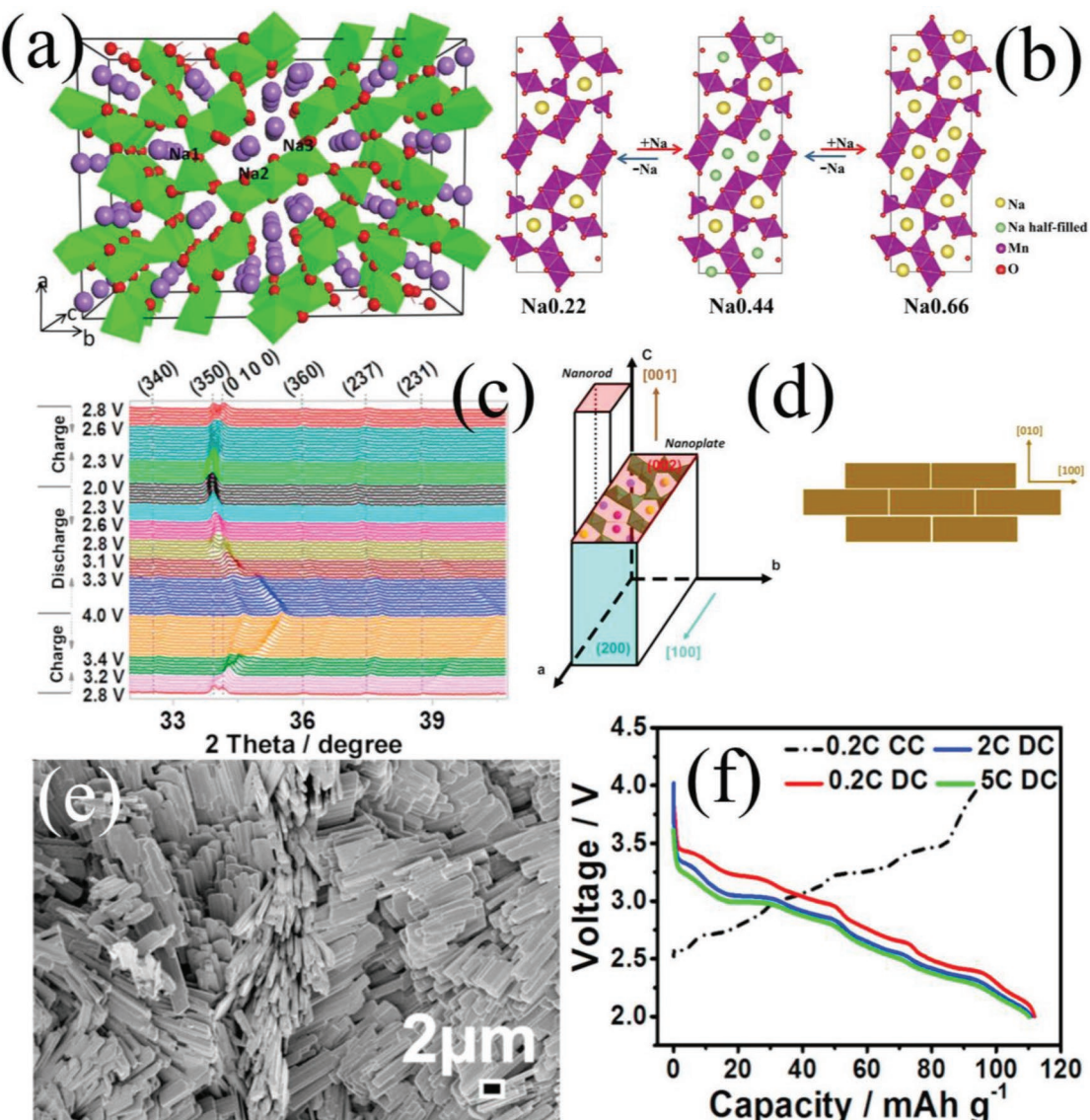


Figure 2. a) Structure of $\text{Na}_{0.44}\text{MnO}_2$ and b) illustration of the phase transformation of upon sodiation and desodiation process. Reproduced with permission.^[4] Copyright 2018, Elsevier. c) Crystal growth of nanorod and nanoplate and the structural formation of nanoplate particles. d) In situ evolution of the XRD patter. e) SEM microscopy image of $\text{Na}_{0.44}\text{MnO}_2$ nanoplates and f) the discharge profiles at 0.2, 2, and 5 C. Reproduced with permission.^[7] Copyright 2016, Elsevier.

of calcination temperature on the electrochemical performance of $\text{Na}_{0.44}\text{MnO}_2$ and found that 900 °C is the optimal annealing condition. The obtained $\text{Na}_{0.44}\text{MnO}_2$ nanowire has a longer length and a smaller width than the control samples, battery tests showed that the cathode delivered a capacity of 99 mAh g⁻¹ at 20 C.^[3,6] Recently, a symmetric sodium-ion capacitor based on $\text{Na}_{0.44}\text{MnO}_2$ with high power was also reported.^[2] Some researchers elaborately attempted to achieve enhanced rate capability and volumetric energy density by morphology regulation. Showing in Figure 2e, Li and co-workers obtained bidimensional $\text{Na}_{0.44}\text{MnO}_2$ (nanoplates) with a limited crystal growth along [001] in acidic and reductive environment, compared to unidimensional structure, this bidimensional structure extending perpendicularly the Na^+ favorable insertion path ways would allow limiting surface defects, increasing the

tap density and fast Na^+ (de)insertion. Consequently, the material delivered a discharge capacity of 96 mAh g⁻¹ at 10 C rate.^[7]

The appealing performance of $\text{Na}_{0.44}\text{MnO}_2$ linked to its open structure with interconnected and large tunnels that is able to sustain the multiple phase change during the Na^+ (de)-intercalation processes, endowing $\text{Na}_{0.44}\text{MnO}_2$ as a promising cathode material for high power SIBs.

2.1.2. Layer Oxides

In General, sodium-storage layered oxides with stable output capacity can be categorized into two main groups: P2 type and O3 type, according to the surrounding Na^+ environment and the number of unique oxide layer stacking. To be specific, “P”

or “O” represents that Na ions accommodated at prismatic or octahedral sites, and the “2” or “3” suggests the distinguishable number of MeO_2 -layer in a single cell unit. Usually, P3-type structure, the thermodynamic stable phase, can be obtained if the synthesis temperature is lower than 800 °C rather than P2 that is the high-temperature phase.

Unfortunately, P2 phase would transform into O2 phase due to the gliding ($\pi/3$ rotation) of some TMO_6 octahedral sheets if a certain amount of Na^+ is extracted, leading to a significant contraction on crystal lattice and a decrease in interlayer distance. Because the large prismatic sites are energetically stabilized by large Na^+ in the P2-type phase, while TMO_2 slabs glide (move) to form octahedral sites after Na^+ extraction and also by Na^+/Li^+ exchange, resulting in the formation of a new O2 phase with a unique AB AC AB oxygen stacking. More details regarding the structure evolutions of P2-type layered oxides could be found in Figure 3.^[8]

P2 Type: The crystal structure of P2-type Na_xTMO_2 oxides is shown in Figure 3. The redox center is available for many earth abundant elements, such as Fe, Mn, Ni, etc., Na ions in this structure have trigonal prismatic coordination in between two $(\text{MO}_2)_n$ slabs per unit cell. This type of material could deliver a high capacity due to the initial Na-rich phase. For instance, $\text{P2-Na}_{2/3}[\text{Fe}_{1/2}\text{Mn}_{1/2}]\text{O}_2$ reported by Komaba exhibited a higher reversible capacity of 190 mAh g^{-1} by introducing the

electrochemically active $\text{Fe}^{3+}/\text{Fe}^{4+}$ redox, and manganese partly substitution for iron was aimed to stabilize Fe^{4+} , the electrode turned out to achieve a high power density of $\approx 2000 \text{ W kg}^{-1}$.^[9]

A series of Mn-based oxides 2D layered polymorphs could be unambiguously fabricated. With high sodium content, $\alpha\text{-NaMnO}_2$ (space group $C2/m$) and $\beta\text{-NaMnO}_2$ (space group $Pmmn$) could be prepared at low temperature and high temperature, respectively. However, former works have found that NaMnO_2 suffers from a severe capacity fading due to the detrimental Jahn–Teller distortion of Mn^{3+} ($t_{2g}^3 e_g^1$). In this context, Mg or Li was used to partially replace Mn to suppress the Jahn–Teller distortion [10,11].

$\text{Na}_{2/3}[\text{Ni}_{1/3}\text{Mn}_{2/3}]O_2$ electrode was proved to have a relatively high operating voltage and high specific capacity.^[12] But the deintercalation of Na^+ can induce a serious phase transition from P2 to O2 and $\text{Na}^+/\text{vacancy}$ ordering, making $\text{Na}_{2/3}[\text{Ni}_{1/3}\text{Mn}_{2/3}]O_2$ susceptible to severe voltage and capacity decay. To suppress the phase change, Cao et al. employed the electrochemically active copper (II) as a unique substituent to stabilize the P2 phase, forming $\text{Na}_{0.67}\text{Ni}_{0.3-x}\text{Cu}_x\text{Mn}_{0.7}\text{O}_2$ ($x = 0, 0.1, 0.2$ and 0.3). The existence of Cu can not only stabilize the crystal structure against the detrimental phase transition, thus suppress the severe voltage and capacity decay, but also offer high potential due to the high $\text{Cu}^{2+}/\text{Cu}^{3+}$ redox. Consequently,

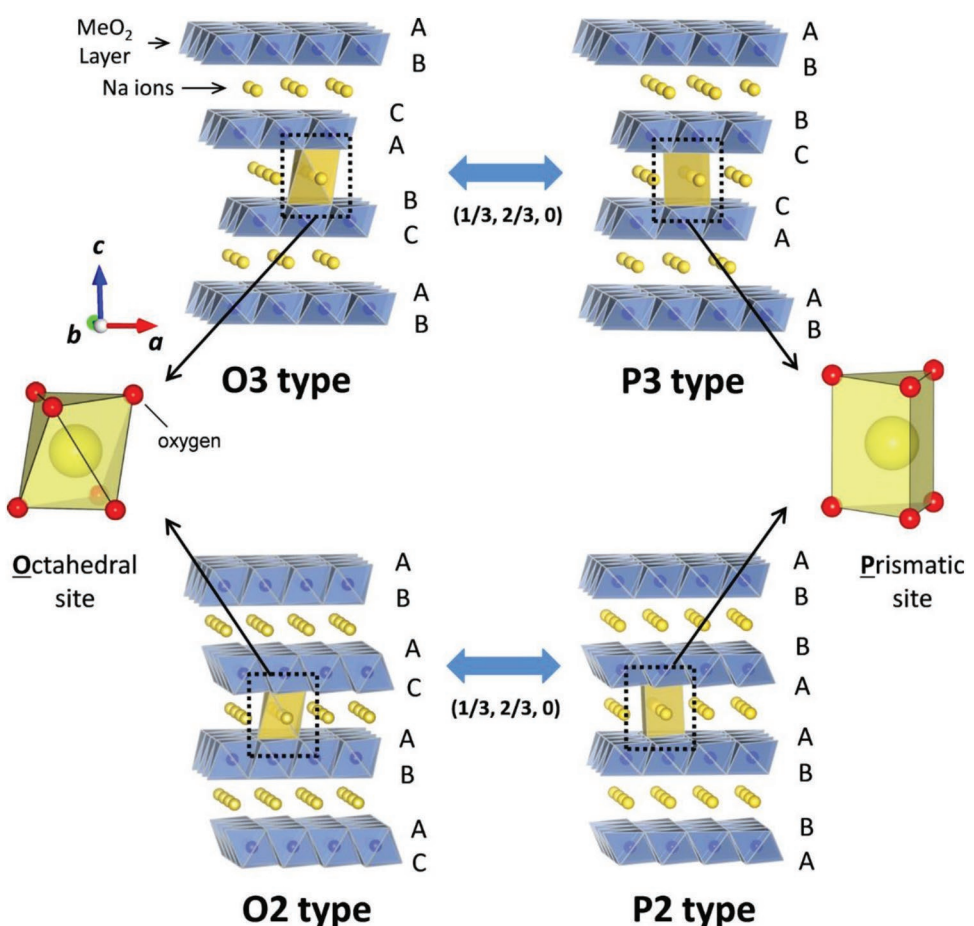


Figure 3. The classification of Na-Me-O layered materials with the sheets of edge-sharing MeO_6 octahedra and phase transition processes induced by sodium extraction. Reproduced with permission.^[16] Copyright 2014, National Institute for Materials Science.

the formulated P2-type $\text{Na}_{0.67}\text{Ni}_{0.1}\text{Cu}_{0.2}\text{Mn}_{0.7}\text{O}_2$ showed much-alleviated structural degradation and favorable battery performance with a moderate rate capability.^[13] This strategy paved new ways to prepare high power materials.

NaCoO_2 has been expected as a promising cathode for SIBs due to the triumph of its counterpart LiCoO_2 .^[14] However, as illustrated in Figure 4a, NaCoO_2 revealed surprising differences in full cells with respect to analogue lithium-based materials, and did not show attractive charge/discharge performance due to the larger radius of Na^+ . Delmas et al. systematically studied its performance in the electrolyte of NaClO_4 (1 M) solution in propylene carbonate, and they revealed complicated phase.^[14] Recently, Scrosati's group first designed a novel, high-power sodium-ion full cell (SIFC), which consisted of a layered P2- $\text{Na}_{0.7}\text{CoO}_2$ cathode coupled with a graphite anode in an optimized ether-based electrolyte. In their system, the formed passivation layer at the cathode would be modified during the following sodiation/desodiation process, and the use of glyme-based electrolyte enables the cointercalation of solvated sodium ions by forming ternary graphite intercalation compounds.^[15] The cathode delivered capacities of about 100 mAh g^{-1} at 0.2 C and 80 mAh g^{-1} at 1 C. Also it exhibited a decent residual capacity of about 70 mAh g^{-1} with a desirable average discharge voltage of 2.9 V at 10 C (1 C = 175 mA g^{-1}), that was, 203 Wh Kg^{-1} at the corresponding power density of 5075 W Kg^{-1} (Figure 4b). In addition, based on total masses of cathode and anode, the full cell could achieve an energy density of \approx 59.5 Wh Kg^{-1} under a power density of \approx 2975 W Kg^{-1} .

In short, P2 type $\text{Na}_{0.7}\text{CoO}_2$ and $\text{Na}_{2/3}[\text{Ni}_{1/3}\text{Mn}_{2/3}]\text{O}_2$ or their derivatives show a large reversible capacity and acceptable kinetic performance, but the poor cyclability and high cost of cobalt/nickel resources remain the major obstacle for their large-scale applications.

O3 Type: As a complementary to layered oxide cathodes, O3 type material is also easy to be obtained by tuning element species and ratios. The layer stacking sequence is O3-type, which can be described as octahedral coordinated Na ions in between three $(\text{MO}_2)_n$ slabs per unit cell.

Fe centered O3 type layered structure shows inferior performance due to the migration of iron ions. For example, NaFeO_2 is known as a representative of O3-type layered structures, but possesses poor sodium storage capability, because Fe^{3+} would migrate into vacant tetrahedral sites when Na^+ is extracted out during charge (Figure 4c). This migration is irreversible and would become severer with increased upper cut off voltage. As a result, solid-state diffusion of sodium ions is disturbed, leading to the rapid degradation and a limited working voltage window of Na_xFeO_2 .^[16]

To overcome this problem, Fe ions in Na_xFeO_2 were partially substituted by Ni, Mn, or Co ions and the substituted forms $\text{Na}_x[\text{Fe}_{y/2}\text{M}_{1-y}]\text{O}_2$ have been reported with a wider charge/discharge voltage window. In these materials,^[17–19] O3-type $\text{Na}_x[\text{Fe}_{1/2}\text{Co}_{1/2}]\text{O}_2$ shows much stable plateaus (Figure 4e,f) and excellent rate capability with a power density of 16 600 W kg^{-1} , the authors attributed this outstanding performance to the fast ionic conductivity of P3 phase formed by the O3–P3 phase transition during the desodiation process.^[20]

Metal ions' substitution is also effective in stabilizing binary/ternary-metal-based oxides even in the presence of a small

amount. Specially, polyoxometalates were developed to employ the synergistic effects of multiple metal ions. For example, Liu and colleagues designed O3-type $\text{NaMn}_{0.48}\text{Ni}_{0.2}\text{Fe}_{0.3}\text{Mg}_{0.02}\text{O}_2$, in which the incorporation of Mg not only enlarges the interlayer spacing, thus enhancing the Na^+ diffusion kinetics and the rate capability, but also minimizes Jahn-Teller effect. Consequently, an enhanced reversible capacity of 40 mAh g^{-1} was achieved at 5 C compared with that for Mg-free sample.^[21]

Yu et al. reported the layered O3-type NaCrO_2 material as the cathode in Na-ion batteries, which was fabricated via an emulsion-drying method.^[22] The rate performance of NaCrO_2 electrode with 3.4 wt% carbon content was surprising, an unexpectedly high capacity (106 mAh g^{-1}) at a rate of 50 C (5.5 A g^{-1}) was obtained, corresponding to 87% of its capacity at a rate of 0.5 C (55 mA g^{-1}). Even at an ultrahigh rate of 150 C (16.5 A g^{-1} , discharge in 27 s), a high power density of 39 600 W Kg^{-1} and a discharge capacity of 99 mAh g^{-1} can still be attained. Notably, a superior rate capability in full sodium-ion batteries, based on NaCrO_2 cathode coupled with hard carbon anode in pouch-cell configure, was observed at a high rate of 100 C (10 A g^{-1}), which demonstrates a great potential for high-power applications (Figure 4d). The authors ascribed the impressive performance to the presence of crystalline carbon layers, which assists the immediate migration of electrons so that sodium ions can be inserted or extracted at ultrafast rates.

P2–O3 Intergrowth Type: The P2 phase is only found in sodium deficient compositions (i.e., $\text{Na}/\text{M} < 1$), and it has been revealed that in O3 type electrode, the diffusion of Na^+ from one octahedral site to another should take place through the edge sharing tetrahedral site between them, involving with an intermediate site with high-energy barrier, which is detrimental for high rate performance.^[23] Therefore, designing P2–O3 intergrowth structure that combines the advantages of both P2 and O3 phase might be a feasible approach to achieve high capacity as well as good rate capability.

Ni/Mn-based binary metal oxides containing Ni^{2+} and Mn^{4+} are also the most widely studied electrode materials because of their relatively high operating voltage and highly symmetric and stable crystal structure. However, the phase transition from P2 to O2 and Na^+ /vacancy ordering make P2- $\text{Na}_{2/3}\text{Ni}_{1/3}\text{Mn}_{2/3}\text{O}_2$ vulnerable to severe voltage and capacity decay. Johnson et al. demonstrated that the cation substitution and constructing layered intergrowth structures are promising strategies to improve the performance. They fulfilled the incorporation of Li into O3- $\text{NaNi}_{0.5}\text{Mn}_{0.5}\text{O}_2$, forming a P2/P3-intergrowth $\text{Na}_{1-x}\text{Li}_x\text{Ni}_{0.5}\text{Mn}_{0.5}\text{O}_{2+d}$ (Figure 4g), which could promote the smooth diffusion of Na^+ .^[23] Similarly, Liu and co-workers also developed a P2/O3 biphasic derived from Ni/Mn-based binary metal oxides, $\text{Na}_{0.67}\text{Mn}_{0.55}\text{Ni}_{0.25}\text{Ti}_{0.2-x}\text{Li}_x\text{O}_2$ ($x = 0, 0.1, 0.2$), which shows multiple electrons transfer. An average discharge potential of \approx 2.65 V at 1920 mA g^{-1} (8 C) could be attained (Figure 4h), that is, a 5088 W kg^{-1} in power density.^[24]

2.2. Prussian Blue Analogs

Prussian blue analogs (PBAs) appear to be suitable host materials to accommodate reversible Na^+ insertion reactions because of their compositional tenability and rigid open channel

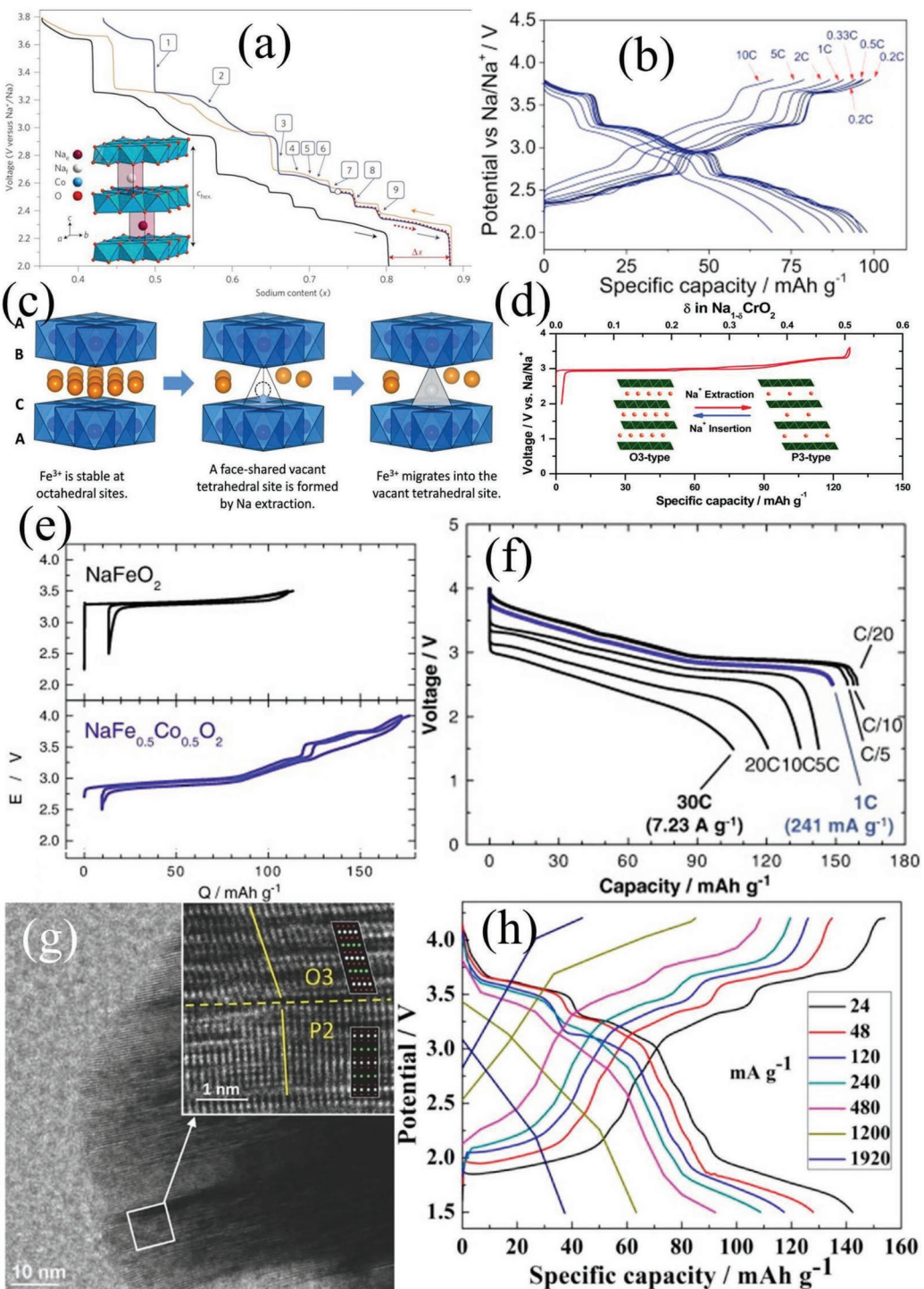


Figure 4. a) Galvanostatic cycling curve of a $\text{Na}/\text{P}2-\text{Na}_x\text{CoO}_2$ battery giving an overview of the phase diagram. Reproduced with permission.^[14] Copyright 2011, Macmillan Publishers Limited. b) Voltage profiles of the $\text{Na}/1 \text{ M NaClO}_4 \text{ EC:DMC}$ (1:1 w/w)+20% FEC/ $\text{Na}_{0.7}\text{CoO}_2$ cell studied at increasing currents. Reproduced with permission.^[15] Copyright 2016, Elsevier. c) A proposed mechanism of the iron migration process in $\text{O}3$ type NaFeO_2 during sodium extraction. Reproduced with permission.^[16] Copyright 2014, National Institute for Materials Science. d) Charge and discharge profile of NaCrO_2 (inset: structure revolution during Na^+ de/embedding). Reproduced with permission.^[22] Copyright 2015, Royal Society of Chemistry. e) Charge/discharge curves of NaFeO_2 and $\text{NaFe}_{0.5}\text{Co}_{0.5}\text{O}_2$ in Na cells. f) Rate-capability of $\text{NaFe}_{0.5}\text{Co}_{0.5}\text{O}_2$: charged to 4.0 V at a rate of 12 mA g^{-1} . Reproduced with permission.^[20] Copyright 2018, Elsevier. g) High-resolution TEM image directly showing the intergrowth stacking of the $\text{P}2$ and $\text{O}3$ lattices. Reproduced with permission.^[23] Copyright 2014, WILEY-VCH Verlag GmbH & Co. KGaA, Weinheim. h) Rate curves of $\text{Na}_{0.67}\text{Mn}_{0.55}\text{Ni}_{0.25}\text{Ti}_{0.2-x}\text{Li}_x\text{O}_2$ ($x = 0.2$) in the voltage range of 1.5–4.2 V versus Na^+/Na at various density currents. Reproduced with permission.^[24] Copyright 2016, American Chemical Society.

structure with large interstitial sites to endow great durability and fast kinetics (Figure 5a).^[25,26] Despite this, the practical performance of PBAs is greatly affected by phase purity, crystallinity, defects, water content, and carbon decoration.

$\text{Na}_x\text{Fe}[\text{Fe}(\text{CN})_6]$ (FeFe-PB) is one of the oldest coordination materials with strong electrochemical activity already known for many years and has been widely studied for electrochemical applications. FeFe-PB exhibits an eligible capacity at high potential, specifically, the voltages of the two plateaus at 3.11 and 3.30 V on charge, 3.00 and 3.29 V on discharge could be found. A full cell with rhombohedral $\text{Na}_{1.92}\text{Fe}_2(\text{CN})_6$ as cathode and hard carbon as anode witnessed no obvious voltage decay with increased rate test.^[27]

Many approaches have been developed to unravel the underlying full utilization of its potential of two-electron redox reaction. Morphological modification is an effective mean widely used to construct a favorable surface layer and to guarantee the structural stability of bulk phase in materials technology. A high quality PB nanocrystals $\text{Na}_{0.61}\text{Fe}[\text{Fe}(\text{CN})_6]_{0.94}$ (HQ-NaFe) (Figure 5b) were prepared through a facile synthetic procedure. The HQ-NaFe exhibited a low zeolite water content and a small number of $[\text{Fe}(\text{CN})_6]$ vacancies in the crystal framework, which further resulted in sufficient transportation pathways for Na^+ and electrons, effective maintenance of the crystal structure integrity upon cycling and an enhanced rate performance.^[28]

Introducing carbon is another way often used to improve the electronic conductivity of the PBA materials. Dou and colleagues prepared an FeFe-PB@C composite, $\text{Na}_{0.647}\text{Fe}[\text{Fe}(\text{CN})_6]_{0.93} \cdot 0.07 \cdot 2.6\text{H}_2\text{O}$ by embedding homogeneous PB cubes uniformly in the conductive carbon matrix (Ketjen black), ensuring intimate electronic contact between the PB crystals and the carbon. Compared with bare sample, this FeFe-PB@C composite showed a greatly enhanced reversible capacity of 120 mAh g⁻¹ and an outstanding rate capability with capacity of 77.5 mAh g⁻¹ at 90 C (1 C = 100 mA g⁻¹), also an impressive cycling stability with 90% capacity retention after 2000 cycles at 20 C was obtained.^[29]

Among various redox couples of transition metal ions, $\text{Mn}^{2+}/^{3+}$ couple seems to proper to be used for substitution of $\text{Fe}^{2+}/^{3+}$ couples in the PBA lattice through introducing the higher reversible redox, $\text{Mn}^{2+}/^{3+}$, to bring out another abundant class of sodium manganese(II) hexacyanoferrates(II) ($\text{Na}_{2-\delta}\text{MnHFC}$) compositions. The Mn and Fe are coordinated by different atoms of the -CN group, Mn by N and Fe by C, the Fe ions are in a low spin state while the Mn ions are in a high spin state.^[30] A hydrated $\text{Na}_{1.32}\text{Mn}[\text{Fe}(\text{CN})_6]_{0.83} \cdot 3.5\text{H}_2\text{O}$ thin film was synthesized by an electrochemical method, which showed a discernible rate curve up to 40 C (1 C = 109 mA g⁻¹) with a high power density of ≈11 300 W kg⁻¹.^[31]

At present, many high quality PBA crystals are synthesized by hydrothermal or controlled slow chemical precipitation methods in aqueous solutions, resulting in a certain amount of coordinated water in lattices or interstitial water, which will lead to several adverse effects during long-term cycles. For example, the occupancy of interstitial sites by H_2O molecules inhibits Na^+ insertion and the decomposition of water deteriorates the Coulombic efficiency and cycling performance. Goodenough et al. attempted to unravel this problem by drying

the as-obtained sample in air/vacuum for 30 h at 100 °C, and they found removal of interstitial H_2O from the structure of $\text{Na}_2\text{MnFe}(\text{CN})_6 \cdot z\text{H}_2\text{O}$ would generate a new dehydrated phase exhibiting superior electrochemical performance. At a charge/discharge rate of 20 C (1 C = 150 mA g⁻¹), the capacity of the half-cell is 120 mAh g⁻¹ (Figure 5c), rendering a high calculated specific power density of 8700 W kg⁻¹. The structural evolution between monoclinic $\text{M}-\text{Na}_{2-\delta}\text{MnHFC}$ and rhombohedral $\text{R}-\text{Na}_{2-\delta}\text{MnHCF}$ samples was found as well.^[32] In another work, they also elucidated structure change by reporting a sodium rich phase $\text{Na}_{1.72}\text{Mn}[\text{Fe}(\text{CN})_6]_{0.99}$, and revealed that a cooperative Na displacement along a single^[11] direction induces a transition from cubic to rhombohedral symmetry, this phase transition is reversible on cycling. Their electrode delivered a reversible capacity of ≈135 mAh g⁻¹ at a high rate capability of 40 C (1 C = 120 mA g⁻¹) with average discharge potential at 2.25 V, namely, a calculated specific power density of 10 800 W kg⁻¹.^[30]

Other compounds in the form of $\text{Na}_x\text{MFe}(\text{CN})_6$ (M = Co, Ni, Ti, Cu, etc.), such as $\text{Na}_2\text{Co}_3[\text{Fe}(\text{CN})_6]_2$ ^[33] and $\text{Na}_2\text{Cu}_3[\text{Fe}(\text{CN})_6]_2$ ^[34] have similar lattice structure, and they similarly possess two redox sites (M, Fe) to the FeFe-PB lattice, thus potentially serving as SIB cathodes with 2 Na^+ storage capacity, long lifespan and high voltage. Figure 5d shows the replacement of iron by nickel and cobalt in PB structure and the consequent impact changes in their electrochemical performances. Enhanced cycle stability and increased working potential were obtained via nickel and cobalt substitution, respectively.^[35] It is noteworthy that PBAs could be extended into aqueous battery and high power could be attained as well.

Even though PBAs have presented appealing power capability discussed above, major challenges remain at present. Typically, the easily formed vacancies may decrease the electronic conductivity, leading to framework collapse and a disordered lattice during cycling.^[28] Furthermore, the safety hazard of PBA materials at elevated temperature is also an important issue that needs to be considered when they are commercialized used.^[1]

2.3. Polyanion Type

In comparison with 2D oxide cathodes, 3D polyanionic positive electrode materials built up with a series of strongly covalently bonded polyanion units $(\text{XO}_4)^{n-}$ (X = S, P, Si, etc.) could offer many significant advantages, such as minimal structural rearrangements during Na^+ uptake/removal, superior thermal-abuse tolerance, and high output voltages. However, given the presence of heavy polyanion groups, polyanion-based insertion compounds have a relatively low gravimetric capacity and low volumetric energy densities due to their low powder densities as well as the use of small particles and carbon additives.^[36] Therefore, it is worthwhile to explore high-power polyanion materials to extend their utilization.

2.3.1. NASICON Type

Sodium super ionic conductor (NASICON) materials, with the general formula of $\text{Na}_x\text{MM}'(\text{XO}_4)_3$ (M = V, Ti, Fe, Tr or Nb, etc.;

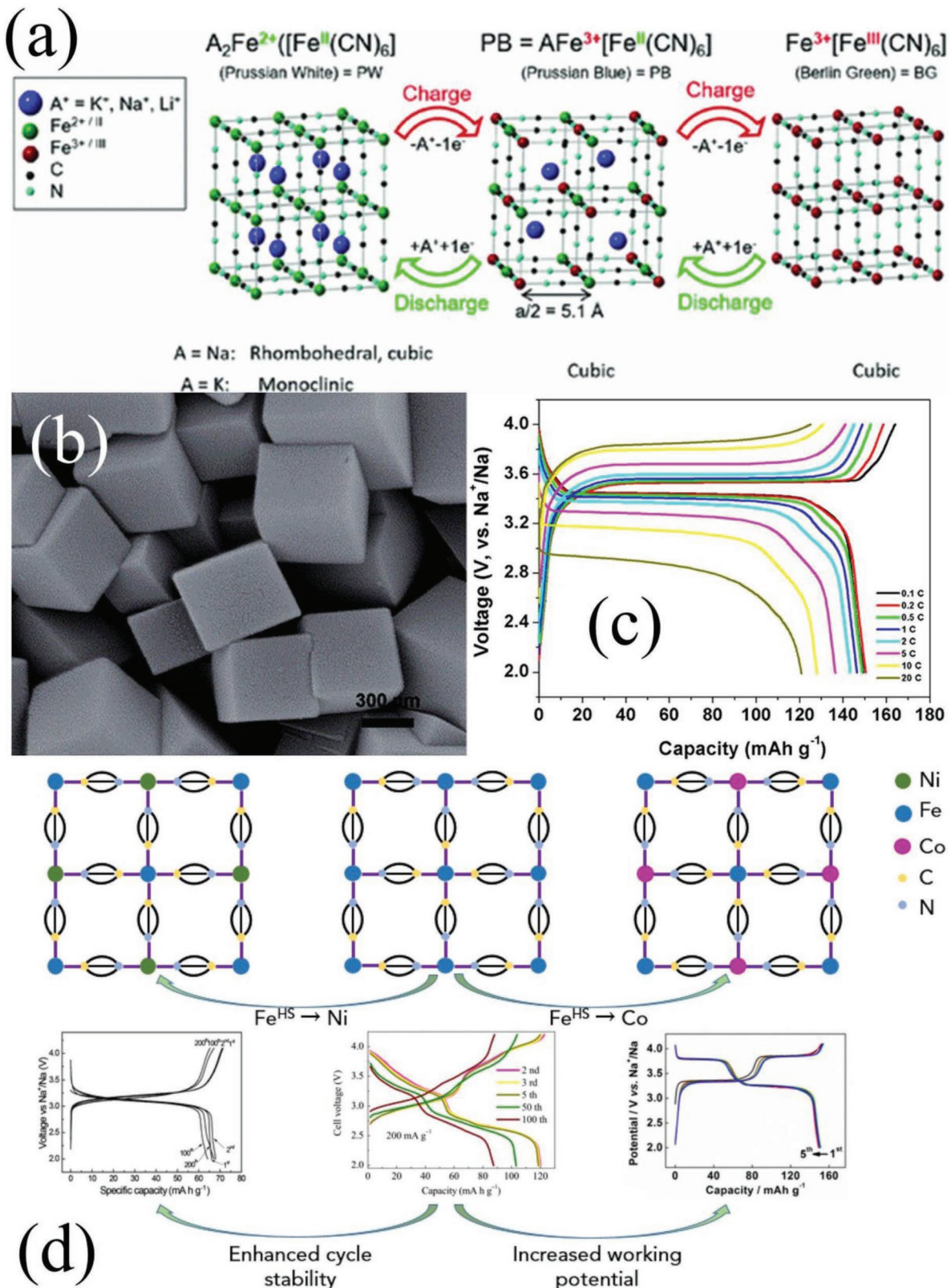


Figure 5. a) Prussian Blue structure and its corresponding oxidized (Berlin Green) and reduced (Prussian White) species. Reproduced with permission.^[25] Copyright 2018, Springer. b) SEM image of NaFeFe-PB nanocubes. Reproduced with permission.^[28] Copyright 2014, Royal Chemical Society. c) Rate capability of a Na/R-Na_{2-δ}MnHCF cell. Reproduced with permission.^[32] Copyright 2015, American Chemical Society. d) Electrochemical performance modifications of PBAs through elemental variation in high-spin sites. Reproduced with permission.^[35] Copyright 2018, Cell Press.

$X = P$, or S , $x = 0\text{--}4$), are appealing cathodes for SIBs due to their high ionic conductivity, chemical flexibility, structural and thermal stability. The framework structure of NASICON is constructed by corner-shared MO_6 (M' O_6) and polyhedral XO_4 groups, providing pronounced Na^+ diffusion channels. Take $Na_3V_2(PO_4)_3$, the representative of NASICON family as an example for elucidation of the framework. Figure 6a demonstrate the framework structure of rhombohedral $Na_3V_2(PO_4)_3$ and Na^+ migration path. The isolated VO_6 octahedral and PO_4 tetrahedral units interlinked via corners to establish the framework anion $[V_2(PO_4)_3]^{3-}$ basic units along the c-axis direction, $[V_2(PO_4)_3]^{3-}$ unit is interlinked to each other by the PO_4 tetrahedron along the a-axis, forming the open 3D framework.

There are two independent sodium ions located in the voids/channels of the framework with two different oxygen environments, with the $Na1$ ions occupy M1 sites (octahedral sites, i.e., O-sites) and $Na2$ ions occupy M2 sites (tetrahedral sites, i.e., T-sites). There are two diffusion paths: move between two adjacent T sites and O-sites to nearest T-sites, and the specific path by which Na migrates between two adjacent T sites is in a curved way. The open framework structure with well-defined 3D ion channels is beneficial for sodium ion migration, resulting in extremely high ionic mobility,^[37–40] and the good thermal stability at charged state could aid safe battery operation.^[41] Unfortunately, NASICON structure materials often suffer from low intrinsic electrical conductivity, which limits their practical electrochemical performance, especially the rate capability.

To address this problem, many strategies have been developed; including i) decreasing the particle size, ii) conductive carbon/heteroatoms doped carbon coating, iii) replacing PO_4 polyanion with other units, and iv) substitution of Na or V with other metal elements.

The strategies (i) and (ii) often used together to bring out synergistic effect. Yang et al. reported a hierarchical carbon framework wrapped $Na_3V_2(PO_4)_3$ (HCF-NVP). The hierarchical carbon framework consists of graphene-like coating layers and interconnected nanofibers, which provide ultra-fast transport of electrons and accommodate for volume changes during reaction. Benefiting from the merits of this structure, a superior high rate capability of 38 mAh g^{-1} at 500 C (58.5 A g^{-1}) could be reached (Figure 6b).^[42] Cao et al. achieved high mass loading of carbon coated $Na_3V_2(PO_4)_3$ uniformly anchored on the surface of carbon fibers (NVP@C-CC). The NVP@C-CC cathode was able to release a high energy density of 396 Wh kg^{-1} and power density as high as 97 kW kg^{-1} .^[43] Notably, a full NASICON battery based on NVP cathode and $NaTi_2(PO_4)_3$ anode was assembled, which could deliver an initial discharge capacity of 104.7 mAh g^{-1} and achieve an ultrahigh rate performance, namely, 80.5 , 73 , and 61 mAh g^{-1} at 20 , 30 , and 50 C , respectively. Specifically, a power density (based on the mass of NVP@C) as high as 8.4 kW kg^{-1} with an energy density of 94 Wh kg^{-1} was reached at a tremendously high rate of 50 C .

Functional carbon (heteroatoms doped) coating also play an import role in improving the electrochemical performance of $Na_3V_2(PO_4)_3$. Recently, a high sodium storage performance of $Na_3V_2(PO_4)_3$ was realized by optimizing nanostructure and rational surface engineering: N, B codoping (denoted as NVP@C-BN). As shown in Figure 6c, the conductive 3D

interconnected porous structure greatly mitigated mechanical stress from Na^+ extraction/insertion. In addition, extrinsic defects and active sites introduced by the co-doping heteroatoms (N, B) both enhanced Na^+ and e^- diffusion. As a result, a reversible capacity of 70% theoretical capacity at 100 C after 2000 cycles and a specific power of 84 mAh g^{-1} at 100 C was obtained ($1 \text{ C} = 110 \text{ mA g}^{-1}$).^[44]

Besides conductive carbon coating, replacing PO_4 polyanion and transition metal substitution of vanadium are also two polished methods to pursue high power NVP and its derivatives. Replacing PO_4 polyanion units with PO_4F , P_2O_7 , or $(P_2O_7)_m(PO_4)$ units would significantly lower the energy of the V^{3+}/V^{4+} redox couple, that is, increase the operating voltage, which is a key approach to address the energy and power density issues for SIBs.^[36]

There are a great number of vanadium-based fluorophosphates materials and could be roughly sorted into two classes: only introducing F and F, O co-substitution. Palacín et al. reported a full Na-ion cell assembled by $Na_3V_2(PO_4)_2F_3$ (NVPF) and hard carbon, which displayed an operation voltage of 3.65 V .^[45] A family of $Na_{3+x}V_2(PO_4)_2F_3$ with high power was obtained as well.^[46] Recently, a high-voltage cathode, $Na_3V_2(PO_4)_2O_2F$ nanotrapirisms (NVPF-NTP) was proposed by Guo and co-workers. The framework of NVPF-NTP is composed of VO_5F octahedrons and PO_4 tetrahedrons. In detail, VO_5F octahedrons are connected with PO_4 tetrahedrons by sharing O atoms in the ab-plane, and pairs of VO_5F octahedrons share corner F atoms along the c-direction, finally forming pseudolayers along the ab-plane (Figure 6d inset). The locations between pseudolayers provide sites for Na storage and transport. Hence, the electrode exhibited considerable performance both in energy and power aspects, specifically, an energy density of 486 Wh kg^{-1} as well as a power density of $\approx 11\,000 \text{ W kg}^{-1}$ at 40 C ($1 \text{ C} = 130 \text{ mA g}^{-1}$) are delivered. Notably, when coupled with a Sb-based anode, the full cell also showed excellent rate performance, a capacity of 65 mAh g^{-1} at 20 C was obtained, providing a preview of practical application.^[47] Wu et al. also prepared an advanced sodium-ion full battery with $Na_3V_2(PO_4)_2O_2F$ and Se/graphene anode, which could operate at low-temperature.^[48,49]

Besides PO_4 polyanion unit's replacement, metal ion doping, either to sodium or to vanadium, is also demonstrated as an efficient strategy to enhance the efficiency and overall performance of NASICON-based batteries.^[50,51] For example, the doping of K^+ to the Na^+ site in NVP can enhance the rate performance of $Na_3V_2(PO_4)_3$ due to the larger atomic size of K^+ than that of Na^+ , which can significantly enlarge the lattice volume along the c-axis and thus increase the Na^+ diffusion pathway. As a result, $K_{0.09}Na_3V_2(PO_4)_3/C$ presented a high reversible capacity of 82 mAh g^{-1} at 5 C .^[52] The metal doping to vanadium can affect the electrochemical performance of $Na_3V_2(PO_4)_3$ as well. Goodenough et al. investigated a class of $Na_xMV(PO_4)_3$ ($M = Mn, Fe, Ni$) obtained through transition metal substitution, and found the NASICON structure could be well maintained after repeated Na^+ extraction and insertion.^[50] Yang et al. found that Mg^{2+} doping did not change the structure of NVP, but could effectively improve ionic/electronic conductivity and obtain optimized particle size, thus enhancing the rate capability: the specific capacity only

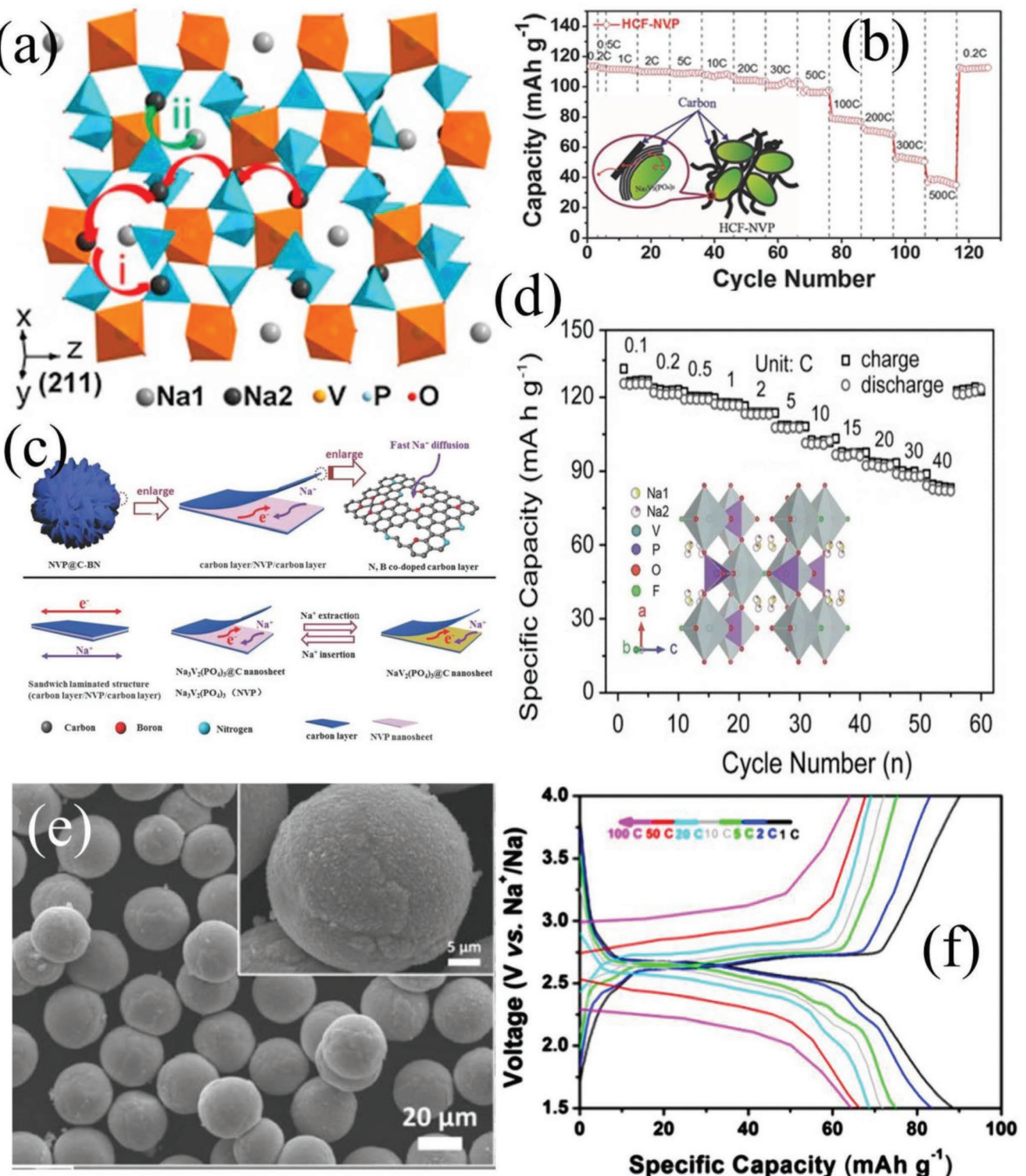


Figure 6. a) Schematic representation of the NASICON- $\text{Na}_3\text{V}_2(\text{PO}_4)_3$ structure and Na^+ migration path. Reproduced with permission.^[37] Copyright 2015, Elsevier. b) Rate capability and schematic illustration (inset) of HCF-NVP electrode. Reproduced with permission.^[42] Copyright 2015, WILEY-VCH Verlag GmbH & Co. KGaA, Weinheim. c) The Schematic illustration of the structure of NVP@C-BN. Reproduced with permission.^[44] Copyright 2018, WILEY-VCH Verlag GmbH & Co. KGaA, Weinheim. d) Rate capabilities from 0.1 C to 40 C and the schematic of the crystal structure (inset) of NVPF-NTP. Reproduced with permission.^[47] Copyright 2015, WILEY-VCH Verlag GmbH & Co. KGaA, Weinheim. e) SEM image of FMO-H and f) charge-discharge curves at different rates. Reproduced with permission.^[55] Copyright 2016, Elsevier.

decreased from 112.5 to 94.2 mAh g⁻¹ when the current density increased from 1 C to 30 C.^[53]

Double substitution for metal ion and PO₄ polyanion was also developed. More recently, Masquelier and co-workers demonstrated that partial substitution of vanadium with aluminum in Na₇V₄(P₂O₇)₄(PO₄) was able to increase the gravimetric capacity due to the lighter weight of Al than V. It's also worthy of mentioning the two derivatives, Na₇V₃Al(P₂O₇)₄(PO₄) and Na₇V₂Al₂(P₂O₇)₄(PO₄), exhibited higher operation voltage due to the activation of the V⁴⁺/V⁵⁺ redox couple, which is of great importance to improve power output. More specifically, the charge/discharge curves of Na₇V₃Al(P₂O₇)₄(PO₄) exhibited two distinct redox processes at 3.87 V (2 Na⁺ extracted) and 3.96 V (1 Na⁺ extracted), higher than those (3.87 and 3.89 V) in Al free sample.^[54] All effective methods brought out to enhance the performance of Na₃V₂(PO₄)₃ is summarized in Figure 7.

Besides the most extensively studied vanadium-centered cathode materials, there are many other materials following the general NASICON formula Na_xMM'(XO₄)₃, such as Na₂TiFe(PO₄)₃, Na₃Fe₂(PO₄)₃, NaNbFe(PO₄)₃, etc., disappointingly, most of them show poor sodium storage capability. Nevertheless, the dawn still comes. Fe₂(MoO₄)₃, which is in monoclinic (*P21/c*) crystal structure comprising of FeO₆

octahedral and tetrahedral interconnected through corner sharing oxygen atoms, is another pragmatic member possessing electrochemical activity in NASICON type family, Fe₂(MoO₄)₃ could exhibit high rate and high power capability through rational design. Mai and colleagues reported graphene wrapped Fe₂(MoO₄)₃ nanoparticle composite (noted as FMO-MG) (Figure 6e), in which graphene coating can enhance the electronic conductivity and shorten the Na⁺ diffusion path. As a result, the composite showed a capacity of 64.1 mAh g⁻¹ at a high current rate of 100 C (1 C = 90.62 mA g⁻¹) (Figure 6f), with a specific power density of 19.9 kW kg⁻¹.^[55] Most recently, Goodenough et al. reported NASICON-structured Na₃MnZr(PO₄)₃ with high-voltage reversibly accessed by Mn⁴⁺/Mn³⁺ and Mn³⁺/Mn²⁺ redox couples. By reducing the concentration of Mn in polyanion framework structure, the cooperative Jahn-Teller distortion does not occur with all Mn³⁺ and the surface disproportionation of the Mn³⁺ to Mn²⁺ and Mn⁴⁺ is also suppressed. When tested in a half-cell, the discharge capacity was 82 and 52 mAh g⁻¹ at 1 C and 10 C, respectively.^[56]

In short, compared to other sodium-based cathodes, NASICON-type compounds are more suitable for power-oriented batteries rather than energy-oriented batteries in terms of their fast electrochemical kinetics and relatively low specific capacity.^[57]

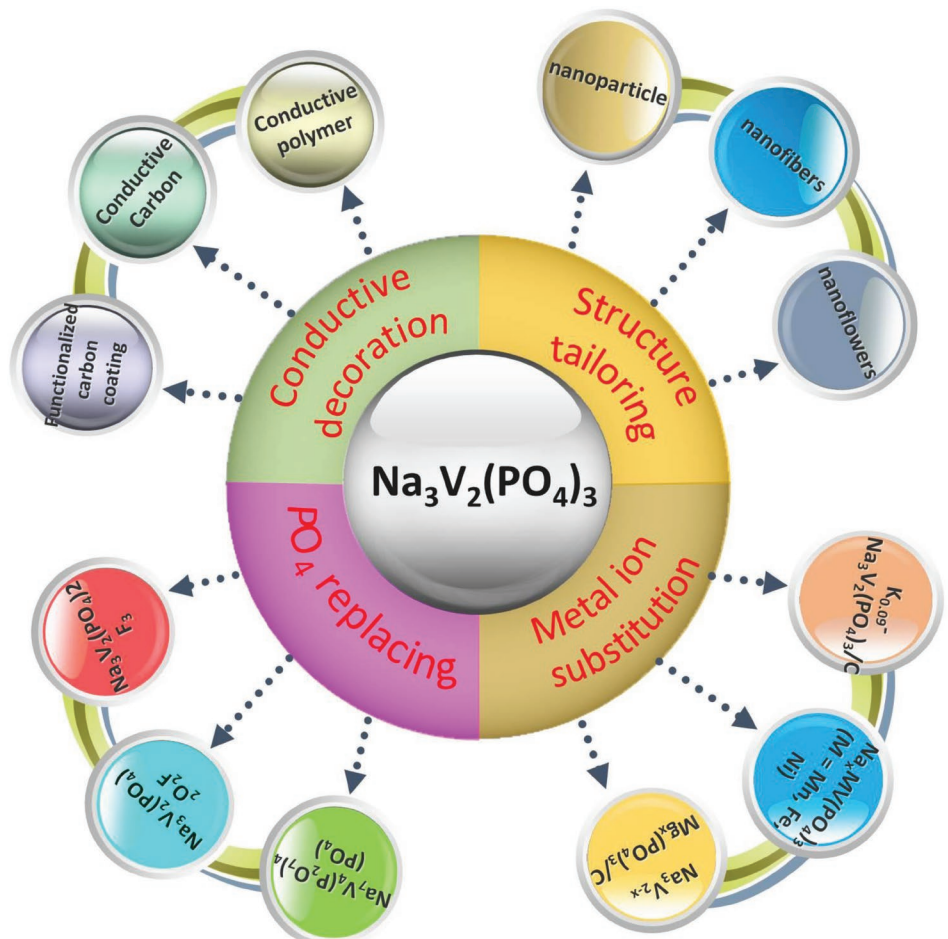


Figure 7. Effective strategies brought out to enhance the performance of Na₃V₂(PO₄)₃.

2.3.2. Others

As discussed above, NASICON-type compounds show attractive potential for high power applications. However, the toxic nature and limited crust abundance of vanadium remain obstacles for scaled-up production. In contrast, iron, the fourth most common element on earth, also shows considerable sodium storage capability when acts as redox center in polyanion materials, such as phosphates, sulfates, oxalates and molybdates. Most of these materials exhibited suitable insertion potentials and superior structural stability, thus drawing tremendous research interests.^[1]

Recent studies have introduced many important types of potential iron based polyanions, especially phosphate electrode materials as cathodes for SIBs. Generally, these phosphate electrode materials could be sorted into two categories: (pyro) phosphates and mixed-anion materials, such as fluor/phosphates and phosphates/pyrophosphates.

The last two decades have witnessed the triumph of LiFePO₄ in the electric vehicle (EV) and hybrid electric vehicle (HEV) markets. As an analog to LiFePO₄, olivine NaFePO₄ (Figure 8a) has also exhibited sodium storage ability.^[58] However, only some unconventional synthetic methods can produce pure olivine-phased NaFePO₄. Amorphous NaFePO₄ delivers a high discharge capacity (152.1 mAh g⁻¹) with long-term cycling stability, however the average working potential is very low (2.32 V) and the rate performance is unsatisfied. Amorphous FePO₄ can be obtained by various facile synthetic routes and exhibit favorable electrochemical performance, but the Na-vacant characteristic and low work potential (2.34 V) restrain its practical use. Loh et al. reported highly pure NaFePO₄ prepared by aqueous ion-exchange method, the cathode exhibited a high reversible capacity of 142 mAh g⁻¹ (0.1 C, 1 C = 154 mA g⁻¹) as well as an impressive cycle stability (6000 cycles at 10 C). Notably, a maximum specific power density of \approx 7546 W kg⁻¹ accompany with energy density of \approx 93 Wh kg⁻¹ could be reached.^[59] As to sodium storage process, the Na insertion and extraction processes show different mechanisms due to the large volumetric mismatch between FePO₄ and NaFePO₄ (17.58% difference in unit volume),^[60] the intermediate phase of Na_{2/3}FePO₄ was confirmed by many groups.^[60,61] However, up until today, olivine NaFePO₄ is not the thermodynamically stable phase and cannot be obtained using traditional solid-state synthesis, which inhibits its large-scale utilization.

As an analogy to phosphate materials, iron-based pyrophosphates, comprising frameworks of octahedral FeO₆ and P₂O₇ units, have drawn some researchers' attentions.^[62] As the typical representative of this family, Na₂FeP₂O₇ has a triclinic *P1*-structure that is built from FeO₆ octahedral and P₂O₇ tetrahedral building blocks, creating large tunnels along the [011] direction to accommodate the Na atoms (Figure 8b).^[63,64] In the light of the large tunnels to accommodate Na⁺ ions, this cathode could achieve high power through rational structure design. Kim and co-workers synthesized Na₂FeP₂O₇ nanoparticles (NFP-NPs) embedded in carbon via a citric acid-assisted sol-gel method, the NFP-NPs exhibited a reversible capacity close to the theoretical value (95 mAh g⁻¹) in the voltage window of 2.0–4.0 V (versus Na/Na⁺) with long lifespan (Figure 8c). Meanwhile, they displayed a superior rate capability of 70, 66 and 65 mAh g⁻¹

even at high rates of 20, 30 and 60 C (1 C = 97 mA g⁻¹), respectively, delivering an energy density of \approx 163.2 Wh kg⁻¹, as well as a power density of \approx 14 608 W kg⁻¹.^[65] Besides Na₂FeP₂O₇, other iron-based pyrophosphates with different element ratios have also been reported. Recently, a class of Na₄₋ α Fe_{2+ α /2(P₂O₇)₂ and its Mn analogs were reported. It is elucidated that the triclinic structure of Na_{3.12}Fe_{2.44}(P₂O₇)₂ (NFPO) is composed of a centrosymmetrical crown of Fe₂P₄O₂₂ and Fe₂P₄O₂₀ moieties connected by corner-sharing to form a 3D framework. Each crown unit consists of two FeO₆ octahedral and two P₂O₇ groups, which is different from monoclinic NaFeP₂O₇ and triclinic Na₂FeP₂O₇ (Figure 8d).^[66,67] The sodium-ion diffusion in Na-rich Na_{3.32}Fe_{2.34}(P₂O₇)₂ via two 1D pathways was revealed by Chou's group through a first-principles calculation, and the sample showed a single-phase-transition process during sodiation and desodiation, accompanied by trivial change in the lattice parameters and impressive rate performance (Figure 8e). Notably, a calculated power density of near 3000 W kg⁻¹ as well as a high energy density of over 300 Wh kg⁻¹ could be reached.^[68]}

NaFePO₄ exhibits a very low operating voltage of 2.6 V,^[60,61] that reduces its competitiveness in comparison with other polyanion cathodes. Despite this, the working potential could be enhanced due to the strong inductive effect of the anions if replacing PO₄³⁻ by PO₄F⁻ group.^[36,69] Na₂FePO₄F consists of pairs of face-sharing Fe octahedral, each coordinated to four oxygen and two fluorine ions, forming Fe₂O₆F₃ bi-octahedral units (Figure 9a, left). These units are connected by corner sharing (via F site) to other pairs of Fe face sharing octahedral along the *a*-axis (Figure 9a, middle). These connected chains of Fe octahedral are bonded through corner-sharing PO₄³⁻ tetrahedral along the *c*-axis (Figure 9a, right). There are two crystallographically unique sites, Na1 and Na2 available for sodium ions (Figure 9a, right),^[70] which result in a more favorable Na migration along different possible channels in this 2D layered Na₂FePO₄F. Na₂FePO₄F was earlier reported by Komba and co-workers, the cathode could deliver an initial discharge capacity of 110 mAh g⁻¹ at a rate of 0.05 C (6.2 mA g⁻¹) with two well-defined voltage plateaus at 3.06 and 2.91 V (vs Na/Na⁺), but the capacity dropped below 20 mAh g⁻¹ when current rate increased to 8 C.^[69] Later, Kawabe et al. attempted to further enhance the discharge voltage by introducing Mn to replace Fe in the crystal structure. They successfully obtained Na₂Fe_{0.5}Mn_{0.5}PO₄F and found it demonstrated a higher average operating voltage than that of Na₂FePO₄F due to the Mn²⁺/Mn³⁺ redox couple centered at 3.53 V, however, the high potential made the reversible capacity decrease at a sacrifice. To address the issue of poor rate, nanostructure construction was proved efficient. Balaya et al. reported a nanostructured Na₂FePO₄F through a soft template method, followed by high-energy ball milling (HEBM) process and postheat treatment. The post-treated sample has an enhanced performance that was attributed to the reduced antisite disorder and improved sodium ion diffusion.^[70] Dunn et al. first used the polyol synthesis route to prepare Na₂FePO₄F nanoparticles with a size of 15–25 nm. After a further electrical conductive decoration, the sample could deliver a reversible capacity of 60 mAh g⁻¹ at 10 C (1 C = 124 mA g⁻¹), that is, a specific power density of \approx 6076 W kg⁻¹ with energy density of \approx 110.3 Wh kg⁻¹.^[71]

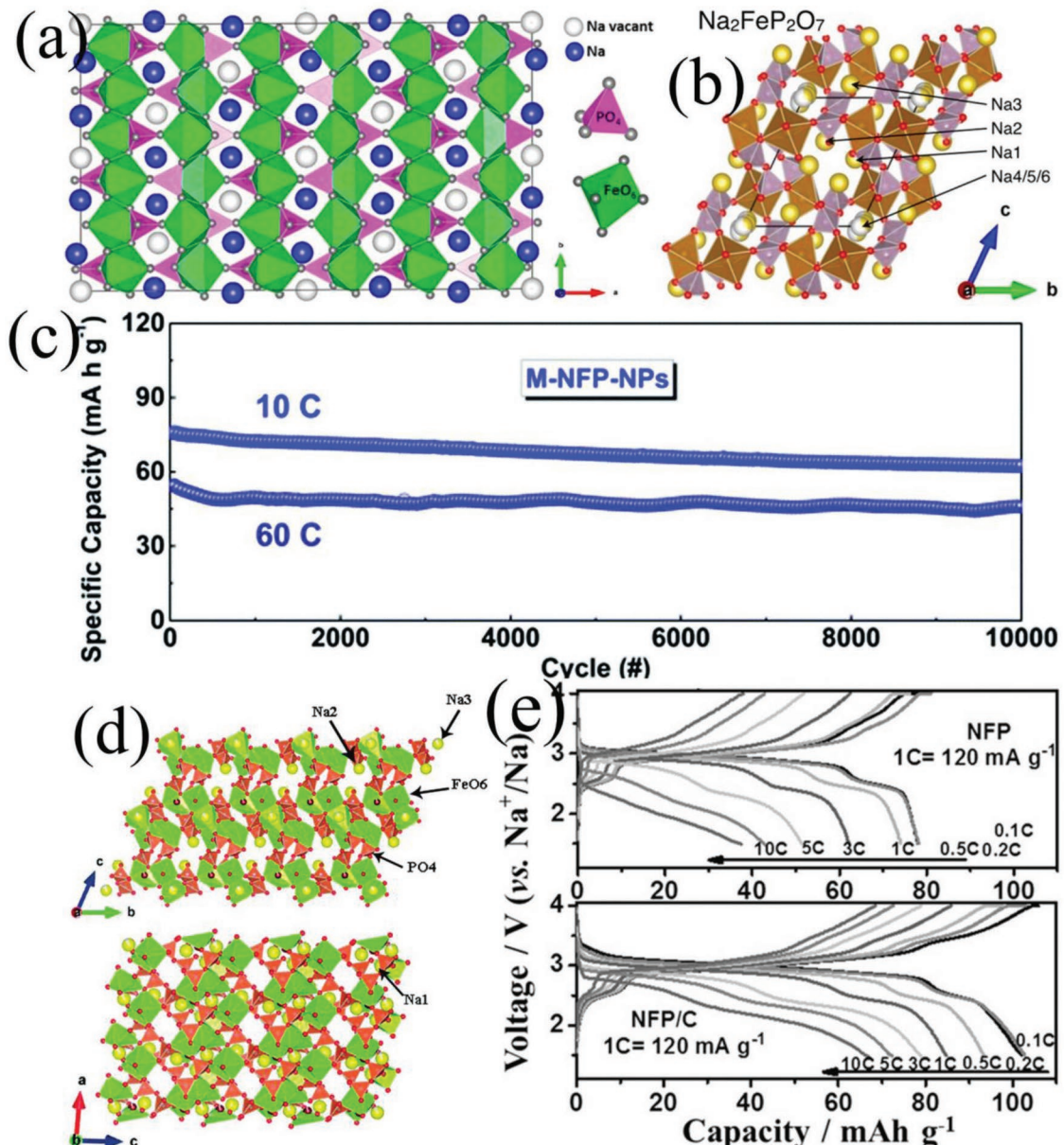


Figure 8. a) Scheme of the refined crystal structure of NaFePO_4 in polyhedral representation Reproduced with permission.^[58] Copyright 2014, American Chemical Society. b) Final refined crystal structure of $\text{Na}_2\text{FeP}_2\text{O}_7$ Reproduced with permission.^[64] Copyright 2013, American Chemical Society. c) Long-term cyclability of M-NFP-NPs at 10 and 60 C. Reproduced with permission.^[65] Copyright 2017, Royal Society of Chemistry. d) Crystal structure model of triclinic $\text{Na}_{3.12}\text{Fe}_{2.44}(\text{P}_2\text{O}_7)_2$ Reproduced with permission.^[67] Copyright 2015, The Royal Society of Chemistry. e) Voltage profiles at different C-rates of bare and carbon coated $\text{Na}_{3.32}\text{Fe}_{2.34}(\text{P}_2\text{O}_7)_2$. Reproduced with permission.^[68] Copyright 2017, WILEY-VCH Verlag GmbH & Co. KGaA, Weinheim.

Similar to the strategy of designing $\text{Na}_2\text{FePO}_4\text{F}$ mentioned above, double polyanion material of mixed phosphates-pyrophosphates was also proposed. The mix-anions compounds integrate the advantages of both phosphates and pyrophosphates, and have become an appealing member in iron-based polyanion family.^[36] $\text{Na}_4\text{Fe}_3(\text{PO}_4)_2(\text{P}_2\text{O}_7)$ (NFPP) has a Pn21a space group and its crystal framework can be described in terms of $[\text{Fe}_3\text{P}_2\text{O}_{13}]_\infty$ infinite layers and $[\text{P}_2\text{O}_7]$ groups (Figure 9b). This arrangement leads to the formation of large tunnels along the b direction, which can provide appropriate pathways with a lower activation barrier for Na^+ diffusion. Kang et al.

revealed that the Na storage mechanism of NFPP electrode involves a one-phase reaction accompanying an exceptionally small volumetric change of less than 4%,^[25,72] thus affording a long cycle life.^[73,74] Recently, Our group reported a 3D graphene decorated $\text{Na}_4\text{Fe}_3(\text{PO}_4)_2(\text{P}_2\text{O}_7)$ microspheres prepared via a spray dry method.^[75] Graphene coating on the surface of particles and the flexible 3D graphene network can not only improve the electronic conductivity, but also accommodate the structural stress of the material during charging and discharging. Accordingly, the NFPP@rGO composite exhibited outstanding rate capability (35 mAh g^{-1} at 200 C) with a

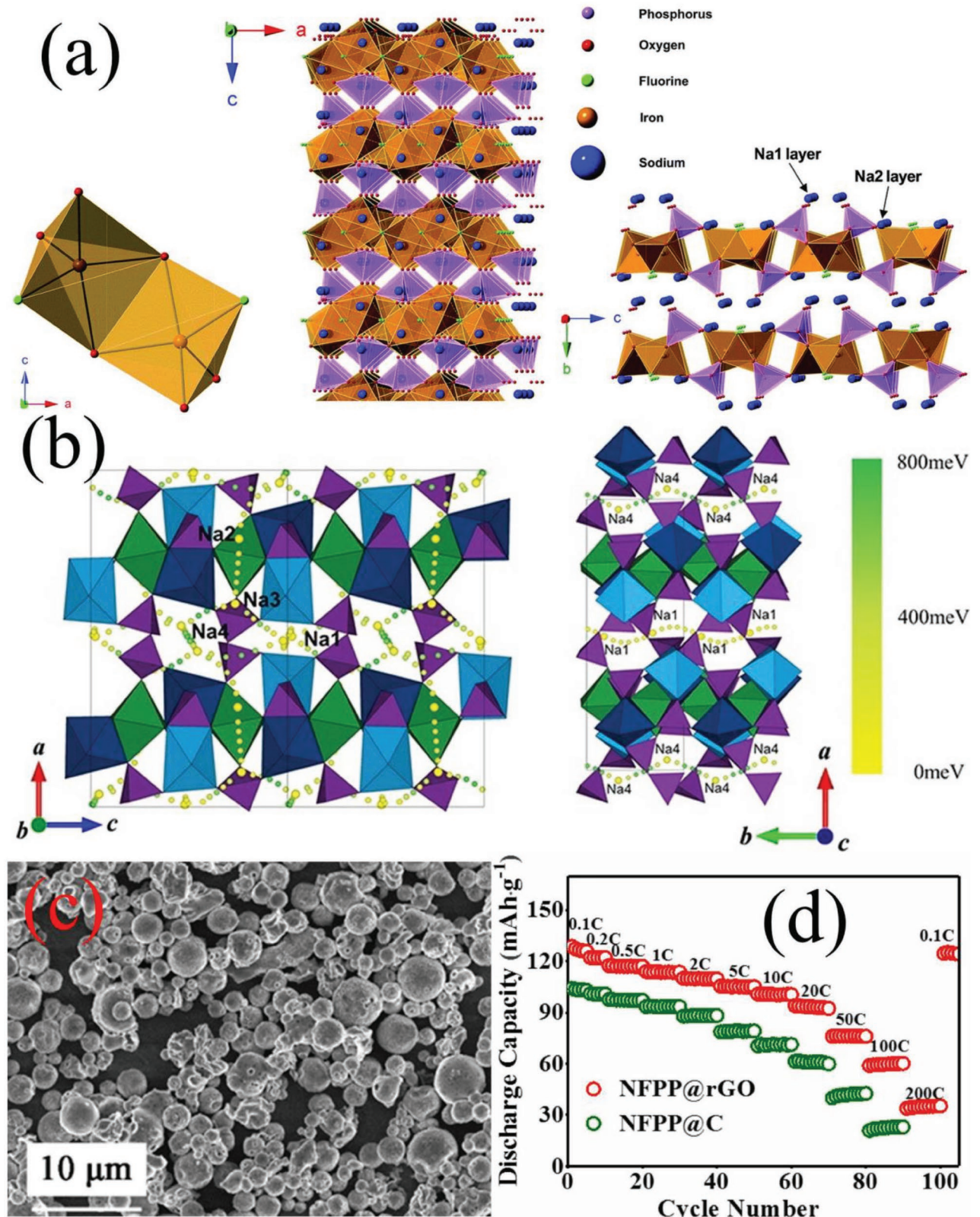


Figure 9. a) Crystal structure of $\text{Na}_2\text{FePO}_4\text{F}$: (left) $\text{Fe}_2\text{O}_6\text{F}_3$ bioctahedral units; (middle) view along $[100]$ showing Fe face-sharing octahedral; and (right) along $[010]$ corner-sharing PO_4^{3-} tetrahedra and the Na layers. Reproduced with permission.^[70] Copyright 2015, Royal Society of Chemistry. b) The 3D sodium diffusion paths in the $\text{Na}_4\text{Fe}_3(\text{PO}_4)_2(\text{P}_2\text{O}_7)$ structure. Reproduced with permission.^[74] Copyright 2012, American Chemical Society. c) SEM image and d) rate capability of NFPP@rGO. Reproduced with permission.^[75] Copyright 2018, Elsevier.

high power density of 52.3 kW kg^{-1} at an energy density of 70.9 Wh kg^{-1} (Figure 9c,d).

Besides iron-based phosphates and their derivatives, sulfate iron-centered polyanions have emerged as promising prototypes for high power SIBs. $\text{Na}_2\text{Fe}_2(\text{SO}_4)_3$ (NFS) has captured great attention since its report by Yamada group's in 2014 that shows high discharge voltage and high rate performance.^[76] In the structure of $\text{Na}_2\text{Fe}_2(\text{SO}_4)_3$, the Fe ions occupy octahedral sites that share edges with a crystallographically equivalent octahedron, forming Fe_2O_{10} dimer units. These isolated edge-sharing Fe_2O_{10} dimers are in turn bridged together by SO_4 units strictly by corner-sharing mode, hence forming a 3D framework with large tunnels along c axis and fast ion conductivity (Figure 10a).^[77] Conductive decoration on NFS is efficient to improve its performance, Liu and co-workers prepared graphene scaffold $\text{Na}_{2+2x}\text{Fe}_{2-x}(\text{SO}_4)_3$ microsphere (NFS@rGO), a superior rate performance (78 mAh g^{-1} at 60°C and 72 mAh g^{-1} at 80°C) were achieved due to the structural stability of NFS@rGO and boosted the electronic conductivity.^[78] Another strategy brought out enhance the electrochemical capability is structure tailoring. Deng et al. introduced a top-down synthesis of muscle-inspired alluaudite $\text{Na}_{2+2x}\text{Fe}_{2-x}(\text{SO}_4)_3$ spindle, the alluaudite sulfate nanoparticles closely anchor on the single-wall carbon nanotubes

(SWNT), the electrode exhibited a calculated specific power of 13.6 kW kg^{-1} (Figure 10b,c).^[79]

Though these frequent iron-centered materials show favorable rate capability and long-term cycle life in some reports, more researches are still needed to thoroughly understand the sodium storage mechanism and further improve their electrochemical performance to meet the requirements of high power systems.

In parallel to the most extensively studied V and Fe based polyanionic compounds, other transition metal based polyanion materials also show decent power features. Barpanda et al. reported a Co-based sulfate $\text{Na}_{2.32}\text{Co}_{1.84}(\text{SO}_4)_3$, and through first principles calculations, they revealed possible $\text{Co}^{3+}/\text{Co}^{2+}$ redox activity at the very high voltages of 4.76 V (partial desodiation) and 5.76 V (complete desodiation), involving both Co redox centers and the O lattice. A mixed-polyanion Co-based $\text{Na}_{4-x}\text{Co}_3(\text{PO}_4)_2\text{P}_2\text{O}_7$ was reported by Iba and colleagues. It shares the same crystal structure with $\text{Na}_{4-x}\text{Fe}_3(\text{PO}_4)_2\text{P}_2\text{O}_7$, the sample showed trivial capacity decrease when rate raised and could achieve a capacity of near 90 mAh g^{-1} at 850 mA g^{-1} . Similarly, $\text{Na}_{4-x}\text{Mn}_3(\text{PO}_4)_2\text{P}_2\text{O}_7$ was reported, and notably in contrast to most manganese-based electrodes, the sodium ion mobility in this crystal structure increased rather than decreased as the structural changes induced by Jahn–Teller distortion (Mn^{3+}),

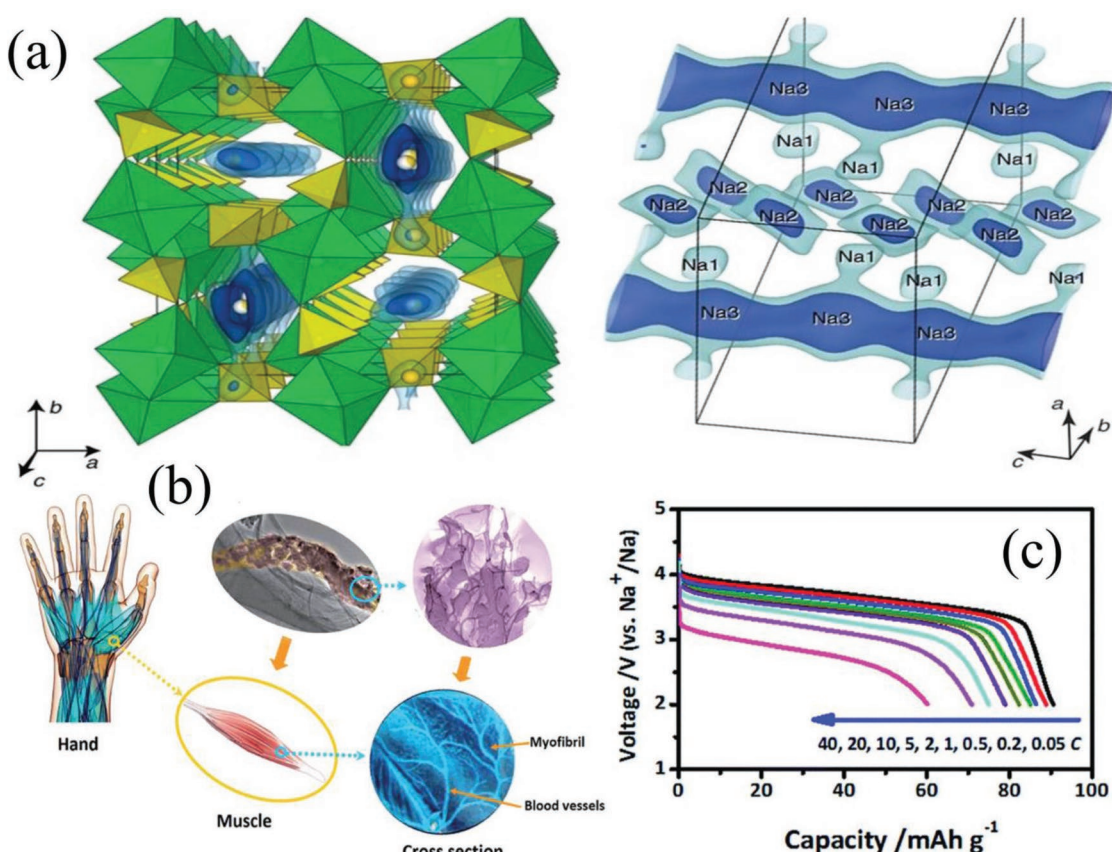


Figure 10. a) Na-ion diffusion in $\text{Na}_2\text{Fe}_2(\text{SO}_4)_3$ where green and yellow polyhedra are that of FeO_6 and SO_4 , respectively. Reproduced with permission.^[76] Copyright 2014, Nature Publishing Group. b) Design of muscle tissue-inspired $\text{Na}_{2+2x}\text{Fe}_{2-x}(\text{SO}_4)_3/\text{SWNT}$ composite and c) discharge curves of the muscle-inspired $\text{Na}_{2+2x}\text{Fe}_{2-x}(\text{SO}_4)_3/\text{SWNT}$ spindle at different rates from 0.05 to 40 C. $1 \text{ C} = 120 \text{ mA g}^{-1}$ Reproduced with permission.^[79] Copyright 2016, The Royal Society of Chemistry.

which opens up sodium diffusion channels. Consequently, a high power density of over 7000 W kg⁻¹ could be found in its Ragone plot.^[80] If breakthroughs in high voltage organic electrolytes are made in future, Co-based polyanionics may serve as potential cathode candidates for high power sodium ion batteries.^[81] In order to fully evaluate the application potential in high power SIBs, a comparison including power density and operation voltage under high current density of typical cathode materials is posted at Figure 11, and a comprehensive overview of more potential cathode materials toward high power applications are summarized in Table 1.

3. Anode

With respect to the anode counterpart, the Coulombic efficiency, working potential, cycling stability and rate capability are the most important characteristics to determine the compatibility of anodes with the above cathodes in high power sodium-ion batteries. Recent researches of high power anodes for SIBs focused on carbonaceous materials, titanium-based compounds, p-block alloying elements (metals, alloys, and phosphorous) and transition metal phosphides (or oxides, sulfides).

3.1. Insertion Materials

3.1.1. Hard Carbon

To date, many carbonaceous materials, such as hard carbon, soft carbon, carbon nanotube, nanofibers, and graphene have been reported with sodium storage activity. Among them, hard carbon is the most promising anode material for sodium-ion batteries due to its high capacity, suitable working potential and sustainability.^[82]

Hard carbon (HC), with the electrochemical capability to accommodate sodium ions was first proposed by Stevens et al. in the year 2000,^[83] it has a “house of cards” structure containing graphite-like microcrystallites and amorphous region. There are many disputes about sodiation/desodiation process since its application in Na-ion battery^[84,85]: adsorption on the surface active sites, nanopore filling analogous to adsorption, and intercalation between the graphene layers with suitable d spacing (Figure 12a–c). Understanding the sodium storage mechanism is of great importance for its further high power application. In this light, consistent efforts have been made. Liu and co-workers thoroughly investigated a series of nanostructured hard carbon materials and shed new insight, an “adsorption–intercalation” mechanism for Na ion storage. Specifically, Na ions adsorb on the defect sites of hard carbon with a wide adsorption energy distribution, producing a sloping voltage profile in the first stage, and in the second stage, Na ions intercalate into graphitic layers

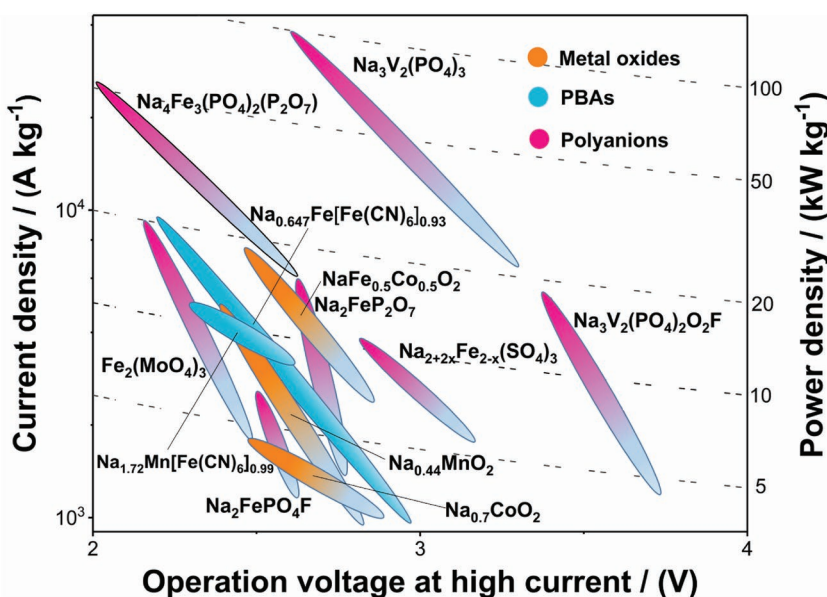


Figure 11. Power density and operation voltage of typical cathode materials under high current density.

with suitable spacing to form NaC_x compounds, similarly to that in Li ion battery.^[84] And under the guidance of this knowledge, they fabricated nonporous hard carbon material and alleviated the macronosia, low Coulombic efficiency in full cell, paving new way for optimizing Na storage capabilities and achieving high performance. To improve the power capability of hard carbon, many researches centered on nanoarchitectures manufacturing. For instance, Figure 12d,e shows Huang et al. synthesized monodispersed hard carbon spherules (HCS) from an abundant biomass of sucrose, the electrode could achieve a reversible charge capacity of 270 mAh g⁻¹ even at a very high charging rate of 20 C (3 min charge, 6000 mA g⁻¹). Moreover, the application of HCS in full cell coupled with an air-stable P2-Na_{2/3}Ni_{1/3}Mn_{2/3}O₂ positive electrode was demonstrated. Based on total masses of cathode and anode, the full cell exhibited a high average operating voltage of 3.5 V, with an estimated energy density of 200 Wh kg⁻¹, highlighting the potential of this system for practical applications.^[86] Liu and co-workers reported hard carbon nanoparticles (HCNP) prepared via the pyrolysis of a polyaniline precursor, the electrode obtained at 1150°C exhibited a prolonged cycling stability and charge capacities of 181, 72 and 45 mAh g⁻¹ at current densities of 250 (1 C), 1250 (5 C) and 2500 (10 C) mA g⁻¹, respectively. The superior rate performance is attributed to an optimum spacing of 0.366 nm between the graphitic layers and the nanoparticulate size, which result in a low-barrier Na⁺ cation insertion.^[87] Zhou et al. restrained the plateau capacity loss for sodium storage in hard carbon at high rates by replacing the ester-based electrolytes with ether-based electrolytes, which might be attributed to the reduced electrochemical polarization and the formation of thin SEI layers on the electrode surface. Owing to the improved plateau capacity, hard carbon showed an extraordinary rate capability with capacity of 217 mAh g⁻¹ at 900 mA g⁻¹.^[82]

Unfortunately, most carbonaceous materials suffer from the low initial Coulombic efficiency and poor sodium (de)-intercalation kinetics. Light-weight heteroatom (such as B, N, P, and S)

Table 1. Comprehensive overview of most potential and typical cathode materials for SIBs toward high power applications (calculated based on the mass of cathode).

| Sample | Cutoff voltage [V] | Reversible Capacity [mAh g ⁻¹], speed | Cycling performance initial capacity [mAh g ⁻¹], % capacity retention, cycle number, speed | Maximum rate capacity [mAh g ⁻¹], speed | Energy under Power [Wh Kg ⁻¹], under [W Kg ⁻¹] | Remarks | Ref. |
|--|--------------------|---|--|---|--|--------------------------------|------|
| Tunnel type Na _{0.44} MnO ₂ | 2.0–4.0 | 122.9, 0.2 C | ≈106, 82.9%, 700, 10 C | 99, 20 C | ≈267, ≈3267 | 1 C = 121 mA g ⁻¹ | [3] |
| P2-type Na _{0.7} CoO ₂ | 2.0–3.8 | 100, 0.2 C | 100, 92%, 100, 0.2 C | 70, 10 C | ≈203, ≈5075 | 1 C = 175 mA g ⁻¹ | [15] |
| O3-type Na _x [Fe _{1/2} Co _{1/2}]O ₂ | 1.5–4.0 | 110 0.2 C | 160, 75%, 50, 10 C | 100, 30 C | ≈230, ≈16 600 | 1 C = 241 mA g ⁻¹ | [20] |
| O3-type NaCrO ₂ | 2.0–3.6 | 121, 0.18 C | 121, 90%, 300, 0.18 C | 106, 50 C 99, 150 C | ≈237, 39 600 | 1 C = 110 mA g ⁻¹ | [22] |
| P2-O3 biphasic Na _{0.67} Mn _{0.55} Ni _{0.25} Li _{0.2} O ₂ | 1.5–4.2 | 158, 0.05 C | 109, 84%, 50, 1 C | 65, 5 C 38, 8 C | ≈100.7, ≈5088 | 1 C = 240 mA g ⁻¹ | [24] |
| Na _{0.647} Fe[Fe(CN) ₆] _{0.93} ·2.6H ₂ O | 2.0–4.0 | 120, 1 C | 100, 90%, 2000, 20 C | 77.5, 90 C | ≈193, ≈22 500 | 1 C = 100 mA g ⁻¹ | [29] |
| Dehydrated Na ₂ MnFe(CN) ₆ | 2.0–4.0 | 150, 0.1 C | 140, 75%, 500, 0.7 C | 120, 20 C | ≈348, ≈8700 | 1 C = 150 mA g ⁻¹ | [32] |
| Na-rich Na _{1.72} Mn[Fe(CN) ₆] _{0.99} | 2.0–4.2 | 135 | ≈125, 96%, 30, 1/20 C | 45, 40 C | ≈101, ≈10 800 | 1 C = 120 mA g ⁻¹ | [30] |
| NASICON-type Na ₃ V ₂ (PO ₄) ₃ | 2.0–3.9 | ≈118, 1 C | 101.9, 82%, 2000, 20 C 95, 78.4%, 2000, 50 C | 96.8, 100 C 69.9, 200 C | 396, 97 000 | 1 C = 117 mA g ⁻¹ | [43] |
| NASICON-type Na ₃ V ₂ (PO ₄) ₂ O ₂ F | 2.0–4.3 | 127.8, 0.1 C | ≈95, 80.9%, 2000, 20 C | 84.3, 40 C | 178.8, 11 000 | 1 C = 130 mA g ⁻¹ | [47] |
| NASICON-type Fe ₂ (MoO ₄) ₃ | 1.5–4.0 | 98.4, 2 C | 85.9, 76%, 100, 10 C | 64.1, 100 C | 88, 19 900 | 1 C = 90.62 mA g ⁻¹ | [55] |
| NaFePO ₄ | 2.0–4.0 | 142, 0.1 C | 60, 70%, 6000, 10 C | 38, 20 C | ≈93, ≈7546 | 1 C = 154 mA g ⁻¹ | [59] |
| Na ₂ FeP ₂ O ₇ | 2.0–4.0 | 95, 0.1 C | 77, 83%, 10 000, 10 C 55, 84%, 10 000, 60 C | 65, 60 C | ≈163.2, ≈14 608 | 1 C = 97 mA g ⁻¹ | [65] |
| Na _{3.32} Fe _{2.34} (P ₂ O ₇) ₂ | 1.5–4.0 | 100, 0.1 C | ≈72, 89.6%, 1100, 5 C | 68, 10 C | ≈149.6, ≈2640 | 1 C = 120 mA g ⁻¹ | [68] |
| Na ₂ FePO ₄ F | 2.0–4.0 | 110, 0.1 C | 60, 70%, 5000, 10 C | 60, 10 C 45, 20 C | 110.3, 6076 | 1 C = 124 mA g ⁻¹ | [71] |
| Na ₄ Fe ₃ (PO ₄) ₂ (P ₂ O ₇) | 2.0–4.5 | 110, 0.05 C | 98, 89%, 300, 0.5 C | 82, 10 C | 230, 3612 | 1 C = 129 mA g ⁻¹ | [72] |
| Na ₄ Mn ₃ (PO ₄) ₂ (P ₂ O ₇) | 3.0–4.5 | 121, C/20 | ≈90, 86%, 100, 0.2 C | 70, 20 C | ≈180, 7000 | 1 C = 130 mA g ⁻¹ | [80] |
| Na _{2+2x} Fe _{2-x} (SO ₄) ₃ (x = 0.45) | 2.0–4.5 | ≈92, 0.05 C | ≈78, 92%, 100, 5 C | 61, 40 C | 176.9, 10 927 | 1 C = 94.2 mA g ⁻¹ | [79] |

doping is regarded as an effective strategy to enhance the electrochemical properties of carbonaceous materials, due to the improvement in electrical conductivity to conduct the electron transport, the enlargement in specific surface area to increase the binding sites, and the improvement of Na⁺ adsorb ability in the charging process.^[88] Huang et al. reported porous hard carbon material synthesized via a simple pyrolysis of H₃PO₄-treated biomass. XPS analysis showed that the carbon material was functionalized by O-containing and P-containing groups. The CV measurements revealed the pseudocapacitive effect for the surface redox reaction of O-containing functional groups. As shown in Figure 12g, the carbon electrode delivered a specific capacity of 118.4, 94.5 and 71 mAh g⁻¹ at 1, 2 and 5 A g⁻¹, respectively.^[89]

3.1.2. Titanium-Based Compounds

Besides the carbonaceous materials, following the sodium insertion mechanism, titanium-based oxides and NaTi₂(PO₄)₃ are of great potential for application in high power sodium-ion battery.

Thus far, a number of potential candidates have been explored. Na₂Ti₃O₇ (NTO7) was first found by Senguttuvan et al. to reversibly uptake 2 Na ions per formula unit (200 mAh g⁻¹) in 2011.^[90] As an insertion electrode for sodium ion batteries at room temperature, NTO7 has a very low sodium insertion potential (around 0.3 V), which is important for the enhancement of the cell voltage and power density.^[91] However, the rate capability of NTO7 was not evidently improved through regularly downsizing the particle or carbon decoration due to its extremely low intrinsic electronic conductivity. To address this trouble, Li and co-workers developed a rational approach to fabricate 3D hydrogenated NTO7 nanoarrays supported on flexible Ti substrates. Benefiting from high surface area, high electrical conductivity and Na⁺ diffusivity, these joint material designs afford a high reversible (desodiation) capacity of 227 mAh g⁻¹ and retain a capacity of 65 mAh g⁻¹ even over 10 000 continuous cycles at a high rate of 35 C (6.2 A g⁻¹) (**Figure 13a,b**).^[92]

In the light of strong P–O covalent, NaTi₂(PO₄)₃ (hereafter denoted as NTP) is an important member in the NASICON family, two sodium ions can be reversibly intercalated in the 3D frameworks which consist of three [PO₄] tetrahedron connected to two [TiO₆] octahedral.^[93] The strong covalent P–O bond

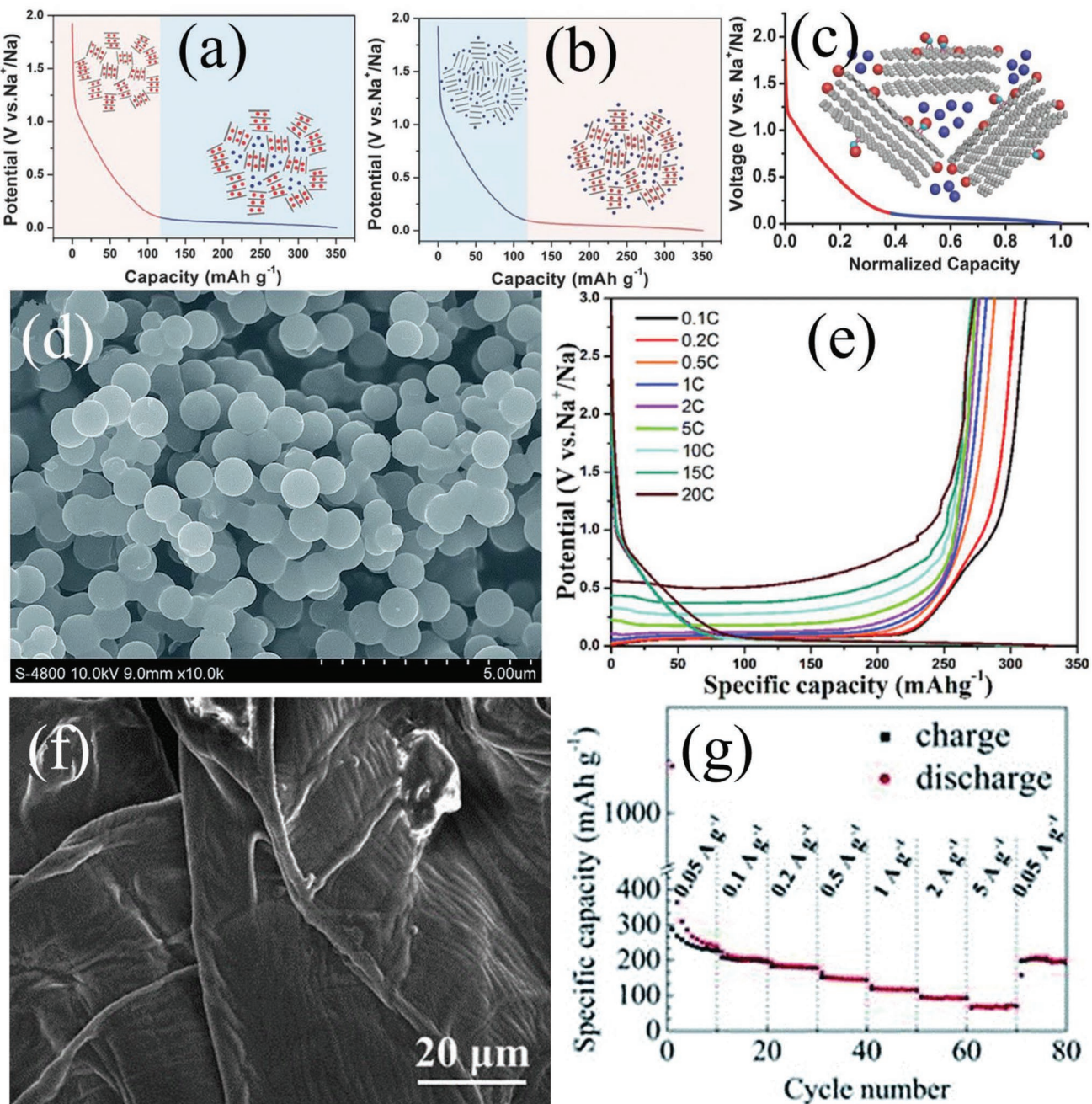


Figure 12. Schematic illustration of the mechanisms for Na-ion storage in hard carbon: a) intercalation–adsorption. b) adsorption–intercalation. c) Adsorption–pore filling. Reproduced with permission.^[84] Copyright 2017, WILEY-VCH Verlag GmbH & Co. KGaA, Weinheim. d) Structure of HCS from abundant sucrose and e) rate performance of the HCS electrode carbonized at 1600 °C discharged at the same current rate of 0.1 C. Reproduced with permission.^[86] Copyright 2015, The Royal Society of Chemistry. f) SEM images of natural pomelo peels after vacuum freeze-drying and g) rate performance of H₃PO₄-activated porous carbon. Reproduced with permission.^[89] Copyright 2014, The Royal Society of Chemistry.

endows with intrinsic safe properties of remarkable structure and thermal stability. NTP has significant advantages, including open 3D framework with the large interstitial spaces, fast Na⁺ diffusion, and trivial volume expansion upon sodium ions insertion/extraction, and high operation voltage that avoids the risk of superficial (dendritic) sodium growth at high power

output endowing appealing electrochemical performance after proper modification. Therefore, it is regarded as an ideal choice for high-power anode materials.^[94]

The practical use of NTP is restricted by inherently low electronic conductivity, accordingly many strategies, especially morphological modification and conductive composite decoration,

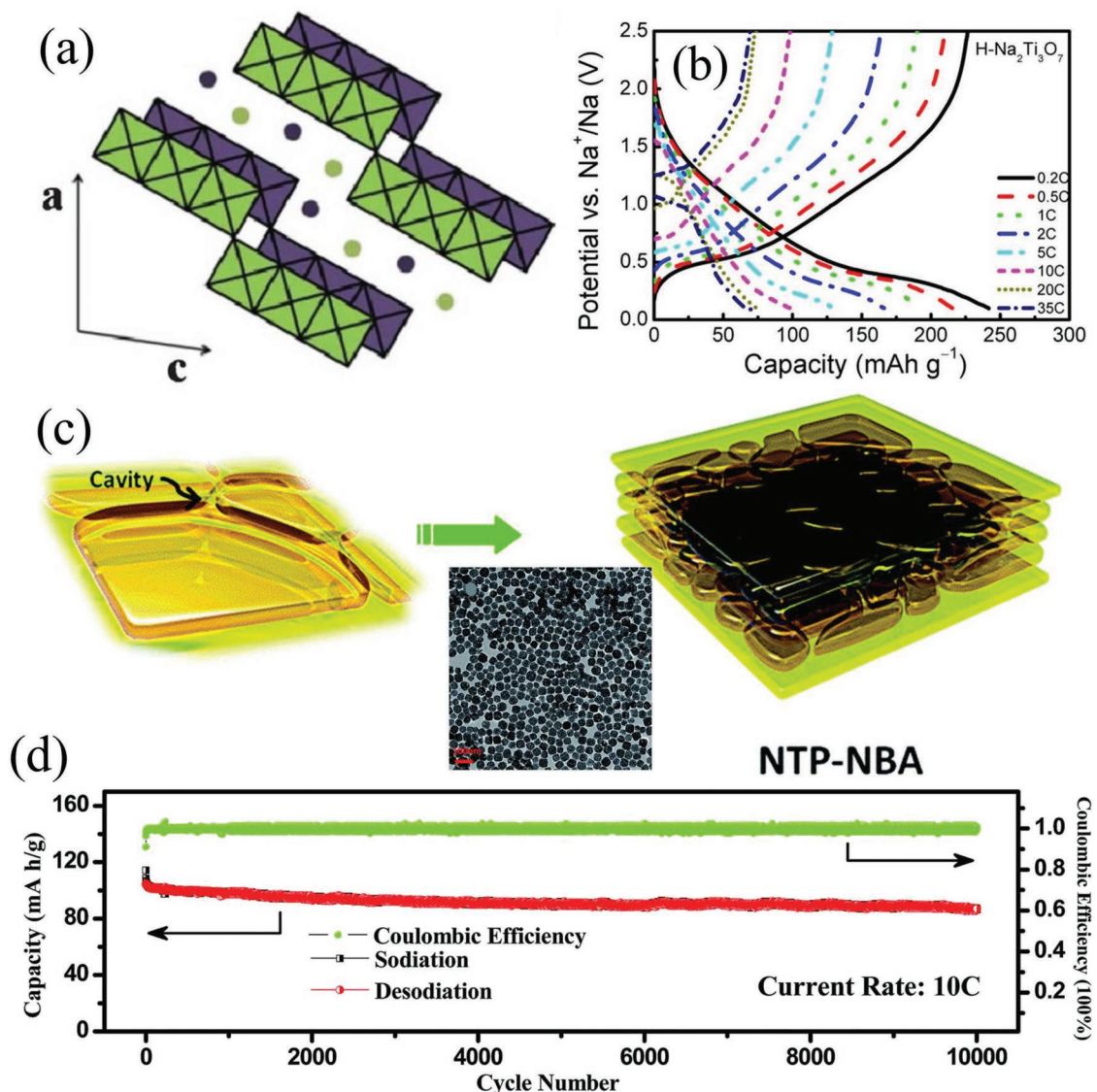


Figure 13. a) The crystal structure of $\text{Na}_2\text{Ti}_3\text{O}_7$. b) Galvanostatic profiles of $\text{H-Na}_2\text{Ti}_3\text{O}_7$ at various current rates. Reproduced with permission.^[92] Copyright 2016, American Chemical Society. c) Schematic illustration of the 3D nanoarchitectures of NTP-NBA products, inset: TEM image of NTP-NBA nanocubes and d) cycling performances of the NTP-NBA electrodes obtained at different current rates of 10 C. Reproduced with permission.^[93] Copyright 2015, The Royal Society of Chemistry.

have been developed by different groups to address the above problem. Wu's group^[95] and Wang et al.^[96] used graphene and carbon nanotube to decorate NTP nanoparticles, respectively, both of their electrodes could bear a high rate of 50 C and the relevant capacities are 67 and 103.4 mAh g^{-1} . A special structure, porous $\text{NaTi}_2(\text{PO}_4)_3$ nanocubes, is controllably synthesized by Yang's group, which exhibited an improved lifespan, more than 10 000 cycles, as well as an excellent rate capability, reaching 90.72 mAh g^{-1} under 10 C (Figure 13c,d).^[93] In parallel to these treatments, some other complicated decoration with conductive layers was also developed. Yang et al.^[97] designed a rational synergistic coating of carbon and rutile TiO_2 on $\text{NaTi}_2(\text{PO}_4)_3$ nanocubes, in which the nanocoating of rutile TiO_2 improves surface stability as well as specific capacity, while further coating of carbon provides enhanced

rate capability. A high rate capability with capacities of 83.5 and 77.2 mAh g^{-1} at a discharge/charge rate of 10 C and 20 C were obtained, respectively. Jiang and co-workers also brought out ultrafast sodium storage of NTP nanoparticles through embedded in nanocarbon networks, giving highly reversible capacity (108 mAh g^{-1} at 100 C) and long cycle life (83 mAh g^{-1} at 50 C after 6000 cycles).^[94] The author ascribed these excellent electrochemical performances to the synergistic effects of nanosized NTP, thinner carbon shell and the interconnected carbon network, which lead to low charge transfer resistance, large surface area for electrolyte soaking and enough void to buffer the volume change during repeated cycling. Interestingly, when the cutoff voltage is lowered to 0.01 V, a new discharge plateau around 0.4 V could be found which was attributed to further reduction of Ti^{3+} to Ti^{2+} . Thus more Na^+

Table 2. Comprehensive overview of typical NTP anodes in Na-ion batteries reported so far.

| Morphology | Cutoff voltages [V] | Reversible capacity [mAh g^{-1}], speed | Cycling performance initial capacity [mAh g^{-1}], % capacity retention, cycle number, speed | Rate capacity [mAh g^{-1}], speed | Remarks | Ref. |
|---|---------------------|--|---|--|---------------------------------------|------|
| NTP/graphene | 1.5–3.0 | 138, 1 C | 96, 80%, 1000, 50 C | 67, 50 C | $1 \text{ C} = 133 \text{ mA g}^{-1}$ | [95] |
| NTP/carbon nanotube | 1.5–3.0 | 116.4, 0.5 C | 96.0, 98%, 1000, 50 C | 103.4, 50 C | $1 \text{ C} = 130 \text{ mA g}^{-1}$ | [96] |
| Porous NTP Nanocubes | 1.5–2.8 | 110, 0.2 C | 115, 75.5%, 10 000, 10 C | 90.72, 100 C | $1 \text{ C} = 133 \text{ mA g}^{-1}$ | [93] |
| NTP/C/TiO ₂ | 1.2–2.8 | 131.2, 0.1 C | 83.5, 89.3%, 10 000, 10 C | 77.2, 20 C | $1 \text{ C} = 133 \text{ mA g}^{-1}$ | [97] |
| NTP/C/C (carbon shell and carbon network) | 1.5–2.8 | 132, 1 C | 118, 70.3%, 6000, 50, C | 108, 100 C | $1 \text{ C} = 133 \text{ mA g}^{-1}$ | [94] |
| NTP/C nanocomposite | 0.01–3.0 | 220, 0.1 C | \approx 100, 68%, 10 000, 20 C | 82, 20, C | $1 \text{ C} = 200 \text{ mA g}^{-1}$ | [98] |
| 3D graphene decorated NTP microspheres | 1.4–3 | 130, 0.2 C | \approx 100, 77%, 1000, 20 C | 75, 100 C | $1 \text{ C} = 133 \text{ mA g}^{-1}$ | [99] |

could insert into NTP and give a desirable initial capacity of 220 mAh g^{-1} ; a reversible capacity of 82 mAh g^{-1} at 20 C could be obtained as well.^[98]

Besides, high power full batteries based on NTP anode and diverse cathodes were explored. Fang et al. reported an all-NASION-type NTP@rGO//Na₃V₂(PO₄)₃/C full battery, which keeps 38.6 Wh kg^{-1} at a power density of 3167 W kg^{-1} (based on the total masses of active materials).^[99] Aqueous full cell based on NTP and Prussian blue analog, NaTi₂(PO₄)₃//Na₂NiFe(CN)₆, also shows potential performance for high-power usage.^[100] The NaTi₂(PO₄)₃ with high performance from different optimizing methods is summarized in **Table 2**.

In short, regardless of requirements in energy density, Ti-based compounds, particularly Na₂Ti₃O₇ and NaTi₂(PO₄)₃ have shown their strong competitiveness among a variety of anode candidates for SIBs in future power-need facilities and grid-scale energy storage systems.

3.2. Alloying Materials

Sodium can alloy with several metallic and nonmetallic elements, including P, Sn, Sb, Ge, Pb, and Bi, with theoretical specific capacities of 2596 (Na₃P), 847 (Na₁₅Sn₄), 660 (Na₃Sb), 369 (NaGe), 484 (Na₁₅Pb₄), and 385 mAh/g (Na₃Bi), respectively.^[101–103] Nevertheless, it has been commonly accepted that the slow ion diffusion kinetics, unstable solid electrolyte interphase (SEI), and large volume change of the electrode material during alloy/dealloy process are the major obstacle to hinder their practical application.^[104–106] With the aim of prolonging the cycle life and advancing the power capability of these alloying anodes, rationalized structure and morphology design in combination with optimized electrode have been developed.

3.2.1. P

Elemental Phosphorus could react with three Na atoms to form Na₃P compounds, giving a theoretical specific capacity of 2596 mAh g^{-1} , encompassing the highest value among all known anode materials for SIBs. However, the tremendous volume variation ($\approx 300\%$) during repeated charge/discharge processes causes severe pulverization of the active material and

thus leads to a rapid decay. There are three main Phosphorus (P) allotropes: white, red and black. White phosphorus is highly reactive and toxic, making it unsuitable for battery use. Therefore, extensive researches focused on red and black phosphorus and their metal phosphides. The common strategy to optimize the sodium storage performance of phosphorus is to introduce carbon matrix as well as rational structure.

Red phosphorus (P) is regarded as a specially promising anode material for SIBs, since it is commercially available. Yang et al. first reported an amorphous red phosphorus/carbon (a-P/C) nanocomposite with extraordinarily considerable lifespan and a high capacity of 640 mAh g^{-1} at a very high rate of 4000 mA g^{-1} .^[107] Rational design of red phosphorus nanodots on reduced graphene oxide sheets (P@RGO) was also developed by Liu and colleagues, the novel structure showed synergetic effects: the red phosphorus nanodots shorten the diffusion distance for sodium ions, and graphene layers act as an elastic buffer layer and function as an electrical highway. As shown in **Figure 14a,b**, the flexible anode achieved a specific charge capacity of 135.3 mAh g^{-1} at $47\ 818.3 \text{ mA g}^{-1}$, which makes a significant performance improvement for red phosphorus anodes for sodium-ion chemistry and flexible power sources for wearable electronics.^[108] As another strategy, Qian and co-workers managed to develop hollow P nanospheres (HPNs) with porous shells (Figure 14c) to alleviate the material pulverization induced by large volume expansion via a wet-chemical synthesis, which is favorable for the practical application. Under the current densities of 3.0 and 4.0 C ($1 \text{ C} = 2596 \text{ mA g}^{-1}$), HPNs-300 electrode showed the discharge capacities of 832.1 and 278.4 mAh g^{-1} , respectively (Figure 14d).^[104] A red P-single-walled carbon nanotube (denoted as red P-SWCNT) composite was fabricated by a modified vaporization-condensation method, which showed a fast rate capability ($\approx 300 \text{ mAh g}^{-1}$ at 2000 mA g^{-1}).^[109] Guo et al. fabricated a 3D hierarchical integrated carbon/red phosphorus/graphene aerogel composite with high surface area and ample active sites, which delivered a capacity of 878.6 at 2 C ($1 \text{ C} = 2600 \text{ mA g}^{-1}$).^[110]

Black phosphorus (BP) closely resembles graphite: a good conductor of electricity ($\approx 300 \text{ S m}^{-1}$ versus $\approx 10^{14} \text{ S m}^{-1}$ for RP) as well as made of puckered sheets of covalently bonded phosphorus atoms. The layered structure has a large enough interlayer channel (3.08 Å) to store sodium ions (2.04 Å), thus showing ascendant trend in SIBs. As shown in **Figure 14e**,

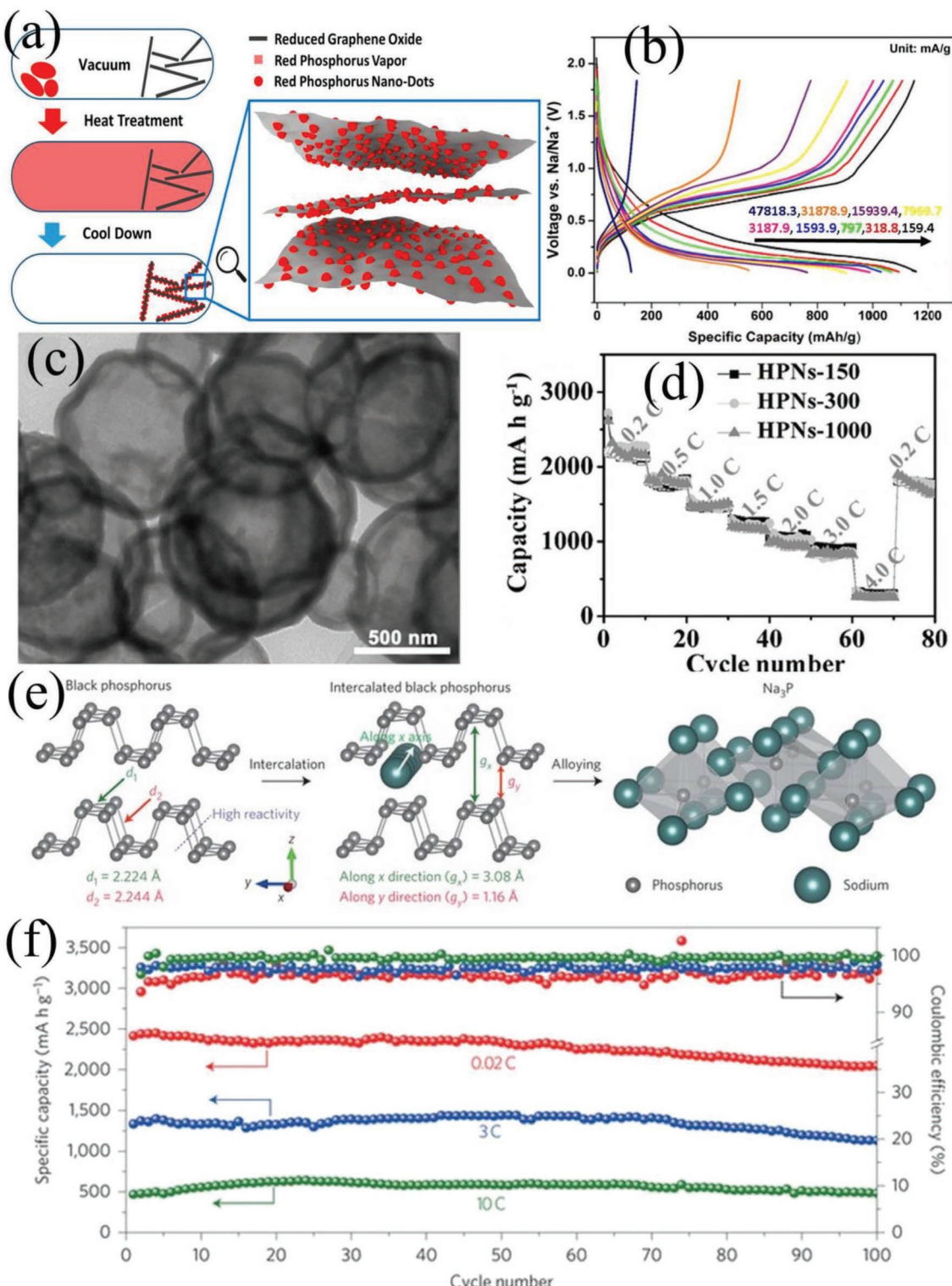


Figure 14. a) Design of P@RGO with its potential profiles at different rates presented in (b). Reproduced with permission.^[108] Copyright 2017, American Chemical Society. c) TEM image of the sample collected from experiments with NaN₃/PCl₅: 0.004 mol/0.0008 mol. d) The rate performance of HPNs with average diameters of 150 (HPN-150), 300 (HPNs-300), and 1000 nm (HPNs-1000) for SIBs at the current densities varying from 0.2 to 4.0 C. Reproduced with permission.^[104] 2017 WILEY-VCH Verlag GmbH & Co. KGaA, Weinheim. e) Schematics mechanism of sodiation in black phosphorus: sodium-ion intercalation followed by alloy reaction to Na₃P. f) Reversible desodiation capacity and coulombic efficiency for the first 100 galvanostatic cycles of the phosphorene/graphene (48.3 wt% P) anode tested under different currents. Reproduced with permission.^[111] Copyright 2015, Macmillan Publishers Limited.

Cui and co-workers proposed a hybrid material made out of a few phosphorene layers sandwiched between graphene layers. Similar to the above-discussed P@RGO, the phosphorene layer is also able to decrease the diffusion distance of sodium ions while the graphene layer serves as electron pathway. They elucidated the mechanism as a two-step reaction: intercalation of sodium ions along the x -axis of the phosphorene layers followed by the formation of a Na_3P alloy. As a result, the hybrid material showed an enhanced performance that a notable reversible capacity of 2440 mAh g^{-1} was obtained at 50 mA g^{-1} . When the currents were raised to 4.6 C (12 A g^{-1}), 7.7 C (20 A g^{-1}) and 10 C (26 A g^{-1}), surprising specific capacities of 1200 (49.2%), 915 (37.5%) and 645 mAh g^{-1} (26.4%) were retained, respectively (Figure 14f).^[111] Similarly, Shahbazian-Yassar and co-workers also confirmed that Na^+ ions prefer to diffuse along the^[100] direction in phosphorene by use of in situ TEM observation.^[112] Compared to the commercially available RP, BP has a good electrical conductivity and layered crystal structure to accommodate Na^+ ions, but the complicated synthesis route hinders its further application.^[113]

3.2.2. Sn

Metallic Sn is one of the most intensively investigated anodes for SIBs owing to its high theoretical capacity of 847 mAh g^{-1} , corresponding to 3.75 Na per Sn . There are no unified mechanisms for the alloy process until today. Based on the theoretical calculations, Chevrier and Ceder proposed a voltage profile to interpret the multisteps alloying reaction between Na and Sn: $\text{Sn} - \text{NaSn}_5 - \text{NaSn} - \text{Na}_9\text{Sn}_4 - \text{Na}_{15}\text{Sn}_4$.^[114] Ellis and co-workers used DFT calculations and in situ X-ray diffraction to reveal another alloying route: $\text{Sn} - \text{NaSn}_3^* - \text{amorphous NaSn} - \text{Na}_9\text{Sn}_4 - \text{Na}_{15}\text{Sn}_4$ (*-new crystalline phase).^[115] Huang's group investigated the microstructural evolution and phase transformation via in situ transmission electron microscopy, and proposed a two-step sodiation process: amorphous NaSn_2 was formed in the first step, followed by the formation of amorphous Na_9Sn_4 , Na_3Sn (336% expansion), and crystalline $\text{Na}_{15}\text{Sn}_4$ (420% expansion) in the second step.^[103] Though various mechanisms lead to different intermetallic phases, the final formation of a crystalline $\text{Na}_{15}\text{Sn}_4$ together with a large volume expansion is now well accepted. The volume evolution was vividly illustrated in Figure 15a by in situ hard X-ray nanotomography.^[116]

The extremely high volumetric expansion–contraction leads to cumulative pulverization, loss of electrical contact and capacity decay during alloying–dealloying reactions. It is extensively proved that the rational and engineered design of nanostructured electrodes with carbon matrix decoration and heteroatom substitution could considerably improve the performance of Sn anode. In this respect, Sn–carbon nanotube (CNT) nanopillar arrays,^[117] yolk–shell Sn/C eglette-like nanocomposites^[118] and Sn nanoparticles@nitrogen-doped carbon nanofiber (Sn@NCNFs)^[119] have been developed in succession. Ultrasmall Sn nanoparticles ($\sim 8 \text{ nm}$) homogeneously embedded in spherical carbon network (denoted as 8-Sn@C) was prepared using an aerosol spray pyrolysis method, and delivered maximum desodiation capacities of 134 and 64 mAh g^{-1}

at 2000 and 4000 mA g^{-1} , respectively. The remarkable electrochemical performance is owing to the synergistic effects between the well-dispersed ultrasmall Sn nanoparticles and the conductive carbon network, which can suppress the volume fluctuation and particle aggregation of Sn during alloying process, thus preventing from pulverization, loss of electrical contact and low utilization rate.^[120] Luo et al. fabricated a hierarchical Sn@carbon composite composed of foam like graphene carbonaceous matrix and well-confined tin nanoparticles with a typical size of $\sim 15 \text{ nm}$ (named as F-G/Sn@C). As shown in Figure 15b, this composite exhibited an impressive reversible capacity of 413 mAh g^{-1} with proper operation voltage and a high-rate capacity, that is, when the current density is gradually increased to 1600 and 3200 mA g^{-1} , the corresponding reversible capacities are 166 and 106 mAh g^{-1} , respectively (Figure 15c). The authors described that the 2D graphene backboned matrix not only acts as a confinement layer to prevent the tin nanoparticles from aggregating during the synthetic process, but also functions as a physical barrier to buffer the volume change effect during charge/discharge processes.^[121]

3.2.3. Sb

Antimony (Sb) is another attractive anode material for SIBs with a high theoretical capacity of 660 mAh g^{-1} . The volume expansion reaches 390% when Sb is alloyed with Na to form Na_3Sb (JCPDS No.74–1162, space group $P63/mmc$).^[122,123] Similar to other alloying anodes, the electrochemical performance of Sb anode can be improved by employing conductive carbon matrix and building nanostructures. As shown in Figure 16a, Liu and co-workers developed a thermal-reduction strategy coupled with carbon coating to synthesize unique Sb@C coaxial nanotubes, in which the inner crystalline Sb and outer amorphous carbon have thicknesses of about 9 and 20 nm , respectively. When tested in half-cell, high capacities of 350 and 310 mAh g^{-1} can be achieved at large current densities of 10 and 20 A g^{-1} , respectively, which represent the best rate performance among the reported Sb-based anode materials so far (Figure 16b). The enhanced sodium storage performance could be attributed to the tailored structure, specifically, the void space inside the tube is large enough to buffer the large volume expansion, and the carbon shell not only enhances the conductivity, but also restricts the aggregation of the Sb nanoparticles and protects Sb from forming an unstable SEI layer. In addition, the 1D structure provides an orientated electronic transport path and strong tolerance to stress change, and the tube-architecture can promote the ionic transport along the radial direction, contributing to the excellent rate capability.^[124] Kovalenko et al. thoroughly compared the performance of microcrystalline Sb and Sb nanocrystals, and revealed that downsizing pristine Sb to 10 – 20 nm can result in significantly faster kinetics and more stable output performance at higher current densities. Consequently, a high capacity of $\sim 500 \text{ mAh g}^{-1}$ could be reached even under 13.2 A g^{-1} .^[125] Cao et al. reported Sb nanoparticles embedded homogeneously in the carbon nanofibers, the unique nanofiber structure could provide a conductive and buffering matrix for effective release of mechanical stress caused by Na ion insertion/extraction and prevent the aggregation

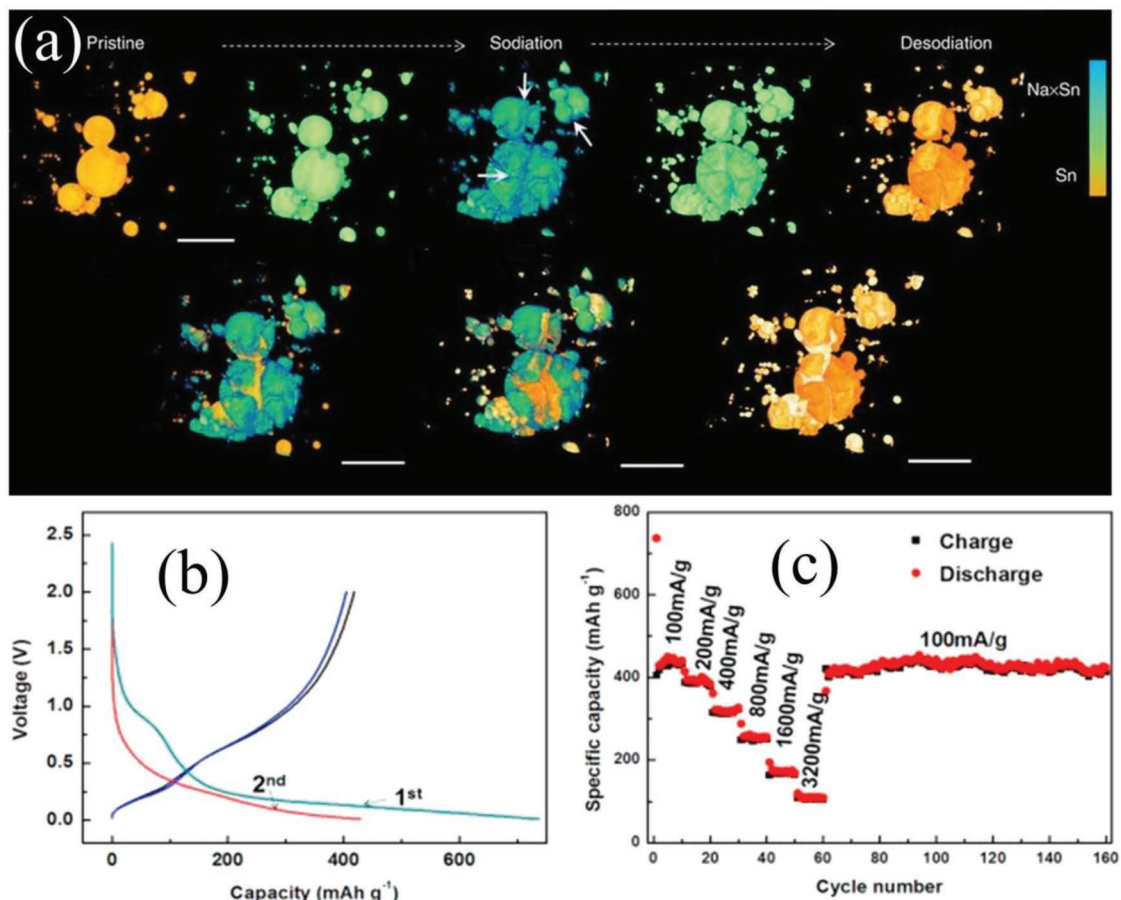


Figure 15. a) 3D morphological change of Sn particles during the first sodiation–desodiation cycle. Reproduced with permission.^[116] Copyright 2015, Macmillan Publishers Limited. b) Galvanostatic discharge–charge voltage profiles of the F-G/Sn@C electrode between 10 mV and 2.0 V versus Na/ Na^+ at a current density of 100 mA g⁻¹. c) Rate capability and cycling performance of the F-G/Sn@C electrodes in the voltage range of 10 mV to 2.0 V for Na ion storage. Reproduced with permission.^[121] Copyright 2016, Elsevier.

of the Sb nanoparticles. When tested as anode for SIBs, it delivered a considerable reversible capacity (631 mAh g⁻¹) at C/15, greatly enhanced rate capability (337 mAh g⁻¹ at 5 C, 1 C = 600 mA g⁻¹) and excellent cycling stability (90% capacity retention after 400 cycles), showing application prototype for high power system.^[126]

However, the weak interaction between the active component and the carbon matrix results in structural instability, which is a common drawback for carbon composite materials. To address this, as shown in Figure 16d, Hu et al. synthesized chemically coupled antimony–multilayer graphene (MLG) by a confined vapor deposition method, in which the chemical bonding between Sb and graphene can not only improve sodium ion diffusion and electronic transport but also stabilize the solid electrolyte interphase against the large volume changes during cycling. Consequently, Figure 16e shows stable long-term cycling performance with 90% capacity retention after 200 cycles, and an excellent rate capability (210 mAh g⁻¹ under 5000 mA g⁻¹).^[127]

Besides, similar to Sn, adopting other elements in Sb is also a feasible strategy to optimize electrochemical performance. Kim et al. proposed a Mo₃Sb₇–C alloy consisting of active–inactive

components as anode for NIBs. The carbon matrix served as a buffer to absorb large volume expansion. They also investigated the effect of fluoroethylene carbonate (FEC) as additive and demonstrated with vol 2% of FEC additive, there would form a more stable and thin SEI layer and represented smaller charge-transfer resistance and better dispersion of the particles during the cycling. As a consequence, it showed impressive rate cyclability, with initial capacity (\approx 250 mAh g⁻¹) retained of 92% at 3 A g⁻¹, 88% at 5 A g⁻¹, and 77% at 10 A g⁻¹.^[128] Yu's group prepared three-dimensionally interconnected NiSb intermetallic hollow nanospheres, where the 3D interconnected hollow structure buffer the volume change during cycling, and the Ni matrix encapsulation Na–Sb alloy leads to the improved structure stability. The electrode delivered high stable and substantial discharge capacities of \approx 300 and \approx 160 mAh g⁻¹ at 5 C and 15 C (1 C = 600 mA g⁻¹), respectively. Notably, a full Na_{0.4}Mn_{0.54}Co_{0.46}O₂//NiSb battery was also exploited and it showed relatively good performance.^[129] A bi-alloy Bi_{0.57}Sb_{0.43}C was synthesized via simple high energy milling, and exhibited an superior electrochemical performance compared their counterparts Bi–C and Sb–C, delivering a specific of 326 mAh g⁻¹ at 1000 mA g⁻¹.^[130]

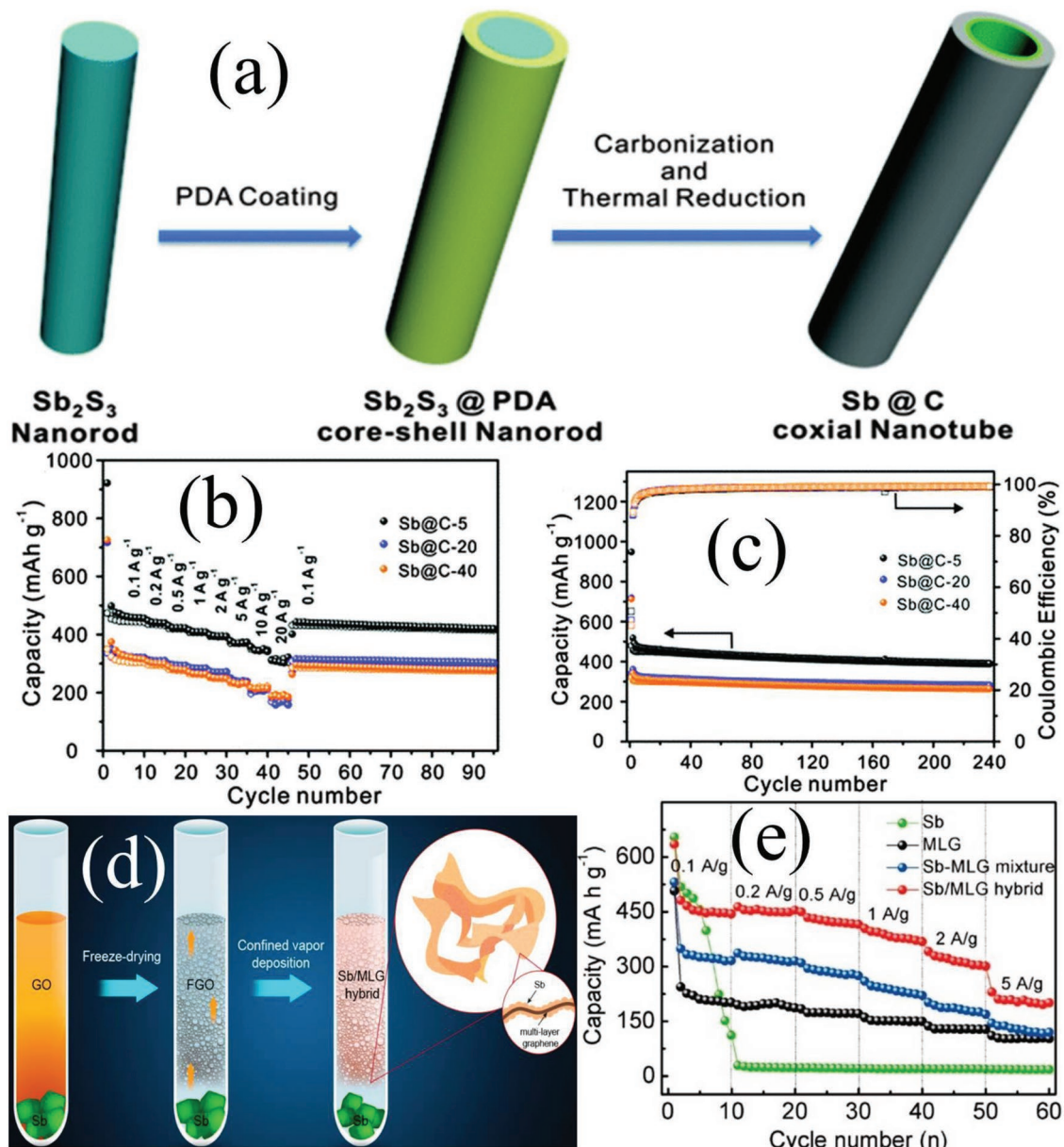


Figure 16. a) Schematic illustration of the formation of Sb@C coaxial nanotubes. b) Rate and c) cycling performance of Sb@C-5, Sb@C-20, and Sb@C-40, where numbers indicate annealing time of 5, 20, and 40 min, respectively. Reproduced with permission.^[124] Copyright 2016, Royal Society of Chemistry. Design of Sb–MLG mixture, and Sb/MLG hybrid electrodes. d) Illustration of the preparation process for the antimony–multilayer graphene hybrid (Sb/MLG) and e) comparison of rate capability of the MLG, Sb, Sb–MLG mixture electrodes. Reproduced with permission.^[127] Copyright 2015, American Chemical Society.

3.2.4. Ge

Besides the promising phosphorus, tin and antimony anodes, recent studies found that germanium (Ge) could also act as a high power anode for SIBs through rational designs.

Germanium possesses a theoretical capacity of 369 mAh g⁻¹ (based on the formation of the fully sodiated Na_xGe phase(s)). Crystalline germanium exhibits extremely sluggish kinetics and high barrier for Na diffusion, in contrast, amorphous Ge manifests surprising electrochemical active toward Na storage. Mitlin et al. first revealed that activation with Li induced amorphization in

Ge nanowires, reducing the barrier for nucleation of the Na_xGe phase(s) and accelerating solid-state diffusion. The electrode achieved a dramatic improvement in the practical capacity, and exhibited a capacity of 103 mAh g⁻¹ at 10 C (3690 mA g⁻¹).^[131] Mullins et al. elaborately fabricated nanocolumnar Ge (Figure 17a) via evaporative deposition. The diffusion coefficient of sodium in germanium was estimated to be $\approx 10^{-13}$ cm² s⁻¹. When tested as anode in half-cell, a capacity of 164 mAh g⁻¹ was obtained at charge/discharge rates up to 10 A g⁻¹ (Figure 17b).^[132,133] Despite promising electrochemical result has been achieved in some reports, the sophisticated synthesis process and intrinsic sluggish

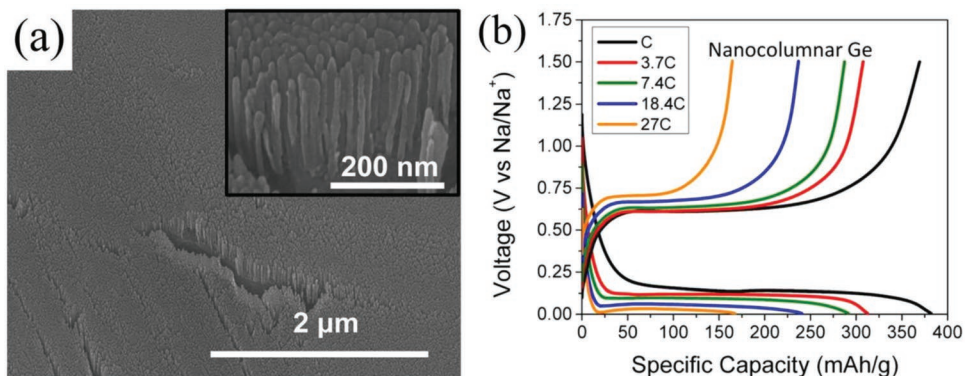


Figure 17. a) SEM image of germanium nanocolumns deposited at 70°. b) voltage profiles for sodium insertion cycles at each rate in the C-rate test (1 C = 0.37 A g⁻¹). Reproduced with permission.^[132] Copyright 2013, American Chemical Society.

kinetics remain the major obstacles for making Ge anode competitively useful in high power SIBs.

Other elements with the ability to alloy with Na, such as lead (Pb), indium (In) and bismuth (Bi), have been reported with theoretical capacities of 485 mAh g⁻¹ (Na₁₅Pb₄), 467 mAh g⁻¹ (Na₂In) and 385 mAh g⁻¹ (Na₃Bi). However, considering the crustal abundance, environmental and safety issues related to their usage, these anodes received limited research interest.^[122]

3.3. Conversion Materials

Analogous to the reaction in LIBs, conversion materials including transition metal oxides, sulfides, nitrides, and phosphides (with M_aX_b as general formula, M = Fe, Co, Mo, Mn, Ni, etc., X = O, S, N, P) have been considered as potential anode materials for SIBs due to their high theoretical specific capacities. However, Most of them, especially oxides, sulfides and nitrides anodes, suffer from low initial Coulombic efficiency, huge volume changes upon cycling, poor cycling stability, and low energy efficiency due to the high voltage hysteresis. These problems have not been solved yet in LIBs; therefore, the anodes mentioned above have little application possibility in high power SIBs, and beyond the scope of this paper.

Combining P with conductive metals, such as Cu, Fe, Ni, Sn and Se can engender a series of metal phosphides. It has been demonstrated that the secondary ingredient can not only enhance the conductivity, but also dilute the concentration of P species and buffer its volume changes during repeated sodiation and desodiation.^[113] A controlled red phosphorus@Ni-P core@shell nanostructure was reported by An et al. The in situ generated Ni₂P on RP particle surfaces can facilitate intimate contact between RP and a mechanically strong amorphous Ni-P outer shell with a high electronic conductivity, which ensures strong electrode structural integrity, a stable solid electrolyte interphase and ultra-fast electronic transport. Consequently, it delivered a good rate capability (491 mAh g⁻¹ at 5200 mA g⁻¹).^[134] Selenium (Se) has good electrical conductivity ($\approx 10^{-5}$ S cm⁻¹) and could storage sodium alone with a high theoretical capacity (678 mAh g⁻¹). An amorphous Se₄P₄ anode was synthesized by a facile mechanical milling method, and the volume change from Se₄P₄ to Na₃P and Na₂Se

produces is about 166%, much lower than that of pure P. The Se₄P₄ anode exhibited excellent rate capability, with capacities of 436 and 332 mA g⁻¹ at the current density of 2000 and 3000 mA g⁻¹, respectively.^[135] Yang's group early uncovered the synergistic sodium storage in Sn₄P₃ that both Sn and P can be reversibly sodiated to contribute their redox capacities, when the current density was increased to 1000 mA g⁻¹, the reversible capacity retained at 349 mAh g⁻¹, which are beyond the Na storage capacities of carbonaceous materials.^[136] Moreover, most of the reversible capacity was delivered at the low potential of ≈ 0.3 V, rendering Sn₄P₃ a promising anode material for high power SIBs. Later, its performance was further enhanced. Liu et al. reported Uniform yolk-shell Sn₄P₃@C nanospheres, in which the Sn₄P₃ nanoparticles were surrounded by a carbon shell, which reached a reversible capacity of about 421 mAh g⁻¹ at 3000 mA g⁻¹.^[137] Mulder et al. reported a Sn₄P₃-P (Sn:P = 1:3) @graphene nanocomposite, which achieved excellent rate capability (≈ 585 and ≈ 315 mAh g⁻¹ at 2 and 10 A g⁻¹, respectively) and unrivaled high rate capacity retentions of > 550 and 371 mAh g⁻¹ at 1 and 2 A g⁻¹, respectively, over 1000 cycles.^[138]

Based on the above discussion, the theoretical, practical capacity and corresponding charge voltage of typical anode materials are summarized in Figure 18 and Table 3, which provides a full picture of recent potential anode materials for high power SIBs.

4. Electrolyte and Aqueous Sodium-Ion Batteries

The electrolyte is an indispensable and decisive component in SIBs, where Na⁺ escapes from one electrode, diffuses through the electrolyte and then reacts with the counter electrode, balancing and transferring charges in the form of ions between the two electrodes during charge and discharge process. Electrolyte could be roughly divided into two types from the perspective of solvent: nonaqueous and aqueous, and the former could be further classified as three main types: solid state, gel polymer and liquid state.

Solid-state electrolytes including solid polymers (SPs) and glass-ceramic composite are still in the early stage of research. They are mainly hindered by low ionic conductivity, for example, the ionic conductivities of SPs are among 10^{-5} to 10^{-7} S cm⁻¹,

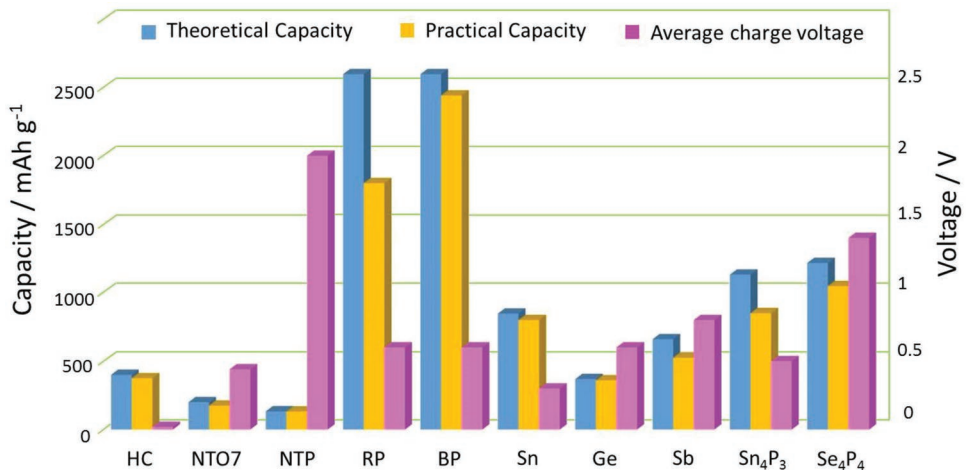


Figure 18. Theoretical, practical capacity and corresponding average charge voltage of typical anode materials (HC: hard carbon, NTO₇: Na₂Ti₃O₇, NTP: NaTi₂(PO₄)₃, RP: Red phosphorus, BP: Black phosphorus).

and that of even the most advanced NASICON type electrolyte, ceramic material, is only around 10⁻⁴ S cm⁻¹.^[139] At present, this severe drawback makes solid state electrolytes unable to meet the high power demand due to the sluggish ionic conductivity, harsh interface between electrodes and electrolyte, and engineering process issues.

Polymers are typically bad solvents for ions because of high viscosities and low dielectric constants—often in the range of 3–5, but these problems could be greatly alleviated by introducing organic solvents into polymer, containing a certain amount of salts, to form gel polymer electrolytes (GPEs). They could achieve a moderate ionic conductivity of 10⁻³ S cm⁻¹ at room-temperature.^[139,140] Goodenough et al. fabricated a low-cost composite gel-polymer electrolyte based on cross-linked poly(methyl methacrylate) and applied it in a sodium-ion full cell Sb//Na₃V₂(PO₄)₃, which could run at high charge and discharge rates, delivering a capacity of 106.8 mAh g⁻¹ at 0.1 C and 61.1 mAh g⁻¹ at 10 C. The extensive growth of the interfacial layer on the surface of the Sb anode with lower Fermi energy instead of the highly active sodium metal, endowing the full cell to run at high charge/discharge current densities with small polarization. And compared with the conventional liquid

electrolyte, the application of the gel-polymer electrolyte is promising to enhance the interfacial properties of the sodium-ion full-cell, especially at elevated temperature.

Liquid electrolytes are the most common electrolytes for SIBs. The compositions of different electrolytes are similar to each other, in which the most common organic solvents are the same, and the sodium salts are often the Na-analogs of the Li salts.^[141] Aprotic organic solvents, in particular cyclic carbonate esters (e.g., PC and EC) and linear carbonates (e.g., EMC, DMC, and DEC) and ethers are widely used because they have advantages such as high dielectric constant ($\epsilon > 15$) to dissolve the Na salts, low viscosity to improve the ionic mobility, chemically inert to the charged surfaces of the cathode and the anode during cell operation, wide liquid range (i.e., low melting point and high boiling point) and slight safe, nontoxic, and economical issues.^[142] As for sodium salt, NaClO₄ and NaPF₆ are widely adopted even though NaClO₄ has a potential safety hazard, and NaPF₆ is unstable to moisture. In fact, binary or ternary carbonate ester solvents, include EC + PC, EC + DEC, EC + PC + DMC, etc., with 1 M NaClO₄ or NaPF₆ are commonly used to supplement each other. Earlier research suggested graphite was unsuitable as the anode for SIBs, but recent studies showed

Table 3. Comprehensive overview of most potential and typical anode materials for SIBs toward high power applications.

| Sample | Cutoff voltages [V] | Reversible Capacity [mAh g ⁻¹] speed | Cycling Performance initial capacity [mAh g ⁻¹], % capacity retention, cycle number, speed | Maximum rate capacity [mAh g ⁻¹], speed | Remarks | Ref. |
|---|---------------------|--|--|---|-------------------------------|-------|
| Hard carbon | 0–3 | 335, 0.1 C | 290, 93%, 100, 0.1 C | 270, 20 C | 1 C = 300 mA g ⁻¹ | [86] |
| P, O codoped-hard carbon | 0–3 | 402 at 50 mA g ⁻¹ | 214, 84.6%, 220, 200 mA g ⁻¹ | 71 at 5 A g ⁻¹ | – | [89] |
| NaTi ₂ (PO ₄) ₃ | 1.5–2.8 | 110 0.2 C | 115 75.5% 10 000 10 C | 90.72, 100 C | 1 C = 133 mA g ⁻¹ | [93] |
| Red phosphorus | 0.01–1.75 | ≈1000 at 1593.9 mA g ⁻¹ | 1074.5, 86.6%, 300, 1593.9 mA g ⁻¹ | 135.3 at 47 818.3 mA g ⁻¹ | – | [108] |
| Black phosphorus | 0–1.5 | 2440 at 50 mA g ⁻¹ | 2440, 83%, 100, at 50 mA g ⁻¹ | 645, 10 C | 1 C = 2608 mA g ⁻¹ | [111] |
| Sn | 0.01–2.0 | 493.6 at 200 mA g ⁻¹ | 415, ≈100%, 500, at 1000 mA g ⁻¹ | 349 at 4000 mA g ⁻¹ | – | [120] |
| Sb | 0.01–2.0 | 407 at 100 mA g ⁻¹ | 240, ≈100%, 2000, at 1000 mA g ⁻¹ | 310 at 20 000 mA g ⁻¹ | – | [124] |
| Mo ₃ Sb ₇ | 0–2 | ≈400 at 100 mA g ⁻¹ | 400, 90%, 100, at 100 mA g ⁻¹ | 192.5 at 10 000 mA g ⁻¹ | – | [128] |
| Ge | 0.005–1.5 | 430, 0.2 C | 372, 88%, 100, 0.2 C | 164 at 10 000 mA g ⁻¹ | 1 C = 370 mA g ⁻¹ | [132] |

that the use of glyme-based electrolyte enables the co-intercalation of solvated sodium ions by forming ternary graphite intercalation compounds.^[15,143]

Incorporation of a small dose of foreign molecules, that is, additives, often brings vast benefits to the electrolytes, increasing the electrochemical capability. Additives is mainly used to modify the electrolyte through the formation of stable electrode-electrolyte interface (EEI), namely, SEI on the anode and CEI on the cathode, dictating the overall performance with respect to reversible capacity, long-term cycling, Coulombic efficiency, safety, and so forth of the battery system. The EEI layers are supposed to be insulator for electrons between electrolyte and electrode but good conductor for Na^+ ions. Fluoroethylene carbonate (FEC) with a higher reduction potential is the mostly widely used film additive for SEI and CEI. A higher reduction means it tends to preferentially reduced before solvent molecules/polymer or conducting sodium salts, leading to the formation of SEI layer.^[144] By introducing 2 vol% FEC, Wang and co-workers attempted to achieve a rate capability of as much as 103.9 and 89.9 mAh g^{-1} at current rates of 2 and 5 A g^{-1} , respectively, and prolonged the lifespan of a nitrogen-doped hollow carbon nanospheres to 136.4 mAh g^{-1} after 2500 cycles, while the FEC bare sample only retained a capacity less than 50 mAh g^{-1} at the end.^[145] Chou et al. elucidated that an addition of 5% FEC into electrolyte, their $\text{Na}_{3.32}\text{Fe}_{2.34}(\text{P}_2\text{O}_7)_2/\text{C}$ cathode material can deliver an initial capacity of 72.5 mAh g^{-1} at a discharge rate of 5 C, and about 90% of the initial capacity was maintained after 1100 cycles, implying the protective surface films on the cathode was beneficial for the improved passivation and suppression of side reactions between the Na metal and the PC solution containing Na salts, especially for long cycling stability.^[146] There are also additives with more functions that are more global to the electrolyte, flame-retardants, fluidity enhancers/viscosity decreasers, impurity or radical scavengers and so forth,^[140] which would eventually affect the sodium ion batteries operating at high power conditions.

Despite nonaqueous electrolyte-based SIBs have displayed superior electrochemical performance, serious safety issues from flammable and volatile liquid solvents, including electrolyte leakage, flammability, dendrite growth, and severe side reactions between electrolytes and electrodes still continue to be the major bottleneck in designing and applying SIBs. To some extent, the safety issue in SIBs is even more severe than that of LIBs due to the high chemical reactivity of sodium. In this context, low cost aqueous sodium-ion batteries (ASIBs, Figure 19a) drew increasing attention in the past few years due to their high safety, environmental friendliness in large-scale applications and long cycle life.

However, unlike the nonaqueous SIBs, the choice of electrode materials in aqueous SIBs is seriously limited due to the narrow stable electrochemical window of water (≈ 1.23 V), side reaction with water or with oxygen, proton coininsertion along with insertion of metal ion, dissolution of electrode materials in aqueous electrolyte, etc. As mentioned before, $\text{Na}_{0.44}\text{MnO}_2$ has been widely reported as a cathode material for a rechargeable aqueous sodium-ion battery (SIB) because of its stable tunnel structure, abundant resources, and environmental benignity. Yuan developed an alkaline Zn- $\text{Na}_{0.44}\text{MnO}_2$ dual-ion battery, which exhibited a high reversible capacity

(80.2 mAh g^{-1} at 0.5 C), high rate capability (32 mAh g^{-1} at 50 C), and long cycle life (73% capacity retention over 1000 cycles).^[147] Prussian blue materials have an open-framework crystal structure containing large interstitial sites that allows fast insertion and extraction of Na^+ with very little crystallographic lattice strain in ASIBs. Cui et al demonstrated insertion/extraction of sodium ions in a low-strain nickel hexacyanoferrate electrode material for at least five thousand deep cycles at high current densities in inexpensive aqueous electrolytes. Its open-framework structure allows retention of 66% of the initial capacity even at a very high rate (41.7 C).^[148] Similarly, as discussed before, another full aqueous rechargeable Na-ion battery by use of Na-deficient $\text{NaTi}_2(\text{PO}_4)_3$ anode, Na-rich $\text{Na}_2\text{NiFe}(\text{CN})_6$ cathode and aqueous Na_2SO_4 electrolyte was developed by Yang and co-workers, showing in Figure 19b. This battery revealed a specific energy density of 42.5 Wh kg^{-1} at a power density of 130 W kg^{-1} , and still retained 34 Wh kg^{-1} at a high power density of 1200 W kg^{-1} (based on the total masses of active materials).^[100] In light of open framework and structure stability, a number of polyanion materials related publications have also come out in the past few years. Zhang et al. developed a new ASIB based on all NASICON-structured electrodes with $\text{NaTi}_2(\text{PO}_4)_3$ anode and $\text{Na}_3\text{V}_2(\text{PO}_4)_3$ cathode in the Na_2SO_4 electrolyte.^[149] Such battery reached the theoretical working window of aqueous electrolyte and exhibited a high output voltage of 1.2 V (Figure 19c).

To further improve the power capability of ASIBs, two main strategies have been documented: developing hybrid sodium-ion battery and employing concentrated electrolyte. Sharma's group introduced a hybrid device with $\text{Na}_{0.44}\text{MnO}_2$ as working electrode, activated carbon as counter electrode and 1 M Na_2SO_4 as electrolyte. With the proper negative to positive electrode mass ratio (0.8:1), energy storage cells capable of working under 18 C and being charged to at least 1.7 V without significant water electrolysis were detected.^[150]

Despite the high safety and low cost, the narrow thermodynamic stability window (1.23 V) of water hinders the application of high-voltage electrode couples, thus limiting the power density of the ASIBs. Meanwhile, the water consumption (decomposition) and side reactions always lead to the failure of sealed aqueous battery system. To some extent, the above-mentioned shortcomings could be virtually eliminated by employing highly concentrated electrolytes. In a super-concentrated solution, the intimate Na^+ -water interaction generating $(\text{Na}^+(\text{H}_2\text{O}))_n$ polymer-like chains to replace the ubiquitous hydrogen bonding between water molecules, such structure is mainly responsible for the expanded electrochemical stability window. With this regard, Many studies have paid attention to the relationship between the electrolyte concentration and the electrochemical performance of ASIBs, and numerous successful cases are reported, where salts including NaClO_4 ,^[152] NaNO_3 ,^[153] NaFSI (Figure 19d)^[154] and so forth. Wang el al. applied "water-in-salt" concept to develop highly concentrated electrolyte based on sodium trifluoromethane sulfonate (NaCF_3SO_3 , or NaOTF), that could offer a 2.5 V window through suppressing hydrogen evolution on anode with the formation of a Na^+ -conducting SEI and reduce the overall electrochemical activity of water on cathode. The full ASIB constructed on $\text{Na}_{0.66}[\text{Mn}_{0.66}\text{Ti}_{0.34}]\text{O}_2$ as cathode and $\text{NaTi}_2(\text{PO}_4)_3$ as anode exhibited excellent cycling

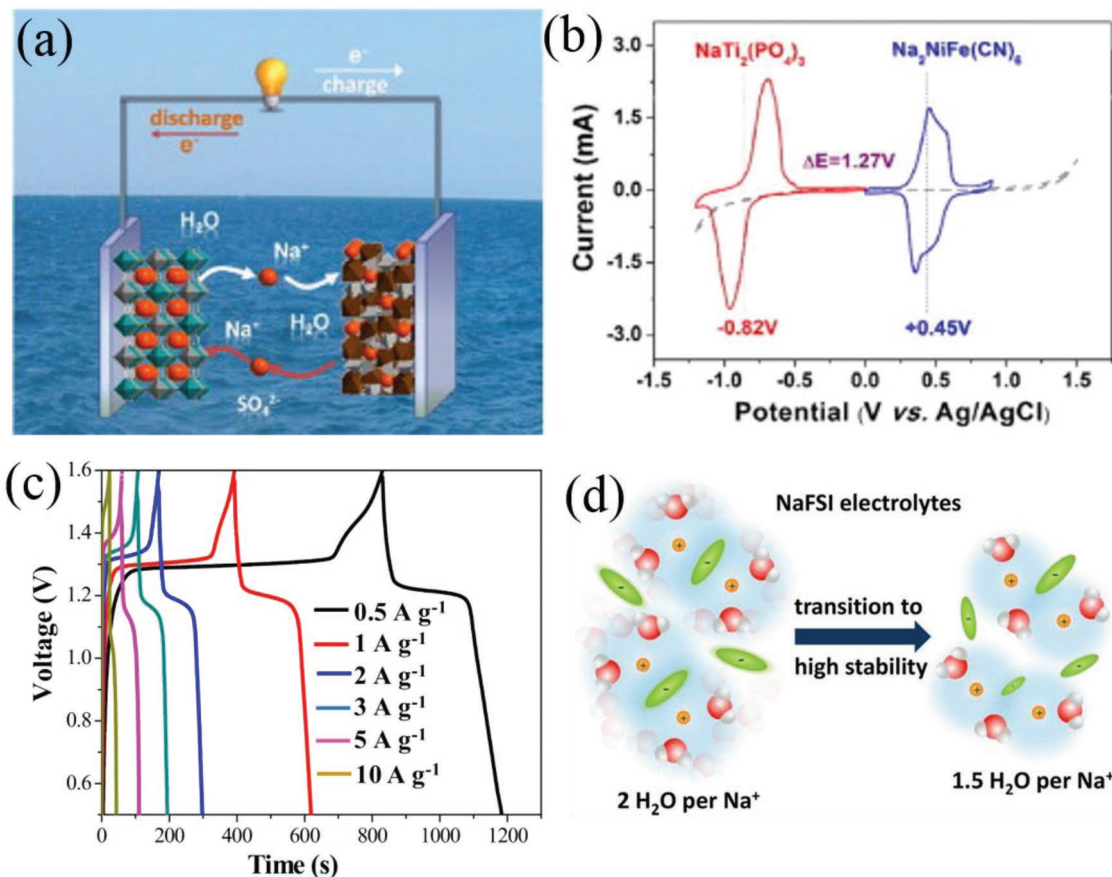


Figure 19. a) Schematic illustration of the working mechanism of aqueous sodium-ion batteries and b) CV curves of Na-deficient NaTi₂(PO₄)₃ anode, Na-rich Na₂NiFe(CN)₆ cathode in aqueous Na₂SO₄ solution. Reproduced with permission.^[100] Copyright 2013, Elsevier. c) Charge-discharge curves of the NTP/NVP full cell at various current. Reproduced with permission.^[148] Copyright 2016, Elsevier. d) Sodium bis(fluorosulfonyl)imide based aqueous electrolytes exhibit a wide electrochemical stability window of up to 2.6 V when the water-to-salt molar ratio falls below 2:1. Reproduced with permission.^[152] Copyright 2017, American Chemical Society.

stability with negligible capacity losses (0.006% per cycle) at a high rate (1 C) for >1200 cycles.^[151]

5. Conclusion and Outlook

The shortage of fossil fuels and the deterioration of environment have stimulated the exploitation of renewable energy and the usage of electric vehicle. As the most advanced rechargeable batteries, currently LIBs have occupied the HEV and EV markets, and the representative LiFePO₄-based batteries have attempted to enter electricity storage system. However, suffering from the limited crust abundance of lithium in the interior of the earth, the ability of LIBs to meet the massive demands of grid-scale energy storage systems (EES) is called into question. Sodium ion batteries are a novel class of secondary batteries, its similar intercalation/deintercalation chemistry to LIBs and low cost of sodium resources provides key advantages that may make SIBs as the storage platform of choice for their applicability in large-scale EES. In practice, power density is a more important parameter than energy density for SIBs, since they are fulfilling the regulation role to an expanding degree in grid frequency regulation services. Though remarkable progress and great achievements have

been made in advancing electrode electrodes for SIBs in the last few years by borrowing from material synthesis routes used to manufacture LIB cells, searching for appropriate electrode materials for SIBs with high power density, long-term cycling life as well as high safety remains a great challenge. In this review, we summarized the development of the emerging promising electrode materials as well as full cell prototypes toward the practical commercialization of high power SIBs, focusing on the exploration of cathode and anode materials, including their inherent host structures, sodium storage mechanisms, and capable strategies to enhance Na⁺ diffusion kinetics.

Regarding to the cathodes materials for SIBs, layered oxides and their derivatives show a large reversible capacity, high operation voltage and acceptable kinetic performance, but the poor cyclability (often < 500 cycles) and high cost of precious metals, such as cobalt and nickel resources, remain major obstacle for their large-scale applications. Moreover, their underlying thermally unsafe character is also an intractable issue. The tunnel structured families with Na_{0.44}MnO₂ as the typical member are ideal choice for high power SIBs; their appealing rate performance is linked to the open structure with interconnected and large tunnels that is able to accommodate fast and repeated de/sodiation. Though this type of cathodes have multiple

charge/discharge plateaus, thus may result in an unstable power supply, several researches revealed that their discharge curves can be smoothed by element doping. PBAs appear to be suitable host materials because of their compositional tenability and rigid open channel structure with large interstitial sites to endow great durability and fast kinetics. But the practical performance of PBAs is greatly affected by phase purity, crystallinity, defects, water content, toxicity and safety hazard at elevated temperature. By removing the coordinated water in lattices or interstitial water and proper metal ion substitution, an enhanced cycle stability and increased working potential could be obtained. NASICON materials, with $\text{Na}_3\text{V}_2(\text{PO}_4)_3$ as the representative, are attracting great interests and regarded as the most promising cathodes for SIBs in recent years due to their high ionic conductivity, chemical flexibility, structural and thermal stability. Their low intrinsic electrical conductivity can be addressed by four main strategies including nanostructure building, conductive composite coating, replacing PO_4 polyanion with other units and metal elements substitution. If significant breakthroughs in lowering the toxic effect and cost of vanadium are achieved in the future, these electrodes will be very competitive. Iron centered polyanion materials are not drawing enough research interests and their potential in SIBs is greatly undervalued due to the relatively low potential and energy density. But the volumetric and gravimetric energy density of batteries for grid-scale EES are less important than those for EVs and HEVs, and based on the fact that these iron-centered polyanions have shown favorable rate capability and long-term cycle life in some works, we believe that this type of cathodes will play a crucial role to develop a well-functioning power-oriented SIBs.

With respect to anode, hard carbon (HC) is undoubtedly the most appealing anode for SIBs due to the relatively high capacity, raw material sustainability, high structural stability, and capability to couple with various cathodes in many emerging prototype sodium-ion full cells. The sodium storage mechanism in hard carbon remains unrevealed completely, thus fundamental studies to this question is still imperative to further its application. Nanoarchitectures manufacturing is able to improve its rate capability, and heteroatom doping is an effective strategy to enhance the low initial Coulombic efficiency and poor sodium (de)-intercalation kinetics. The relatively low operating voltage of hard carbon generally contributes to an increase of the overall cell voltage as well as power output in full-cell configuration, but resulting in safety concerns related to sodium plating and dendrite growth in an improper operation or during fast charging. These tough problems may be alleviated by employing Ti-based compounds operating with insertion/extraction mechanism, which generally offer a higher working voltage and a higher safety benefits due to the absence of metal plating. $\text{Na}_2\text{Ti}_3\text{O}_7$ is able to reversibly uptake Na^+ with proper insertion potential, but its inferior intrinsic electronic conductivity often leads to high polarization and Na^+ insertion causes substantial lattice expansion and strain. NASICON type $\text{NaTi}_2(\text{PO}_4)_3$ could entail fast Na^+ diffusion due to the open 3D framework and trivial volume expansion upon sodium ions insertion/extraction. A considerable rate performance has been achieved by many researchers after morphological engineering, structural design or conductive agents' decoration. However,

the low capacity and high charge potential of $\text{NaTi}_2(\text{PO}_4)_3$ often pose gravimetric energy output of full cell at a sacrifice. Besides, the Ti-based compounds may potentially trigger severe side reactions and gassing in carbonate solvents due to their high catalytic activity. Alloy compounds, in our view, including P, Sn, Sb, Ge are promising options owing to the striking capacity, acceptable operating voltage and raw materials abundance. Their commonly intractable problems, volume expansion that causes unstable SEI and sluggish ionic diffusion, could be effectively addressed at a great extent by rational structure tailoring or morphology decoration approaches. They may come into the field of practical application when the structural stability and prolonged cycling life are further prompted. Typical conversion materials, including transition metal oxides, sulfides and nitrides (with M_aX_b as general formula, M = Fe, Co, Mo, Mn, Ni, etc., X = O, S, N) may not be able to act as alternative anodes in high power SIBs due to some major snags which have not been solved yet in LIBs, including sodium deficiency start phase, low initial Coulombic efficiency, huge volume change upon cycling, poor cycling stability, large voltage hysteresis, and poor reaction irreversibility. Perhaps phosphides are exception, in many cases; the secondary ingredients after conversion reaction, often exhibit a remarkable capacity, high rate capability and ultrastable capacity retention.

Electrolyte is considered to be a critical element, and its rational design and formulation is of top priority. In order to practically assess the viability of the SIB technology, although a variety of organic electrolyte formulas and new electrolyte systems are reported, optimization of each individual component and comprehensive studies to build laboratory-scale prototypes even commercial system are compulsory. Aqueous SIBs with high ionic conductivity and prominent safe feature may be a choice for grid scale energy storage system, but two main challenges remain for future works: broadening the operation potential window and exploring promising electrode materials with higher capacity and prolonged lifespan.

Till now, a vast of SIB full cells based on different types of cathode and anode materials have been proposed in order to promote their practical applications. Most of these full cells demonstrate appreciable energy density of over 200 Wh kg⁻¹ (calculated based on the total electroactive materials), some of them even offer specific energy exceeding 300 Wh kg⁻¹, but seldom with high power capability. According to widely accepted published reports, several prototype^[155] and near-commercialization SIB full cells which are capable of producing very high power output are summarized in Figure 20, in which the energy and power density are calculated based on total masses of both cathode and anode materials. It is of significance to note that the cell performance, including the cycling performance, output power and energy density, is sensitive to the Coulombic efficiencies (CEs) of the electrodes. As for the cathodes, an impractical Coulombic efficiency between 60 and 80% was reported for Prussian blue analogs due to the interstitial water,^[156] but it could be improved to 90% through efficient control of lattice defects and phase transitions. The initial CE of most O3, P2-type layered oxides and iron-centered polyanions could reach 90% in case their crystal structures, composition and configuration is rationally designed. Impressively, a high Coulombic efficiency of over 99% was achieved

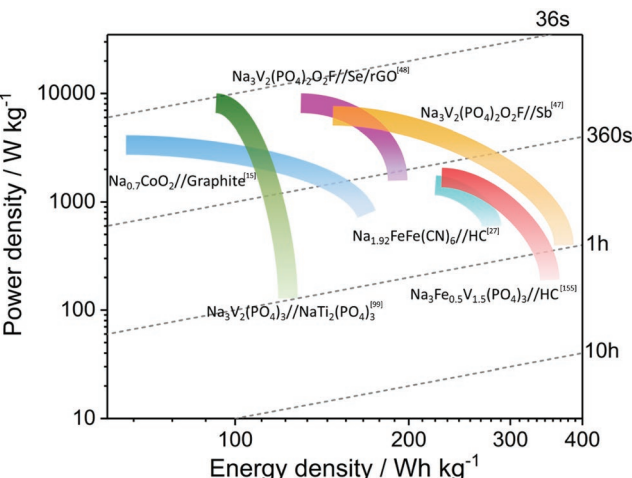


Figure 20. Several emerging prototype sodium-ion full cells with high power capability (HC: hard carbon).

for $\text{Na}_3\text{V}_2(\text{PO}_4)_3$, demonstrating a well compatibility with commercial products. As for the anodes, both alloying materials and Ti-based compounds exhibited a low initial CE less than 80%, because of the irreversible capacity related to SEI formation and/or side reactions occurring within the cell. Nanostructured hard carbon and its functionalized derivatives with high specific surface area were intensively pursued to promote enhanced Na storage capacity and kinetic properties; however the accompanied prominent SEI formation results in massively irreversible capacity loss with initial CE lower than 80%. The highest Coulombic efficiency upon the first cycle reported to date is 88% for amorphous carbon made from the mixture of hard and soft carbon precursors.^[157] In this context, an excess of cathode material is needed to properly balance low CE anode material, thus leading to a lowered power and energy density of full cells. Decreasing surface area, optimizing the electrolyte and designing compatible binder are suggesting as feasible strategies to improve the CE of anode materials. Generally, considering that the sodium-ion batteries technology is still at an early stage, great successes will be achieved in the development of high rate electrode materials. Whereas one thing needs to be emphasized is that SIBs have little competition in energy density compared to LIBs, thus exploring cathode and anode materials with low cost, long cycle life and high safety would be the prime emphasis of future researches of SIBs.

This summary not only sheds a new insight on the classification and screening of alternative high rate electrode materials, but also provides guidance for the design and application of high power SIBs in the future.

Acknowledgements

This work was financially supported by the National Key Research Program of China (No. 2016YFB0901500), the National Natural Science Foundation of China (21875171, 21673165 and 21333007), the Science and Technology Project of State Grid (SGRIDGKJ[2017]841), the Fundamental Research Funds for the Central Universities (2042018kf0007), and the China Postdoctoral Science Foundation (2016M592383 and 2017T100574).

Conflict of Interest

The authors declare no conflict of interest.

Keywords

anode materials, cathode materials, grid-scale energy storage, high power, sodium-ion batteries

Received: December 20, 2018

Revised: January 16, 2019

Published online: February 18, 2019

- [1] Y. Fang, Z. Chen, L. Xiao, X. Ai, Y. Cao, H. Yang, *Small* **2018**, *14*, 1703116.
- [2] Z. Chen, T. Yuan, X. Pu, H. Yang, X. Ai, Y. Xia, Y. Cao, *ACS Appl. Mater. Interfaces* **2018**, *10*, 11689.
- [3] K. Dai, J. Mao, X. Song, V. Battaglia, G. Liu, *J. Power Sources* **2015**, *285*, 161.
- [4] D. Zhang, W. Shi, Y. Yan, S. Xu, L. Chen, X. Wang, S. Liu, *Electrochim. Acta* **2017**, *258*, 1035.
- [5] E. Hosono, T. Saito, J. Hoshino, M. Okubo, Y. Saito, D. Nishio-Hamane, T. Kudo, H. Zhou, *J. Power Sources* **2012**, *217*, 43.
- [6] Q. Liu, Z. Hu, M. Chen, Q. Gu, Y. Dou, Z. Sun, S. Chou, S. X. Dou, *ACS Appl. Mater. Interfaces* **2017**, *9*, 3644.
- [7] X. He, J. Wang, B. Qiu, E. Paillard, C. Ma, X. Cao, H. Liu, M. C. Stan, H. Liu, T. Gallash, Y. S. Meng, J. Li, *Nano Energy* **2016**, *27*, 602.
- [8] P. F. Wang, Y. You, Y. X. Yin, Y. G. Guo, *Adv. Energy Mater.* **2018**, *8*, 1701912.
- [9] N. Yabuuchi, M. Kajiyama, J. Iwatake, H. Nishikawa, S. Hitomi, R. Okuyama, R. Usui, Y. Yamada, S. Komaba, *Nat. Mater.* **2012**, *11*, 512.
- [10] M.-S. Kwon, S. G. Lim, Y. Park, S.-M. Lee, K. Y. Chung, T. J. Shin, K. T. Lee, *ACS Appl. Mater. Interfaces* **2017**, *9*, 14758.
- [11] D. Sehrawat, J. Zhang, D. Y. W. Yu, N. Sharma, *Small Methods* **2018**, 1800092.
- [12] H. Wang, B. Yang, X.-Z. Liao, J. Xu, D. Yang, Y.-S. He, Z.-F. Ma, *Electrochim. Acta* **2013**, *113*, 200.
- [13] L. Wang, Y. G. Sun, L. L. Hu, J. Y. Piao, J. Guo, A. Manthiram, J. M. Ma, A. M. Cao, *J. Mater. Chem. A* **2017**, *5*, 8752.
- [14] R. Berthelot, D. Carlier, C. Delmas, *Nat. Mater.* **2011**, *10*, 74.
- [15] I. Hasa, X. Dou, D. Buchholz, Y. Shao-Horn, J. Hassoun, S. Passerini, B. Scrosati, *J. Power Sources* **2016**, *310*, 26.
- [16] N. Yabuuchi, S. Komaba, *Sci. Technol. Adv. Mater.* **2014**, *15*, 043501.
- [17] Y. Bai, L. Zhao, C. Wu, H. Li, Y. Li, F. Wu, *ACS Appl. Mater. Interfaces* **2016**, *8*, 2857.
- [18] D. Kim, E. Lee, M. Slater, W. Lu, S. Rood, C. S. Johnson, *Electrochim. Commun.* **2012**, *18*, 66.
- [19] N. Yabuuchi, M. Yano, H. Yoshida, S. Kuze, S. Komaba, *J. Electrochem. Soc.* **2013**, *160*, A3131.
- [20] H. Yoshida, N. Yabuuchi, S. Komaba, *Electrochim. Commun.* **2013**, *34*, 60.
- [21] C. Zhang, R. Gao, L. Zheng, Y. Hao, X. Liu, *ACS Appl. Mater. Interfaces* **2018**, *10*, 10819.
- [22] C.-Y. Yu, J.-S. Park, H.-G. Jung, K.-Y. Chung, D. Aurbach, Y.-K. Sun, S.-T. Myung, *Energy Environ. Sci.* **2015**, *8*, 2019.
- [23] E. Lee, J. Lu, Y. Ren, X. Luo, X. Zhang, J. Wen, D. Miller, A. DeWahl, S. Hackney, B. Key, D. Kim, M. D. Slater, C. S. Johnson, *Adv. Energy Mater.* **2014**, *4*, 1400458.
- [24] Z.-Y. Li, J. Zhang, R. Gao, H. Zhang, L. Zheng, Z. Hu, X. Liu, *J. Phys. Chem. C* **2016**, *120*, 9007.

- [25] M. J. Piernas Muñoz, E. Castillo Martínez, *Prussian Blue Based Batteries*, Springer International Publishing, Cham **2018**, pp. 9–22.
- [26] J. Qian, C. Wu, Y. Cao, Z. Ma, Y. Huang, X. Ai, H. Yang, *Adv. Energy Mater.* **2018**, *8*, 1702619.
- [27] L. Wang, J. Song, R. Qiao, L. A. Wray, M. A. Hossain, Y.-D. Chuang, W. Yang, Y. Lu, D. Evans, J.-J. Lee, S. Vail, X. Zhao, M. Nishijima, S. Kakimoto, J. B. Goodenough, *J. Am. Chem. Soc.* **2015**, *137*, 2548.
- [28] Y. You, X.-L. Wu, Y.-X. Yin, Y.-G. Guo, *Energy Environ. Sci.* **2014**, *7*, 1643.
- [29] Y. Jiang, S. Yu, B. Wang, Y. Li, W. Sun, Y. Lu, M. Yan, B. Song, S. Dou, *Adv. Funct. Mater.* **2016**, *26*, 5315.
- [30] L. Wang, Y. Lu, J. Liu, M. Xu, J. Cheng, D. Zhang, J. B. Goodenough, *Angew. Chem., Int. Ed.* **2013**, *52*, 1964.
- [31] T. Matsuda, M. Takachi, Y. Moritomo, *Chem. Commun.* **2013**, *49*, 2750.
- [32] J. Song, L. Wang, Y. Lu, J. Liu, B. Guo, P. Xiao, J. J. Lee, X. Q. Yang, G. Henkelman, J. B. Goodenough, *J. Am. Chem. Soc.* **2015**, *137*, 2658.
- [33] Y. Yuan, J. Wang, Z. Hu, H. Lei, D. Tian, S. Jiao, *J. Alloys Compd.* **2016**, *685*, 344.
- [34] S. Jiao, J. Tuo, H. Xie, Z. Cai, S. Wang, J. Zhu, *Mater. Res. Bull.* **2017**, *86*, 194.
- [35] B. Wang, Y. Han, X. Wang, N. Bahlawane, H. Pan, M. Yan, Y. Jiang, *iScience* **2018**, *3*, 110.
- [36] Y. You, A. Manthiram, *Adv. Energy Mater.* **2018**, *8*, 1701785.
- [37] H. Wang, D. Jiang, Y. Zhang, G. Li, X. Lan, H. Zhong, Z. Zhang, Y. Jiang, *Electrochim. Acta* **2015**, *155*, 23.
- [38] K. Saravanan, W. Mason Chad, A. Rudola, H. Wong Kim, P. Balaya, *Adv. Energy Mater.* **2013**, *3*, 444.
- [39] J. Fang, S. Wang, Z. Li, H. Chen, L. Xia, L. Ding, H. Wang, *J. Mater. Chem. A* **2016**, *4*, 1180.
- [40] Q. Wang, J. Xu, W. Zhang, M. Mao, Z. Wei, L. Wang, C. Cui, Y. Zhu, J. Ma, *J. Mater. Chem. A* **2018**, *6*, 8815.
- [41] K. Saravanan, C. W. Mason, A. Rudola, K. H. Wong, P. Balaya, *Adv. Energy Mater.* **2013**, *3*, 444.
- [42] Y. Fang, L. Xiao, X. Ai, Y. Cao, H. Yang, *Adv. Mater.* **2015**, *27*, 5895.
- [43] D. Guo, J. Qin, Z. Yin, J. Bai, Y.-K. Sun, M. Cao, *Nano Energy* **2018**, *45*, 136.
- [44] Y. Jiang, X. Zhou, D. Li, X. Cheng, F. Liu, Y. Yu, *Adv. Energy Mater.* **2018**, *8*, 800068.
- [45] A. Ponrouch, R. Dedryvere, D. Monti, A. E. Demet, J. M. Ateba Mba, L. Croguennec, C. Masquelier, P. Johansson, M. R. Palacin, *Energy Environ. Sci.* **2013**, *6*, 2361.
- [46] W. Ren, Z. Zhu, Q. An, L. Mai, *Small* **2017**, *13*, 1604181.
- [47] J. Guo, P. Wang, X. Wu, X. Zhang, Q. Yan, H. Chen, J. Zhang, Y. Guo, *Adv. Mater.* **2017**, *29*, 1701968.
- [48] Y. Wang, B. Hou, J. Guo, Q. Ning, W. Pang, J. Wang, C. Lü, X. Wu, *Adv. Energy Mater.* **2018**, *8*, 1703252.
- [49] P. Ge, S. Li, H. Shuai, W. Xu, Y. Tian, L. Yang, G. Zou, H. Hou, X. Ji, *Adv. Mater.* **2019**, *31*, 1806092.
- [50] W. Zhou, L. Xue, X. Lü, H. Gao, Y. Li, S. Xin, G. Fu, Z. Cui, Y. Zhu, J. B. Goodenough, *Nano Lett.* **2016**, *16*, 7836.
- [51] H. Gao, Y. Li, K. Park, J. B. Goodenough, *Chem. Mater.* **2016**, *28*, 6553.
- [52] S. Lim, D. Han, D. Nam, K. Hong, J. Eom, W. Ryu, H. Kwon, *J. Mater. Chem. A* **2014**, *2*, 19623.
- [53] H. Li, X. Yu, Y. Bai, F. Wu, C. Wu, L. Liu, X. Yang, *J. Mater. Chem. A* **2015**, *3*, 9578.
- [54] V. M. Kovrugin, J. Chotard, F. Fauth, A. Jamali, R. David, C. Masquelier, *J. Mater. Chem. A* **2017**, *5*, 14365.
- [55] J. Sheng, H. Zang, C. Tang, Q. An, Q. Wei, G. Zhang, L. Chen, C. Peng, L. Mai, *Nano Energy* **2016**, *24*, 130.
- [56] H. Gao, I. D. Seymour, S. Xin, L. Xue, G. Henkelman, J. B. Goodenough, *J. Am. Chem. Soc.* **2018**, *140*, 18192.
- [57] S. Chen, C. Wu, L. Shen, C. Zhu, Y. Huang, K. Xi, J. Maier, Y. Yu, *Adv. Mater.* **2017**, *29*, 1700431.
- [58] M. Galceran, V. Roddatis, F. J. Zúñiga, J. M. Pérez-Mato, B. Acebedo, R. Arenal, I. Peral, T. Rojo, M. Casas-Cabanas, *Chem. Mater.* **2014**, *26*, 3289.
- [59] W. Tang, X. Song, Y. Du, C. Peng, M. Lin, S. Xi, B. Tian, J. Zheng, Y. Wu, F. Pan, K. P. Loh, *J. Mater. Chem. A* **2016**, *4*, 4882.
- [60] M. Casas-Cabanas, V. V. Roddatis, D. Saurel, P. Kubiak, J. Carretero-González, V. Palomares, P. Serras, T. Rojo, *J. Mater. Chem.* **2012**, *22*, 17421.
- [61] Y. Fang, Q. Liu, L. Xiao, X. Ai, H. Yang, Y. Cao, *ACS Appl. Mater. Interfaces* **2015**, *7*, 17977.
- [62] Y. Fang, J. Zhang, L. Xiao, X. Ai, Y. Cao, H. Yang, *Adv. Sci.* **2017**, *4*, 1600392.
- [63] C. Y. Chen, K. Matsumoto, T. Nohira, R. Hagiwara, *J. Electrochem. Soc.* **2015**, *162*, A176.
- [64] P. Barpanda, G. Liu, C. D. Ling, M. Tamaru, M. Avdeev, S.-C. Chung, Y. Yamada, A. Yamada, *Chem. Mater.* **2013**, *25*, 3480.
- [65] H. J. Song, D.-S. Kim, J.-C. Kim, S.-H. Hong, D.-W. Kim, *J. Mater. Chem. A* **2017**, *5*, 5502.
- [66] K.-H. Ha, S. H. Woo, D. Mok, N.-S. Choi, Y. Park, S. M. Oh, Y. Kim, J. Kim, J. Lee, L. F. Nazar, K. T. Lee, *Adv. Energy Mater.* **2013**, *3*, 770.
- [67] Y. Niu, M. Xu, S. J. Bao, C. M. Li, *Chem. Commun.* **2015**, *51*, 13120.
- [68] M. Chen, L. Chen, Z. Hu, Q. Liu, B. Zhang, Y. Hu, Q. Gu, J. L. Wang, L. Z. Wang, X. Guo, S. L. Chou, S. X. Dou, *Adv. Mater.* **2017**, *29*, 1605535.
- [69] Y. Kawabe, N. Yabuuchi, M. Kajiyama, N. Fukuhara, T. Inamasu, R. Okuyama, I. Nakai, S. Komaba, *Electrochim. Commun.* **2011**, *13*, 1225.
- [70] M. Law, V. Ramar, P. Balaya, *RSC Adv.* **2015**, *5*, 50155.
- [71] J. S. Ko, Vicky V. T. Doan-Nguyen, H.-S. Kim, X. Petrisans, R. H. DeBlock, C. S. Choi, J. W. Long, B. S. Dunn, *J. Mater. Chem. A* **2017**, *5*, 18707.
- [72] X. Wu, G. Zhong, Y. Yang, *J. Power Sources* **2016**, *327*, 666.
- [73] H. Kim, I. Park, S. Lee, H. Kim, K.-Y. Park, Y.-U. Park, H. Kim, J. Kim, H.-D. Lim, W.-S. Yoon, K. Kang, *Chem. Mater.* **2013**, *25*, 3614.
- [74] H. Kim, I. Park, D. H. Seo, S. Lee, S. W. Kim, W. J. Kwon, Y. U. Park, C. S. Kim, S. Jeon, K. Kang, *J. Am. Chem. Soc.* **2012**, *134*, 10369.
- [75] T. Yuan, Y. Wang, J. Zhang, X. Pu, X. Ai, Z. Chen, H. Yang, Y. Cao, *Nano Energy* **2019**, *56*, 160.
- [76] P. Barpanda, G. Oyama, S. Nishimura, S. C. Chung, A. Yamada, *Nat. Commun.* **2014**, *5*, 4358.
- [77] Y. Meng, S. Zhang, C. Deng, *J. Mater. Chem. A* **2015**, *3*, 4484.
- [78] X. Liu, L. Tang, Q. Xu, H. Liu, Y. Wang, *Electrochim. Acta* **2019**, *296*, 345.
- [79] Y. Meng, T. Yu, S. Zhang, C. Deng, *J. Mater. Chem. A* **2016**, *4*, 1624.
- [80] H. Kim, G. Yoon, I. Park, K.-Y. Park, B. Lee, J. Kim, Y.-U. Park, S.-K. Jung, H.-D. Lim, D. Ahn, S. Lee, K. Kang, *Energy Environ. Sci.* **2015**, *8*, 3325.
- [81] D. Dwibedi, R. Gond, A. Dayamani, R. B. Araujo, S. Chakraborty, R. Ahuja, P. Barpanda, *Dalton Trans.* **2016**, *46*, 55.
- [82] Y. Zhu, L. Yang, X. Zhou, F. Li, J. Wei, Z. Zhou, *J. Mater. Chem. A* **2017**, *5*, 9528.
- [83] D. A. Stevens, J. R. Dahn, *J. Electrochem. Soc.* **2000**, *147*, 1271.
- [84] S. Qiu, L. Xiao, M. L. Sushko, K. S. Han, Y. Shao, M. Yan, X. Liang, L. Mai, J. Feng, Y. Cao, X. Ai, H. Yang, J. Liu, *Adv. Energy Mater.* **2017**, *7*, 1700403.
- [85] P. Bai, Y. He, X. Zou, X. Zhao, P. Xiong, Y. Xu, *Adv. Energy Mater.* **2018**, *8*, 1703217.
- [86] Y. Li, S. Xu, X. Wu, J. Yu, Y. Wang, Y.-S. Hu, H. Li, L. Chen, X. Huang, *J. Mater. Chem. A* **2015**, *3*, 71.
- [87] L. Xiao, Y. Cao, W. A. Henderson, M. L. Sushko, Y. Shao, J. Xiao, W. Wang, M. H. Engelhard, Z. Nie, J. Liu, *Nano Energy* **2016**, *19*, 279.
- [88] J. Yang, X. Zhou, D. Wu, X. Zhao, Z. Zhou, *Adv. Mater.* **2017**, *29*, 1604108.

- [89] K.-I. Hong, L. Qie, R. Zeng, Z.-q. Yi, W. Zhang, D. Wang, W. Yin, C. Wu, Q.-J. Fan, W.-X. Zhang, Y.-H. Huang, *J. Mater. Chem. A* **2014**, *2*, 12733.
- [90] P. Senguttuvan, G. Rousse, V. Seznec, J.-M. Tarascon, M. R. Palacín, *Chem. Mater.* **2011**, *23*, 4109.
- [91] W. Wang, C. Yu, Y. Liu, J. Hou, H. Zhu, S. Jiao, *RSC Adv.* **2013**, *3*, 1041.
- [92] S. Fu, J. Ni, Y. Xu, Q. Zhang, L. Li, *Nano Lett.* **2016**, *16*, 4544.
- [93] G. Yang, H. Song, M. Wu, C. Wang, *J. Mater. Chem. A* **2015**, *3*, 18718.
- [94] Y. Jiang, J. Shi, M. Wang, L. Zeng, L. Gu, Y. Yu, *ACS Appl. Mater. Interfaces* **2016**, *8*, 689.
- [95] C. Wu, P. Kopold, Y. L. Ding, P. A. van Aken, J. Maier, Y. Yu, *ACS Nano* **2015**, *9*, 6610.
- [96] L. Wang, B. Wang, G. Liu, T. Liu, T. Gao, D. Wang, *RSC Adv.* **2016**, *6*, 70277.
- [97] J. Yang, H. Wang, P. Hu, J. Qi, L. Guo, L. Wang, *Small* **2015**, *11*, 3744.
- [98] D. Wang, Q. Liu, C. Chen, M. Li, X. Meng, X. Bie, Y. Wei, Y. Huang, F. Du, C. Wang, G. Chen, *ACS Appl. Mater. Interfaces* **2016**, *8*, 2238.
- [99] Y. Fang, L. Xiao, J. Qian, Y. Cao, X. Ai, Y. Huang, H. Yang, *Adv. Energy Mater.* **2016**, *6*, 1502197.
- [100] X. Wu, Y. Cao, X. Ai, J. Qian, H. Yang, *Electrochim. Commun.* **2013**, *31*, 145.
- [101] L. Baggetto, P. Ganesh, R. P. Meisner, R. R. Unocic, J.-C. Jumas, C. A. Bridges, G. M. Veith, *J. Power Sources* **2013**, *234*, 48.
- [102] L. Baggetto, P. Ganesh, C.-N. Sun, R. A. Meisner, T. A. Zawodzinski, G. M. Veith, *J. Mater. Chem. A* **2013**, *1*, 7985.
- [103] J. W. Wang, X. H. Liu, S. X. Mao, J. Y. Huang, *Nano Lett.* **2012**, *12*, 5897.
- [104] J. Zhou, X. Liu, W. Cai, Y. Zhu, J. Liang, K. Zhang, Y. Lan, Z. Jiang, G. Wang, Y. Qian, *Adv. Mater.* **2017**, *29*, 1700214.
- [105] M. Chen, D. Chao, J. Liu, J. Yan, B. Zhang, Y. Huang, J. Lin, Z. X. Shen, *Adv. Funct. Mater.* **2017**, *27*, 1606232.
- [106] H. Zhu, Z. Jia, Y. Chen, N. Weadock, J. Wan, O. Vaaland, X. Han, T. Li, L. Hu, *Nano Lett.* **2013**, *13*, 3093.
- [107] J. Qian, X. Wu, Y. Cao, X. Ai, H. Yang, *Angew. Chem., Int. Ed.* **2013**, *52*, 4633.
- [108] Y. Liu, A. Zhang, C. Shen, Q. Liu, X. Cao, Y. Ma, L. Chen, C. Lau, T.-C. Chen, F. Wei, C. Zhou, *ACS Nano* **2017**, *11*, 5530.
- [109] Y. Zhu, Y. Wen, X. Fan, T. Gao, F. Han, C. Luo, S.-C. Liou, C. Wang, *ACS Nano* **2015**, *9*, 3254.
- [110] H. Gao, T. Zhou, Y. Zheng, Y. Liu, J. Chen, H. Liu, Z. Guo, *Adv. Energy Mater.* **2016**, *6*, 1601037.
- [111] J. Sun, H.-W. Lee, M. Pasta, H. Yuan, G. Zheng, Y. Sun, Y. Li, Y. Cui, *Nat. Nanotechnol.* **2015**, *10*, 980.
- [112] A. Nie, Y. Cheng, S. Ning, T. Foroozan, P. Yasaee, W. Li, B. Song, Y. Yuan, L. Chen, A. Salehi-Khojin, F. Mashayek, R. Shahbazian-Yassar, *Nano Lett.* **2016**, *16*, 2240.
- [113] F. Yang, H. Gao, J. Chen, Z. Guo, *Small Methods* **2017**, *1*, 1700216.
- [114] V. L. Chevrier, G. Ceder, *J. Electrochem. Soc.* **2011**, *158*, A1011.
- [115] L. D. Ellis, T. D. Hatchard, M. N. Obrovac, *J. Electrochem. Soc.* **2012**, *159*, A1801.
- [116] J. Wang, C. Eng, Y. C. Chen-Wiegart, J. Wang, *Nat. Commun.* **2015**, *6*, 7496.
- [117] X. Xie, K. Kretschmer, J. Zhang, B. Sun, D. Su, G. Wang, *Nano Energy* **2015**, *13*, 208.
- [118] S. Li, Z. Wang, J. Liu, L. Yang, Y. Guo, L. Cheng, M. Lei, W. Wang, *ACS Appl. Mater. Interfaces* **2016**, *8*, 19438.
- [119] M. Sha, H. Zhang, Y. Nie, K. Nie, X. Lv, N. Sun, X. Xie, Y. Ma, X. Sun, *J. Mater. Chem. A* **2017**, *5*, 6277.
- [120] Y. Liu, N. Zhang, L. Jiao, Z. Tao, J. Chen, *Adv. Funct. Mater.* **2015**, *25*, 214.
- [121] B. Luo, T. Qiu, D. Ye, L. Wang, L. Zhi, *Nano Energy* **2016**, *22*, 232.
- [122] H. Zhang, I. Hasa, S. Passerini, *Adv. Energy Mater.* **2018**, *8*, 1702582.
- [123] L. Xiao, Y. Cao, J. Xiao, W. Wang, L. Kovarik, Z. Nie, J. Liu, *Chem. Commun.* **2012**, *48*, 3321.
- [124] Z. Liu, X.-Y. Yu, X. W. Lou, U. Paik, *Energy Environ. Sci.* **2016**, *9*, 2314.
- [125] M. He, K. Kravchyk, M. Walter, M. V. Kovalenko, *Nano Lett.* **2014**, *14*, 1255.
- [126] L. Wu, X. Hu, J. Qian, F. Pei, F. Wu, R. Mao, X. Ai, H. Yang, Y. Cao, *Energy Environ. Sci.* **2014**, *7*, 323.
- [127] L. Hu, X. Zhu, Y. Du, Y. Li, X. Zhou, J. Bao, *Chem. Mater.* **2015**, *27*, 8138.
- [128] J. Hur, I. T. Kim, *Bull. Korean Chem. Soc.* **2015**, *36*, 1625.
- [129] J. Liu, Z. Yang, J. Wang, L. Gu, J. Maier, Y. Yu, *Nano Energy* **2015**, *16*, 389.
- [130] Y. Zhao, A. Manthiram, *Chem. Mater.* **2015**, *27*, 3096.
- [131] A. Kohandehghan, K. Cui, M. Kupsta, J. Ding, E. Memarzadeh Lotfabad, W. P. Kalisvaart, D. Mitlin, *Nano Lett.* **2014**, *14*, 5873.
- [132] P. R. Abel, Y.-M. Lin, T. de Souza, C.-Y. Chou, A. Gupta, J. B. Goodenough, G. S. Hwang, A. Heller, C. B. Mullins, *J. Phys. Chem. C* **2013**, *117*, 18885.
- [133] J. H. Kim, J. H. Yun, D. K. Kim, *Adv. Energy Mater.* **2018**, *8*, 1703499.
- [134] S. Liu, J. Feng, X. Bian, J. Liu, H. Xu, Y. An, *Energy Environ. Sci.* **2017**, *10*, 1222.
- [135] Y. Lu, P. Zhou, K. Lei, Q. Zhao, Z. Tao, J. Chen, *Adv. Energy Mater.* **2017**, *7*, 1601973.
- [136] J. Qian, Y. Xiong, Y. Cao, X. Ai, H. Yang, *Nano Lett.* **2014**, *14*, 1865.
- [137] J. Liu, P. Kopold, C. Wu, P. A. van Aken, J. Maier, Y. Yu, *Energy Environ. Sci.* **2015**, *8*, 3531.
- [138] Y. Xu, B. Peng, F. M. Mulder, *Adv. Energy Mater.* **2018**, *8*, 1701847.
- [139] H. Che, S. Chen, Y. Xie, H. Wang, K. Amine, X.-Z. Liao, Z.-F. Ma, *Energy Environ. Sci.* **2017**, *10*, 1075.
- [140] A. Ponrouch, D. Monti, A. Boschin, B. Steen, P. Johansson, M. R. Palacín, *J. Mater. Chem. A* **2015**, *3*, 22.
- [141] G. Åvall, J. Mindemark, D. Brandell, P. Johansson, *Adv. Energy Mater.* **2018**, *8*, 1703036.
- [142] S. Y. Hong, Y. Kim, Y. Park, A. Choi, N.-S. Choi, K. T. Lee, *Energy Environ. Sci.* **2013**, *6*, 2067.
- [143] B. Jache, P. Adelhelm, *Angew. Chem.* **2014**, *126*, 10333.
- [144] H. Kumar, E. Detsi, D. P. Abraham, V. B. Shenoy, *Chem. Mater.* **2016**, *28*, 8930.
- [145] Y. Wen, B. Wang, B. Luo, L. Wang, *Eur. J. Inorg. Chem.* **2016**, *2016*, 2051.
- [146] M. Chen, L. Chen, Z. Hu, Q. Liu, B. Zhang, Y. Hu, Q. Gu, J.-L. Wang, L.-Z. Wang, X. Guo, S.-L. Chou, S.-X. Dou, *Adv. Mater.* **2017**, *29*, 1605535.
- [147] T. C. Yuan, J. X. Zhang, X. J. Pu, Z. X. Chen, C. Y. Tang, X. H. Zhang, X. P. Ai, Y. H. Huang, H. X. Yang, Y. L. Cao, *ACS Appl. Mater. Interfaces* **2018**, *10*, 34108.
- [148] C. D. Wessells, S. V. Peddada, R. A. Huggins, Y. Cui, *Nano Lett.* **2011**, *11*, 5421.
- [149] Q. Zhang, C. Liao, T. Zhai, H. Li, *Electrochim. Acta* **2016**, *196*, 470.
- [150] J. F. Whitacre, A. Tevar, S. Sharma, *Electrochim. Commun.* **2010**, *12*, 463.
- [151] L. M. Suo, O. Borodin, Y. S. Wang, X. H. Rong, W. Sun, X. L. Fan, S. Y. Xu, M. A. Schroeder, A. V. Cresce, F. Wang, C. Y. Yang, Y. S. Hu, K. Xu, C. S. Wang, *Adv. Energy Mater.* **2017**, *7*, 1701189.
- [152] F. Zhang, W. Li, X. Xiang, M. Sun, *Chem. - Eur. J.* **2017**, *23*, 12944.
- [153] H. Qin, Z. P. Song, H. Zhan, Y. H. Zhou, *J. Power Sources* **2014**, *249*, 367.
- [154] R.-S. Kühnel, D. Reber, C. Battaglia, *ACS Energy Lett.* **2017**, *2*, 2005.
- [155] R. Zhan, B. Shen, Q. Xu, Y. Zhang, Y. Luo, H. Liu, H. Chen, F. Liu, C. Li, M. Xu, *Electrochim. Acta* **2018**, *283*, 1475.
- [156] W. Ren, M. Qin, Z. Zhu, M. Yan, Q. Li, L. Zhang, D. Liu, L. Mai, *Nano Lett.* **2017**, *17*, 4713.
- [157] Y. Li, L. Mu, Y.-S. Hu, H. Li, L. Chen, X. Huang, *Energy Storage Mater.* **2016**, *2*, 139.